

Analysis of plasma extracellular vesicle-derived microRNAs from patients with
nonalcoholic fatty liver disease and hepatocellular carcinoma



A Dissertation Submitted in Partial Fulfillment of the Requirements
for the Degree of Doctor of Philosophy in Medical Biochemistry
Department of Biochemistry
Faculty Of Medicine
Chulalongkorn University
Academic Year 2023

การศึกษา microRNAs ใน extracellular vesicles ในผู้ป่วยไขมันพอกตับและมะเร็งตับเพื่อการ
วินิจฉัยและพยากรณ์โรค



วิทยานิพนธ์นี้เป็นส่วนหนึ่งของการศึกษาตามหลักสูตรปริญญาวิทยาศาสตรดุษฎีบัณฑิต
สาขาวิชาชีวเคมีทางการแพทย์ ภาควิชาชีวเคมี
คณะแพทยศาสตร์ จุฬาลงกรณ์มหาวิทยาลัย
ปีการศึกษา 2566

บุษกร บุญแก้ว : การศึกษา microRNAs ใน extracellular vesicles ในผู้ป่วยไขมันพอกตับและมะเร็งตับเพื่อการวินิจฉัยและพยากรณ์โรค. (Analysis of plasma extracellular vesicle-derived microRNAs from patients with nonalcoholic fatty liver disease and hepatocellular carcinoma) อ.ที่ปรึกษาหลัก : ศ. นพ.พิสิฐ ตั้งกิจวานิชย์, อ.ที่ปรึกษาร่วม : อ. ดร.ณัฐธยาน์ ช่วยเพ็ญ

miRNAs Extracellular vesicle-derived microRNAs (EV-miRNAs) เป็นตัวบ่งชี้ทางชีวภาพที่มีประสิทธิภาพในโรคตับ งานนี้ได้ศึกษา EV-miRNAs จากพลาสมาของผู้ป่วยโรคมะเร็งตับที่ไม่ได้มีสาเหตุจากไวรัสตับอักเสบบีและไวรัสตับอักเสบบี (NBNC-HCC) โดยเปรียบเทียบกับ EV-miRNA จากพลาสมาของผู้ป่วยโรคมะเร็งตับ NBNC-HCC กับผู้ป่วยโรคไขมันพอกตับ (NAFLD) และกลุ่มคนสุขภาพดี โดยใช้วิธี NanoString และ qRT-PCR พบว่า EV-miRNA หัวตัวได้แก่ miR-19-3p, miR-16-5p, miR-223-3p, miR-30d-5p และ miR-451a มีการแสดงออกสูงขึ้นในกลุ่มผู้ป่วยโรคมะเร็งตับ NBNC-HCC เทียบกับผู้ป่วยโรคไขมันพอกตับ (NAFLD) และกลุ่มคนสุขภาพดี และ EV-miR-19-3p แสดงประสิทธิภาพการวินิจฉัยที่ดีที่สุด โดยมีความไวสูง สามารถตรวจจับได้ในผู้ป่วยโรคมะเร็งตับ NBNC-HCC ที่มีระดับ AFP ต่ำและผู้ป่วยในระยะเริ่มต้น ซึ่งบ่งชี้ว่า EV-miR-19-3p สามารถทำหน้าที่เป็นตัวบ่งชี้สำหรับการวินิจฉัย และการพยากรณ์โรคของ NBNC-HCC เพื่ออธิบายกลไกการเกิดโรค NAFLD ได้มีการศึกษาบทบาทของ EVs ในการเป็นตัวกลางสื่อสารระหว่างเซลล์แมคโครฟาจและเซลล์ตับที่สะสมไขมัน หลังจากเลี้ยงเซลล์แมคโครฟาจที่มี Cy3-miR-223 ร่วมกับเซลล์ตับที่สะสมไขมัน พบว่า miR-223 มีการแสดงออกสูงขึ้นในทั้ง EVs ที่ได้จากเซลล์แมคโครฟาจและเซลล์ตับที่สะสมไขมัน ยังพบว่าเซลล์ตับที่สะสมไขมันมีการเรืองแสงของ Cy3 การเพิ่มขึ้นของระดับ miR-223 และการลดลงของยีนเป้าหมายของ miR-223 ได้แก่ FOXO3 และ TAZ เมื่อยับยั้งการหลั่งของ EVs จากแมคโครฟาจด้วย GW4869 ทำให้การส่ง miR-223 ไปยังเซลล์ตับลดลง นอกจากนี้เมื่อย้อม EVs จากมาโครฟาจด้วยสี MemGlow แล้วนำไปบ่มกับเซลล์ตับที่สะสมไขมัน พบสีย้อม MemGlow ยังถูกส่งไปยังเซลล์ตับที่สะสมไขมัน การศึกษาเพิ่มเติมยังชี้ให้เห็นว่าตัวรับไขมันบนผิวเซลล์ชนิด LDLR มีบทบาทในการนำ EVs เข้าเซลล์ตับ กล่าวโดยสรุปได้ว่าเซลล์แมคโครฟาจสามารถส่ง miRNA ไปยังเซลล์ตับที่สะสมไขมันได้

สาขาวิชา ชีวเคมีทางการแพทย์

ปีการศึกษา 2566

ลายมือชื่อนิสิต

ลายมือชื่อ อ.ที่ปรึกษาหลัก

ลายมือชื่อ อ.ที่ปรึกษาร่วม

6273001430 : MAJOR MEDICAL BIOCHEMISTRY

KEYWORD: 1. Extracellular vesicles 2. Nonalcoholic fatty liver disease 3. Hepatocellular carcinoma 4. microRNAs 5. Biomarker

Bootsakorn Boonkaew : Analysis of plasma extracellular vesicle-derived microRNAs from patients with nonalcoholic fatty liver disease and hepatocellular carcinoma. Advisor: Prof. Pisit Tangkijvanich Co-advisor: Dr. NATTHAYA CHUAYPEN, Ph.D.

Extracellular vesicle-derived microRNAs (EV-miRNAs) are promising circulating biomarkers for chronic liver disease. In this study, we explored the potential significance of plasma EV-miRNAs in non-hepatitis B-, non-hepatitis C-related HCC (NBNC-HCC). We compared plasma EV-miRNA profiles between NBNC-HCC and control groups including non-alcoholic fatty liver disease (NAFLD) and healthy controls using NanoString method. The differentially expressed EV-miRNAs were validated in another set of plasma samples by qRT-PCR. Five plasma EV-miRNAs were significantly elevated in HCC, which included miR-19-3p, miR-16-5p, miR-223-3p, miR-30d-5p, and miR-451a. Among them, EV-miR-19-3p exhibited the best diagnostic performance and displayed a high sensitivity for detecting AFP-negative HCC and early-stage HCC, indicating EV-miR-19-3p could serve as a novel circulating biomarker for the diagnosis and prognosis of NBNC-HCC. To mechanistically describe NAFLD, we demonstrated the role of EVs in mediating communication between macrophages and lipotoxic hepatocytes. Macrophages were transfected with a Cy3-miR-223 mimic and co-cultured with lipotoxic hepatocytes. We found that miR-223 was highly expressed in EV fractions from the transfected macrophages, as opposed to the protein fractions. Upon co-culture, the lipotoxic hepatocytes displayed Cy3 fluorescence and exhibited an increase in miR-223 levels and a decrease in miR-223 target genes, *FOXO3* and *TAZ*, as compared to the control group. Blocking EV secretion from macrophages with GW4869 led to reduced transfer of miR-223 to hepatocyte recipient cells. Furthermore, the MemGlow dye was transferred to lipotoxic hepatocytes when incubated with MemGlow-labeled EVs from macrophages. The results also suggested that low-density lipoprotein receptor (LDLR) played a partial role in facilitating EV uptake by lipotoxic hepatocytes. In summary, our findings suggest that macrophages can transfer transfected miRNA to lipotoxic hepatocytes.

Field of Study: Medical Biochemistry

Academic Year: 2023

Student's Signature

Advisor's Signature

Co-advisor's Signature

ACKNOWLEDGEMENTS

I would like to express my heartfelt gratitude to the individuals and organizations who have supported and guided me throughout my thesis journey. I am deeply indebted to my advisor, Professor Pisit Tangkijvanich, and my co-advisor, Lecturer Natthaya Chuaypen. Their unwavering support, mentorship, and expertise were invaluable in shaping this thesis. I would like to express my deepest appreciation to: Assistant Professor Chaiyaboot Ariyachet, whose guidance and insights significantly contributed to the quality of this work especially in molecular cell biology session, and Associate Professor Kenneth W. Witwer, for his valuable input and support during one year for my time at Johns Hopkins University School of Medicine. I extend my sincere thanks to the chairs and members of my thesis defense committees for their time, feedback, and valuable contributions. I am also grateful to C2F scholarship, and I am grateful for the financial support provided by the RGJ scholarship and Fulbright program, which enabled me to pursue my studies and research in US. Special thanks to The Center of Excellence in Hepatitis and Liver Cancer at the Department of Biochemistry, Faculty of Medicine, Chulalongkorn University, for their resources and collaboration. Thanks should also go to the Department of Comparative Pathobiology at Johns Hopkins University School of Medicine, where I had the opportunity to learn and collaborate as well as the members of the KWW lab for their camaraderie and assistance.

TABLE OF CONTENTS

	Page
ABSTRACT (THAI)	iii
ABSTRACT (ENGLISH)	iv
ACKNOWLEDGEMENTS	v
TABLE OF CONTENTS	vi
LIST OF TABLES	ix
LIST OF FIGURES.....	x
CHAPTER 1	1
INTRODUCTION	1
1.1. Introduction.....	1
1.2. Research question.....	3
1.3. Hypothesis.....	3
1.4. Objective	3
1.5. Conceptual framework.....	4
1.6. Research workflow	5
CHAPTER 2.....	7
LITERATURE REVIEW	7
2.1. Chronic liver disease (CLD).....	7
2.2. Nonalcoholic fatty liver disease (NAFLD).....	7
2.3. Risk factors for NAFLD and NASH.....	9
2.4. Non-hepatitis B-, non-hepatitis C-related HCC (NBNC-HCC).....	10
2.5. Diagnostic tool and treatment for NAFLD, NASH, and HCC.....	11

2.6. Extracellular vesicles (EVs).....	14
2.6.1. Role of EVs in liver diseases	19
2.6.2. Role of EVs as biomarkers.....	19
2.6.3. Role of EV-derived miRNAs as biomarkers	20
2.6.4. Role of EV in cellular communication in NAFLD	22
2.6.4.1. Lipotoxicity and inflammation in NAFLD development.....	23
2.6.4.2. EV receptor	24
CHAPTER 3.....	26
MATERIALS AND METHODS.....	26
3.1. Research subjects and participant consent.....	26
3.2. Blood collection and plasma processing.....	27
3.3. Cell culture and differentiation.....	27
3.4. EV isolation	28
3.5. EV characterization.....	29
3.5.1. Nanoparticle tracking analysis (NTA).....	29
3.5.2 Nano flow cytometry measurement (NFCM).....	29
3.5.3. Transmission electron microscopy (TEM).....	29
3.5.4. Immunoblotting analysis.....	30
3.6. Co-culture between lipotoxic hepatocytes and macrophages.....	30
3.7. Induction of lipotoxicity in hepatocytes	31
3.8. NanoString miRNA expression analysis	31
3.9. EV and tissue miRNA extraction	32
3.10. Real-Time Quantitative Reverse Transcription PCR (qRT-PCR).....	32

3.11. EV uptake assay	33
3.12. Immunofluorescence staining	33
3.14. Statistical analysis.....	34
CHAPTER 4.....	36
RESULTS.....	36
4.1. Part I Circulating extracellular vesicle-derived microRNAs as novel diagnostic and prognostic biomarkers for non-viral-related hepatocellular carcinoma.....	36
4.1.1. Characteristics of the participants.....	36
4.1.2. Characterization of EVs.....	36
4.1.3. Profiling of EV-derived microRNAs.....	39
4.1.4. Functional gene annotation and pathway enrichment analysis.....	40
4.2. Part II Macrophages release miRNA-enriched extracellular vesicles that are taken up by lipotoxic hepatocytes.....	50
4.2.1 miR-223 expression in transfected macrophages.....	50
4.2.2. miR-223 in macrophage-derived EVs.....	50
4.2.3. miR-223 in lipotoxic hepatocytes after co-culture with macrophages.....	52
CHAPTER 5.....	62
DISCUSSION.....	62
CHAPTER 6.....	70
CONCLUSION.....	70
APPENDIX	72
REFERENCES	88
VITA.....	99

LIST OF TABLES

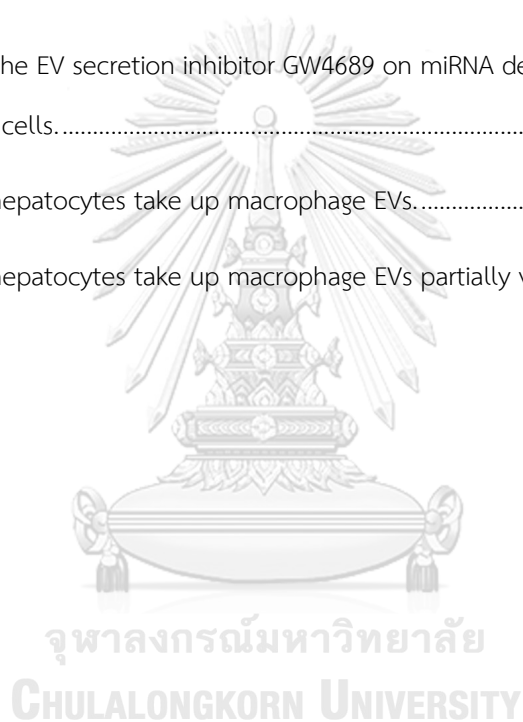
	Page
Table 1 Exosomes, microvesicles, and apoptotic Bodies: main characteristics, adapted from (6) and (51).....	18
Table 2 Sequences of primers used for qRT-PCR analysis	35
Table 3 Baseline characteristic of the validation cohort in this study.....	41
Table 4 Variables associated with overall survival in patients with HCC.....	49



LIST OF FIGURES

	Page
Figure 1 The pathophysiological states and risk factors of NAFLD and HCC.....	11
Figure 2 Histologic features of diagnosis of NAFLD and NASH.	15
Figure 3 Extracellular vesicle biogenesis and release (50).....	17
Figure 4 qRT-PCR analysis of candidate internal controls in the study cohort.	37
Figure 5 Schematic diagram of the study protocol and characterization of EVs derived from plasma.....	38
Figure 6 qRT-PCR analysis of EV miRNAs.....	39
Figure 7 Transcriptome profiling of miRNAs from plasma EVs using NanoString microarray.	40
Figure 8 Venn diagram of intersect genes of miRNA profiling.....	42
Figure 9 Gene Ontology (GO) analysis of the differentially upregulated EV miRNAs.....	43
Figure 10 Gene Ontology (GO) analysis of the differentially downregulated EV miRNAs.....	43
Figure 11 Validation of candidate miRNAs in plasma EV using qRT-PCR.....	45
Figure 12 Validation of candidate miRNAs in plasma EV using qRT-PCR.....	46
Figure 13 Expression of candidate miRNAs in tumor and adjacent non-tumor liver tissue samples using qRT-PCR.....	47
Figure 14 Receiver operating characteristic (ROC) curves of the candidate miRNAs for distinguishing between NBNC-HCC and non-HCC.....	48
Figure 15 Kaplan–Meier survival curves for overall survival analysis of patients with NBNC-HCC.	48
Figure 16 Differentiated macrophages from PBMCs.	51
Figure 17 miR-223 in macrophages and Huh7 hepatocyte cell line by qRT-PCR.....	52
Figure 18 Cy3 fluorescence dye in macrophages after transfection with Cy3-miR-223 mimic.	53

Figure 19 Characterization of EVs from Cy3-miR-223 mimic transfected macrophages.	54
Figure 20 miR-223 in EVs from Cy3-miR-223 transfected macrophages.	55
Figure 21 Induction of lipotoxicity in hepatocytes using palmitic acid.....	56
Figure 22 Cy3 fluorescence dye in hepatocytes after co-culture with Cy3-miR-223 mimic transfected macrophages.	57
Figure 23 miR-223 in lipotoxic hepatocytes after co-culture with Cy3-miR-223 mimic transfected macrophages.....	58
Figure 24 Effects of the EV secretion inhibitor GW4689 on miRNA delivery from macrophages into hepatocyte recipient cells.....	59
Figure 25 Lipotoxic hepatocytes take up macrophage EVs.....	60
Figure 26 Lipotoxic hepatocytes take up macrophage EVs partially via LDLR.....	61



CHAPTER 1

INTRODUCTION

1.1. Introduction

Hepatocellular carcinoma (HCC) is a diverse tumor primarily associated with chronic liver disease (CLD), traditionally linked to chronic viral hepatitis (1). However, a rising number of cases, particularly in Western countries, are now attributed to non-hepatitis B, non-hepatitis C-related HCC (NBNC-HCC) due to the increasing prevalence of non-alcoholic fatty liver disease (NAFLD) (1). In Asian populations, the increasing occurrence of NAFLD is emerging as a significant public health issue, with the potential to result in advancing liver conditions such as cirrhosis and HCC (2). Early detection is crucial for effective treatment, but the prognosis remains challenging due to the aggressive nature of the tumor and high recurrence rates (3). Notably, NBNC-HCC often presents at a late stage, leading to poorer outcomes compared to virus-related HCC (4). Consequently, there is a pressing need for reliable circulating biomarkers to enhance early diagnosis and prognostic prediction in NBNC-HCC.

In recent years, "liquid biopsy" has emerged as a promising method for analyzing circulating cancer components, providing a foundation for precision oncology regarding diagnosis, therapeutic monitoring, and prognosis (5). Among various liquid-biopsy based techniques, extracellular vesicles (EVs) are promising circulating biomarkers for HCC (5). EVs, including exosomes, microvesicles, and apoptotic bodies, play a role in intercellular communication by carrying proteins, lipids, and nucleic acids (6). MicroRNAs (miRNAs), particularly those derived from EVs (EV-miRNAs), are of interest due to their regulatory roles in key pathophysiological processes (7). EV-miRNAs are considered more stable and homogeneous than free miRNAs in serum/plasma,

making them specific and reliable candidates for cancer biomarkers. (8). While "free-circulating" miRNAs have shown utility in distinguishing HCC from non-HCC, limited data are available regarding the role of EV-miRNAs, especially in NBNC-HCC. Further research in this area is essential for improving clinical outcomes in patients with NBNC-HCC.

Lipotoxicity plays a critical role in the development of NAFLD. The excess release of free fatty acids (FFAs), which results from the overtransportation of FFAs from dysfunctional adipose tissue to the liver, leads to lipotoxicity. This, in turn, triggers the recruitment of macrophages to the liver, contributing to the progression of NAFLD. The mediators of crosstalk linking these two scenarios remain elusive. In a recent study using a mouse model of nonalcoholic steatohepatitis, it was demonstrated that neutrophils transfer miR-223-enriched EVs to lipotoxic hepatocytes through the low-density lipoprotein receptor (LDLR), shedding light on the intricate interplay between these phenomena.

In the present study, we aimed to explore the potential clinical significance of EV-miRNAs in patients with NBNC-HCC. First, we compared the profiles of plasma EV-miRNAs of the NBNC-HCC and non-cancerous groups, including patients with NAFLD and healthy controls using the NanoString technique. Additionally, the differentially expressed EV-miRNAs were validated in another set of plasma samples by qRT-PCR to identify novel biomarkers for NBNC-HCC. Indeed, we demonstrated a mechanistic basis for the delivery of miRNA from macrophages to lipotoxic hepatocytes via EVs using a co-culture system of NAFLD model. In summary, our results emphasize the significance of EV miRNAs as biomarkers for diagnosis and the prognosis of NBNC-HCC.

1.2. Research question

1.2.1. Can circulating miRNAs from plasma extracellular vesicles be used as diagnostic and prognostic biomarkers for NBNC-HCC?

1.2.2. Can miRNAs be transported from macrophages to lipotoxic hepatocytes via extracellular vesicles?

1.3. Hypothesis

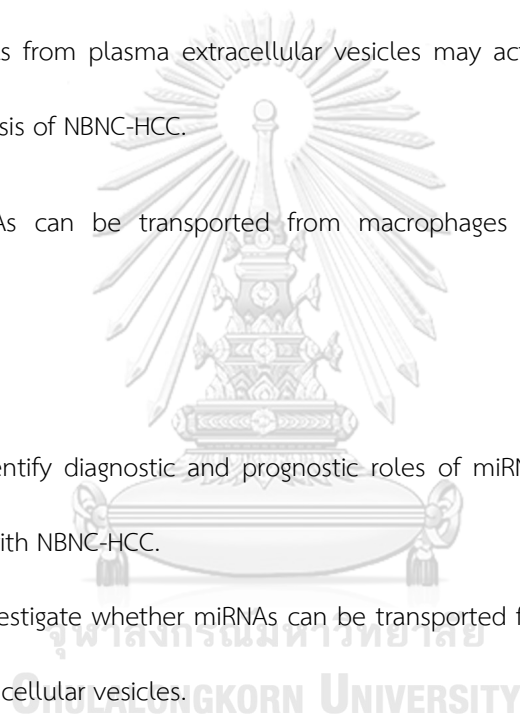
1.3.1. miRNAs from plasma extracellular vesicles may act as circulating biomarkers for diagnosis and prognosis of NBNC-HCC.

1.3.2. miRNAs can be transported from macrophages to lipotoxic hepatocytes via extracellular vesicles.

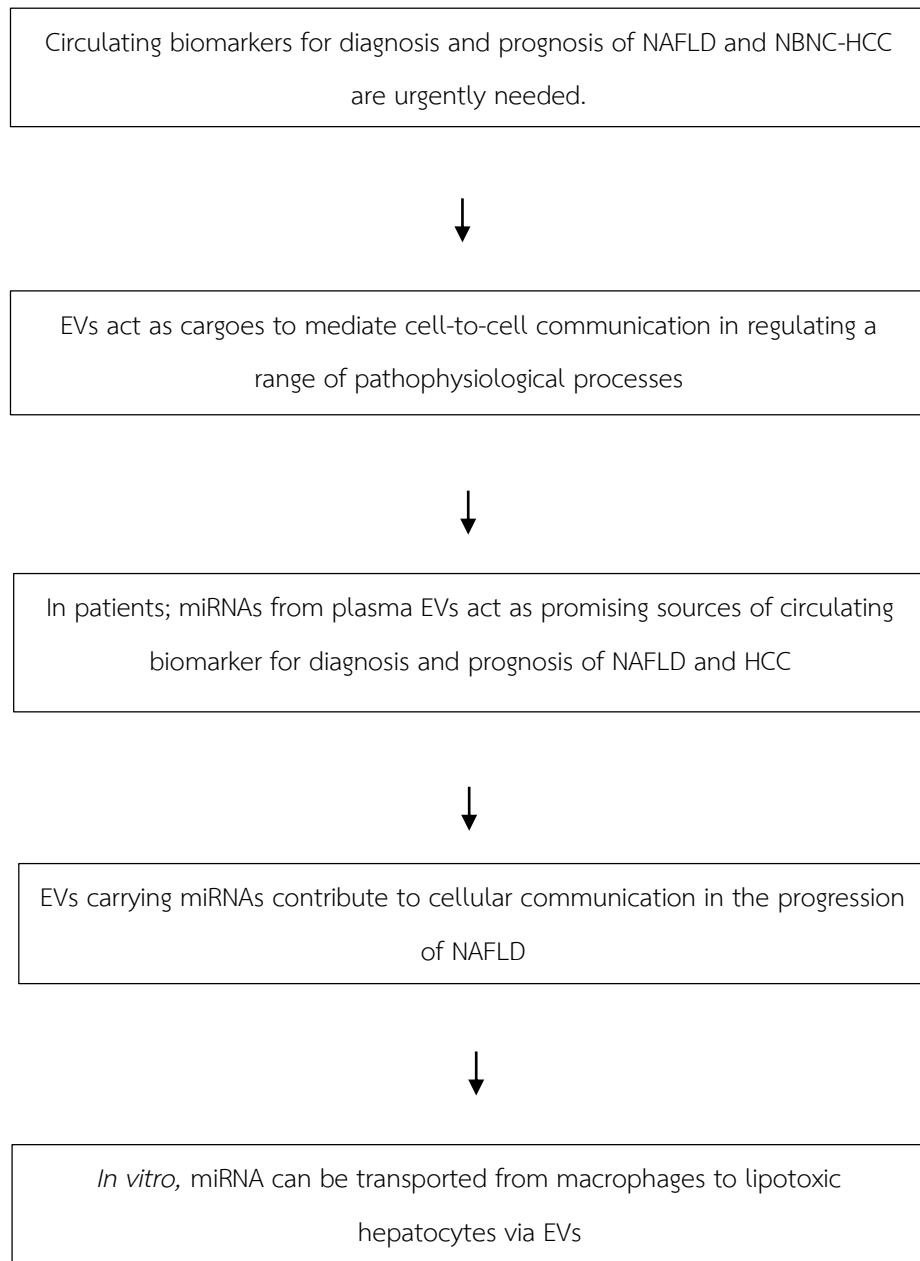
1.4. Objective

1.4.1. To identify diagnostic and prognostic roles of miRNAs from plasma extracellular vesicles in patients with NBNC-HCC.

1.4.2. To investigate whether miRNAs can be transported from macrophages to lipotoxic hepatocytes via extracellular vesicles.

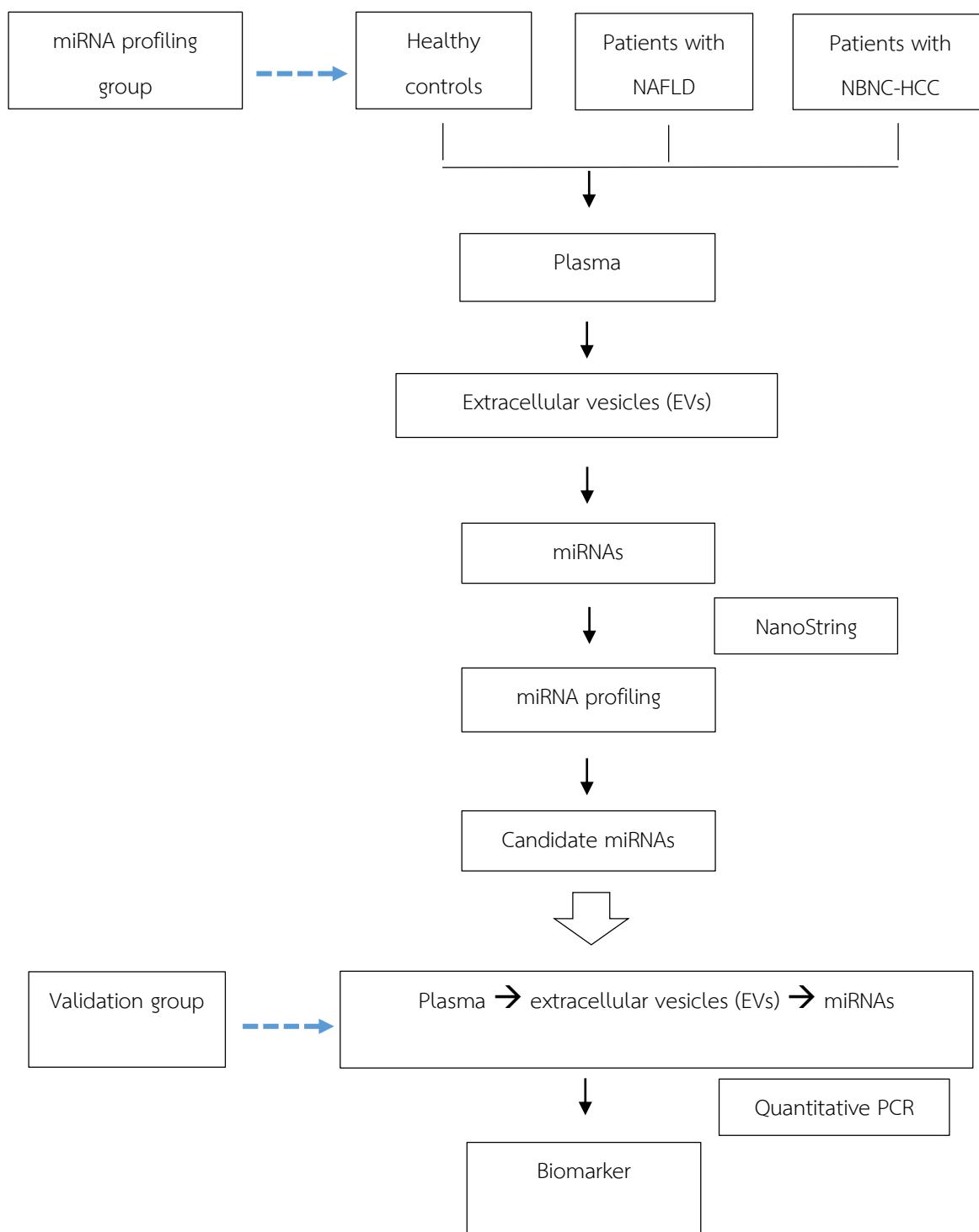


1.5. Conceptual framework

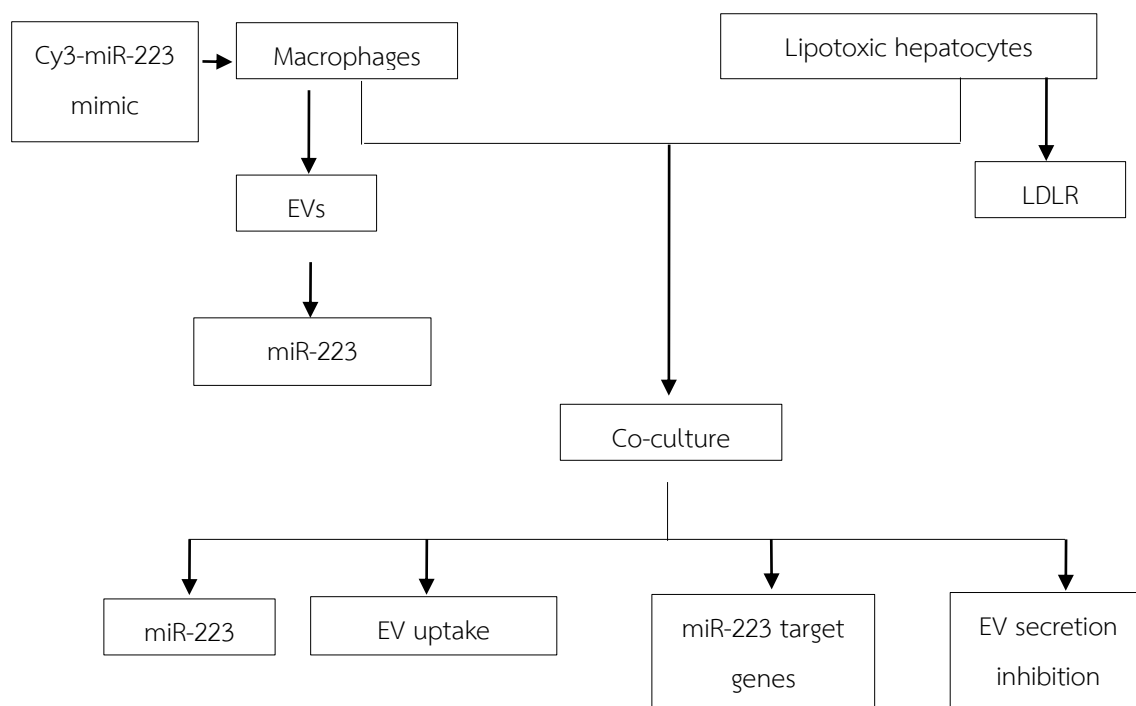


1.6. Research workflow

Part 1



Part 2



CHAPTER 2

LITERATURE REVIEW

2.1. Chronic liver disease (CLD)

The global prevalence of chronic liver disease (CLD) and cirrhosis was approximately 1.5 billion people in 2017 with an annual death rate of up to 2 million people. The most common form of CLD, nonalcoholic fatty liver disease (NAFLD), accounts for about 60%. Other significant risks are hepatitis B virus (HBV) and hepatitis C virus (HCV) infection, and alcohol-related liver disease (ALD), which has been estimated to be approximately 29%, 9%, and 2%, respectively (9). It is estimated that 400 million and 150 million of the world population is infected with HBV and HCV. Additionally, given the increasing global epidemic of non-hepatitis virus (non-B non-C; NBNC) including ALD and NAFLD, which results in more prevalence of CLD especially in moderate-income and high-income countries. Notably, NAFLD is strongly associated with metabolic syndrome. According to alteration of individual environmental modifiers (diet, lifestyle, and gut microbiota), metabolic syndrome such as obesity, diabetes, and hypertension is increasing lead to more prevalence of NAFLD.

2.2. Nonalcoholic fatty liver disease (NAFLD)

NAFLD is the crucial cause of liver disease, accounting for the third-most common cause of cancer-related death worldwide and seventh-most common cause in the United States. Even though highly prevalence of NAFLD worldwide, as estimated at 24%, South America shows the highest rate (31%). The prevalence of NAFLD in the Asia population is 27% as determined by a meta-analysis from terms involving epidemiology and progression of NAFLD from 1989 to 2015 (10). NAFLD is a spectrum of chronic liver disorder characterized by excessive accumulation of triglyceride in hepatocytes that subsequently develop into liver injury and fibrosis (11, 12). The

condition ranges from only isolated fatty liver or hepatic steatosis called nonalcoholic fatty liver (NAFL) to a more severe step, hepatic triglyceride accumulation plus inflammation and hepatocyte injury known as nonalcoholic steatohepatitis (NASH). Patients with NASH may develop fibrosis and finally to cirrhosis and/or HCC (Figure 1). The disease progression is dynamic which steatosis and NASH are typically reversible. The frequency of transition from NASH to early fibrosis (F1-F3) is higher than the reverse step from fibrosis to NASH, which is 34–42% and 18–22%, respectively. However, NAFL and NASH may ultimately progress to HCC with or without the association of cirrhosis, accounting for 2.4% to 12.8% (13).

Insulin resistance plays a critical role in NAFLD pathogenesis (14). In adipose tissue, impaired insulin sensitivity leads to the over transportation of free fatty acids to the liver (15). The disrupted metabolic homeostasis and inflammation, induced by phosphorylated activation of the stress-activated c-Jun NH₂-terminal kinases (JNKs) in adipose tissue, macrophages, and liver promote NAFLD to NASH (16). Taken together, lipotoxicity and inflammation generate oxidative and endoplasmic reticulum (ER) stress, causing hepatocellular damage and apoptosis. Consequently, disease progression is the result of immune cell infiltration, fibrogenesis, and activation of hepatic progenitor cells (HSCs) (17).

The role of chronic inflammation, caused by obesity and metabolic syndrome, in contributing to the progression of NAFLD and NASH leading to HCC formation has been extensively explored. Inflammatory cells and cytokines, typically originating from the innate immune systems, induce hepatic inflammation through the activation of apoptosis signaling kinase-1(ASK-1)–JNK, RAS–RAF–MAPK (MAP kinases), extracellular signal-regulated kinases (ERK), and nuclear factor- κ B (NF- κ B). Recent studies conducted in mice have revealed that long-term feeding of a choline-deficient high-fat diet results in the activation of intrahepatic CD8⁺ T cells,

natural killer T (NKT) cells, and inflammatory cytokines, thereby facilitating the transition from NASH to-HCC via NF- κ B signaling (18). Furthermore, the significance of Kupffer cells, the resident macrophages in the liver, in initiating liver inflammation and contributing to the progression of NAFLD has been demonstrated. The secretion of profibrotic cytokines, such as transforming growth factor- β (TGF β) and platelet-derived growth factor (PDGF), by Kupffer cells leads to immune infiltration, activation of HSCs, and subsequent liver damage (19).

2.3. Risk factors for NAFLD and NASH

NAFLD is strongly associated with metabolic syndromes. Diseases including obesity, type 2 diabetes mellitus (T2DM), dyslipidaemia, insulin resistance, and hypertension, are the main variables in the development of NAFLD. As the global prevalence of these diseases continues to rise, the rate of NAFLD is increasing (20). Among these risk disorders, obesity is considered a key factor that drives NAFLD, especially in an American population. Additionally, individuals who are overweight in childhood and adolescence tend to develop NAFLD. However, some NAFLD patients are nonobese, termed “lean NAFLD”, which is often found more frequently in Asian countries than in Western countries. High-fructose and/or high-fat diet, genetic factors, and drug-related are known as the causes of patients with lean NAFLD (20).

Genetic modifiers are common risk factors in the presence of NAFLD. Single-nucleotide polymorphisms (SNPs) have been found to promote NAFLD and contribute to advanced fibrosis. The importance of gene variants, such as those in the the patatin-like phospholipase domain containing 3 (PNPLA3; rs738409) and transmembrane 6 superfamily member 2 (TM6SF2; rs58542926), has been shown as strongly linked with NAFLD in a large cohort (21, 22). It was found that PNPLA3 variant (23), and insulin resistance (24, 25) significantly affect lean NAFLD.

Notably, environmental modifiers, such as a western diet or a sedentary lifestyle leading to increased weight and obesity, are considered essential causes of NAFLD. Dietary habits involving high-caloric, high fructose, and high-sodium consumptions seem to confer susceptibility to progressive NAFLD. Indeed, individuals with sedentary lifestyles with high sitting times and low physical activity levels, trend to have NAFLD later in life (26).

2.4. Non-hepatitis B-, non-hepatitis C-related HCC (NBNC-HCC)

While chronic viral hepatitis has traditionally posed a significant risk for HCC, there is a rising number of cases attributed to non-hepatitis B, non-hepatitis C-related HCC (NBNC-HCC). This shift is linked to the increasing prevalence of NAFLD. The prevalence of NBNC -HCC is 14.1% (27). Patients with NBNC -HCC are accompanied by metabolic syndromes and strongly age-related disease. NAFLD is an emerging cause of NASH, cirrhosis, and progress to HCC. Nonetheless, the progression of HCC in NASH is often found in the absence of cirrhosis, accounting for up to 25–46% of all NBNC -HCC cases, so it is incidentally detected or undiagnosed (28). The patients are more likely to be diagnosed symptomatically or in the advanced stages (29). To be concern, early diagnosis of NBNC-HCC is recently needed. Moreover, the development of metabolic syndrome and the association of cardiovascular comorbidities are more prominently presented in patients with NBNC-HCC than in other aetiologies. Indeed, cardiovascular disease remains the most common cause of death in individuals with NAFLD, being two-fold more than in liver disease (30).

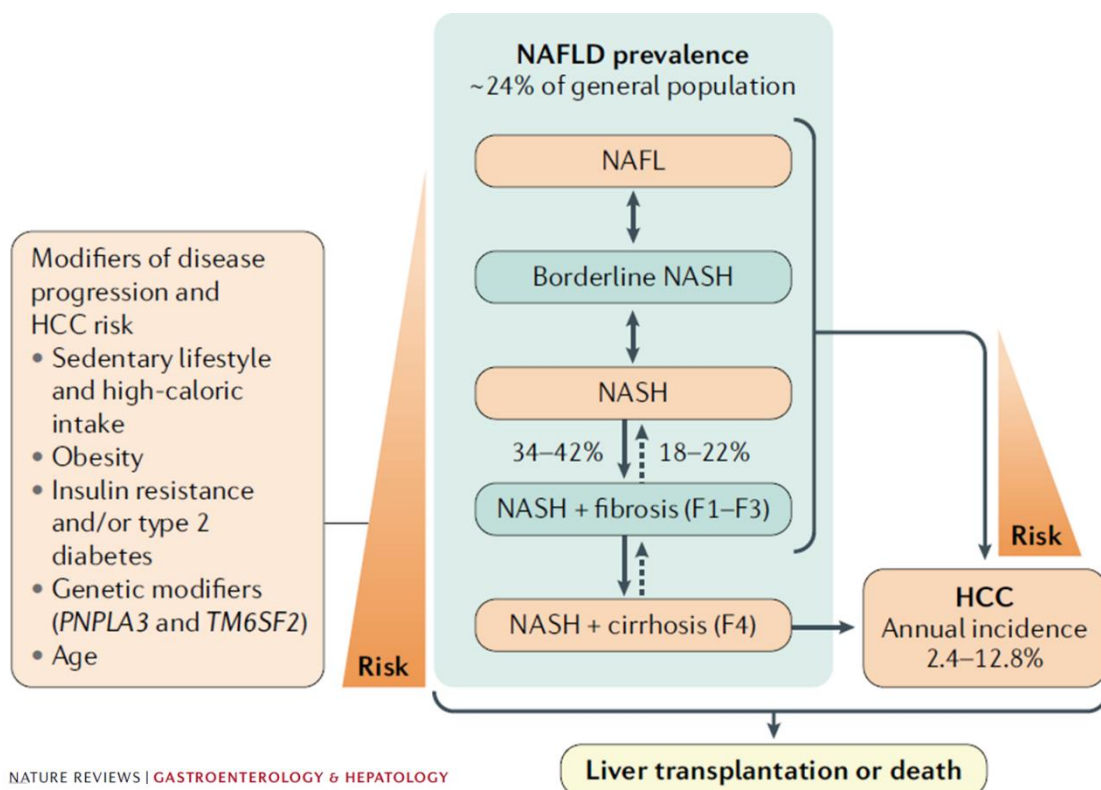


Figure 1 The pathophysiological states and risk factors of NAFLD and HCC (31).

2.5. Diagnostic tool and treatment for NAFLD, NASH, and HCC

To ascertain the presence of NAFLD in individuals, the most common diagnostic methods in the USA involve imaging or other indirect approaches, as indicated in a meta-analysis of worldwide prevalence of NAFLD in 2016 (10). A schema for diagnosing both NAFLD and NASH is depicted in Figure 2. Noninvasive tools, such as serum alanine aminotransferase (ALT) levels and liver ultrasonography imaging, are commonly employed for diagnosis. Reliable imaging methods, including ultrasound, computed tomography (CT), or magnetic resonance imaging (MRI), are used to assess hepatic steatosis in NAFLD. Ultrasound and CT can detect steatosis when it has $\geq 20\%$ of the liver mass, while MRI can identify as little as 5% of steatosis. Clinical prediction rules (CPRs), such as the NAFLD fibrosis score FIB-4 and elastography techniques, offer a dependable

means to determine liver stiffness and detect advanced fibrosis. However, for the diagnosis of NASH, serum ALT levels unfortunately exhibit poor sensitivity (< 50%) (32). Liver biopsy becomes necessary to define NASH through the classification of steatosis, hepatocellular ballooning, lobular inflammation, and varying degrees of fibrosis. Consequently, liver biopsy stands as the definitive technique for diagnosing and classifying NAFLD, as well as determining the presence of NASH. Despite the implementation of these diagnostic modalities, typical challenges hinder accurate diagnoses, including the fluctuation between NAFL and NASH over time, compensated cirrhosis, and asymptomatic with normal laboratory profiles. These challenges impede the diagnosis and estimation of a large population of patients.

While a liver biopsy remains the gold standard for diagnosing and confirming NAFLD and NASH, its routine application is hindered by several limitations. The procedure is invasive, contributing to patient anxiety and discomfort. Additionally, it carries the risk of bleeding and tumor seeding (33). Besides complicated operations, the cost of the procedure is high. Moreover, the sampling error is typically concerned especially in tumor heterogeneity of NAFLD-HCC (34). Therefore, noninvasive approaches such as imaging modalities and serum biomarkers are increasingly employed as alternative tools in diagnosis.

Radiological modalities have been employed for the assessment of NAFLD by detecting fat levels and fibrosis scores. Magnetic Resonance Imaging (MRI) directly measures the specific chemical structure, triglyceride, for quantifying fat in liver tissue. Despite its higher cost, MRI exhibits greater sensitivity compared to ultrasound and CT in this context. The quantification of steatosis relies on the Proton Density Fat Fraction (PDFF), which represents the fraction of MRI-visible protons bound to fat divided by all protons in the liver (bound to both fat and water) (35). On the other hand, fibrosis lacks a specified structure, and indirect methods are employed by measuring liver “stiffness” or “elasticity”. This stiffness arises from collagen deposition and

the rigidity of parenchyma, contributing to fibrosis. Ultrasound-based methods, specifically Controlled Attenuation Parameter (CAP) and Transient Elastography (TE), are utilized to assess liver steatosis and liver stiffness or fibrosis, respectively (36). Magnetic Resonance Elastography (MRE) emerges as the most accurate noninvasive approach for determining stiffness among imaging tests. However, limitations of these imaging modalities include high costs, limited availability, the requirement for expertise, and unreliable applicability for overweight patients with heterogeneous fatty livers (37). Thus, there is an ongoing need for more accessible noninvasive tools.

Remarkably, noninvasive biomarkers based on liquid biopsy methods, involving the determination of specific molecules in body fluids such as blood, have been widely developed. As mentioned above, elevated serum ALT levels can be detected with high sensitivity in NAFLD but not in NASH. The measurement of an increase in cytokeratin-18 (CK-18) in the circulation is found to be a marker of NASH in patients with NAFLD (38). Regarding HCC, an increase in serum alpha-fetoprotein (AFP) is the standard liquid biopsy, which is limited by restricted specificity and sensitivity; that is, some HCC patients have a low level of AFP in their serum (39). Recently, alterations in the expression level of circulating miRNA, and more recently, miRNA from extracellular vesicles, have been intensively investigated to be used as predictors in NAFLD and NASH. To date, there are no ideal clinical applications using these biomarkers. Main complications include difficulties in reproduction in patients due to low sensitivity and specificity, as well as the absence of a standard protocol to be followed, such as a lack of clear cut-off point and the unavailability of commercially clinical test kits (40).

Nowadays, there is a lack of approved drugs of effective treatments for patients with NAFLD, NASH, and fibrosis. Lifestyle modifications, such as dietary changes, exercise, and increased physical activity, are recommended as preventive or corrective measures for these

conditions (41). In the case of HCC patients, based on the Barcelona Clinic Liver Cancer (BCLC) classification, the therapeutic strategy is depended on the disease stages (42). For early-stage HCC (BCLC 0 or A), surgical resection is the primary option, and liver transplantation is the best first-line option for patients with BCLC A tumors. Patients in the intermediate stage (BCLC B) are deemed suitable candidates for chemoembolization, specifically in the form of transcatheter arterial chemoembolization (TACE) (43). Advanced-stage HCC (BCLC C) is addressed with Sorafenib, a multiple tyrosine kinase inhibitor (44). Conversely, in cases of end-stage disease (BCLC D), the focus shifts to supportive care. Therefore, early-stage disease allows for curative treatments, while palliative treatments are indicated for patients in intermediate and advanced stages. However, there currently exists no viable therapeutic option for those in the end-stage.

2.6. Extracellular vesicles (EVs)

Extracellular vesicles (EVs) are membrane-enclosed particles released by various types of cells into the bloodstream, including biological fluids. According to their size and biogenesis pathways, EVs can be typically classified into three main types: exosomes, microvesicles (also called microparticles), and apoptotic bodies. The characteristics of EVs are described in Table 1. The most widely studied are exosomes (50-150 nm), which are homogeneous populations with a cup-like morphology. The biogenesis pathway is initiated by invagination of the endosome membrane, production of a multivesicular endosome, and fusion with the cell membrane to release mature exosomes into the extracellular space (Figure 3). Whereas, microvesicles (100-1000 nm) form a more heterogeneous population, produced via direct outward blebbing of the plasma membrane. Despite differences in the generation processes, these pathways share common Endosomal Sorting Complexes Required for Transport (ESCRT) pathway for transport machinery. Both types of EVs are produced in response to pathophysiological stimuli, as well as hypoxia and inflammation. Recently finding indicate that exosomes and microvesicles overlap in

size (100-150 nm) and density (1.08-1.19 g/ml). Therefore, the International Society for Extracellular Vesicles (ISEV) suggests using the terms small EV (sEV) and large EV instead of exosomes and microvesicles, unless specific evidence supporting their biogenesis pathway is provided, such as through microscopic imaging (46). Another type of EVs, apoptotic bodies (500-2000 nm), is exclusively released through the process of apoptosis, involving caspase-mediated cleavage and subsequent activation of Rho-associated kinase I (6).

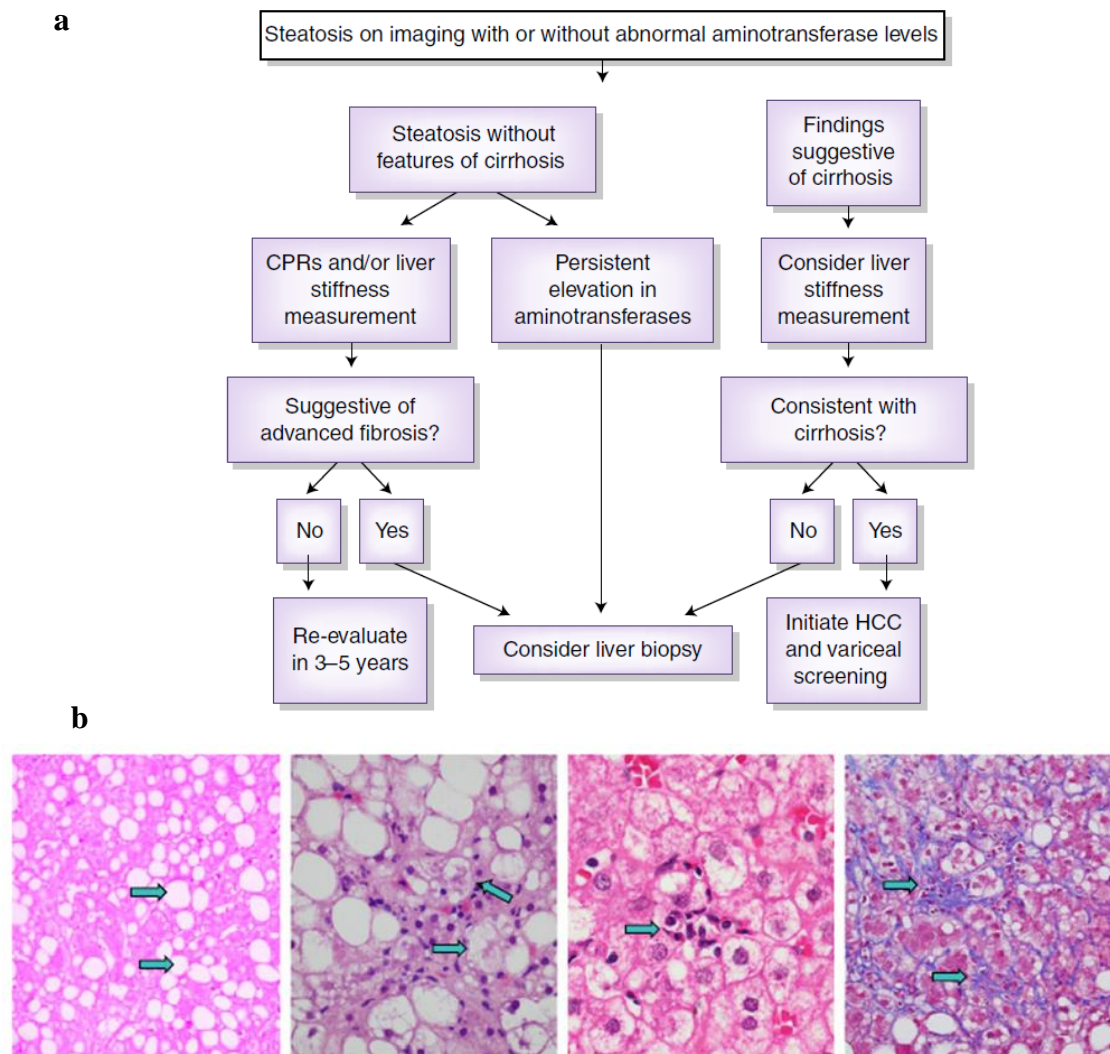


Figure 2 Histologic features of diagnosis of NAFLD and NASH. **(a)** schema diagram for diagnosing NAFLD and NASH. **(b)** liver biopsy images showing macrovesicular steatosis (fat), hepatocellular ballooning, lobular inflammation, and pericellular fibrosis (arrows) (45).

cup-like morphology. The biogenesis pathway is initiated by invagination of the endosome membrane, production of a multivesicular endosome, and fusion with the cell membrane to release mature exosomes into the extracellular space (Figure 3). Whereas, microvesicles (100-1000 nm) form a more heterogeneous population, produced via direct outward blebbing of the plasma membrane. Despite differences in the generation processes, these pathways share common Endosomal Sorting Complexes Required for Transport (ESCRT) pathway for transport machinery. Both types of EVs are produced in response to pathophysiological stimuli, as well as hypoxia and inflammation. Recently findings indicate that exosomes and microvesicles overlap in size (100-150 nm) and density (1.08-1.19 g/ml). Therefore, the International Society for Extracellular Vesicles (ISEV) suggests using the terms small EV (sEV) and large EV instead of exosomes and microvesicles, unless specific evidence supporting their biogenesis pathway is provided, such as through microscopic imaging (46). Another type of EVs, apoptotic bodies (500-2000 nm), is exclusively released through the process of apoptosis, involving caspase-mediated cleavage and subsequent activation of Rho-associated kinase I (6).

EV membrane serves a dual role by not only protecting its constituents from the circulating environment but also harboring specific membrane proteins that enable the traceability of these vesicles back to their parental cells. An illustrative example is evident in EVs secreted by the liver, where the presence of the asialoglycoprotein receptor 1 (ASGPR1) signifies the enrichment of hepatocyte-specific receptors (47). A diverse array of proteins enriched within EVs confers various functions. Noteworthy among these are transmembrane proteins such as tetraspanins (CD9, CD63, CD81, and CD82), which play pivotal roles in cell migration, cell-cell adhesion, and cellular signaling. The involvement of adhesion molecules, specifically integrins, facilitates EV trafficking through the extracellular matrix, guiding them to their targeted cells (48,

49). In addition, intracellular proteins, including heat shock proteins (Hsp70 and Hsp90), members of the Endosomal Sorting Complexes Required for Transport complexes (Tsg101, Alix), and proteins involved in membrane fusion (Rabs, ARF6), are intricately packaged into EVs during the biogenesis process. These proteins, serving as signaling molecules, contribute to the communication between different cell types. As such, EVs emerge as dynamic carriers of molecular cargo, orchestrating intricate cell-cell communication in a highly regulated manner.

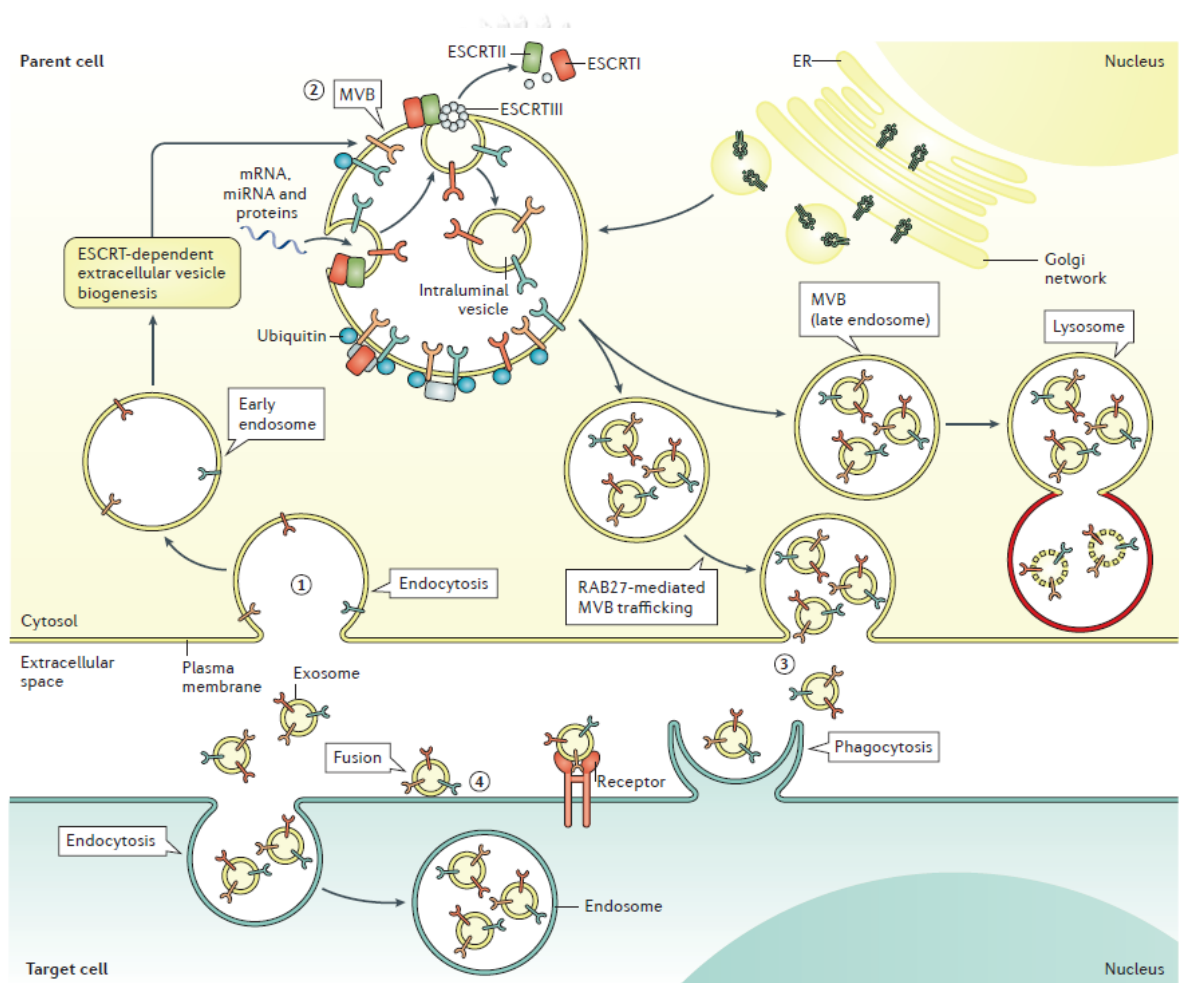


Figure 3 Extracellular vesicle biogenesis and release (50).

Table 1 Exosomes, microvesicles, and apoptotic Bodies: main characteristics, adapted from (6) and (51)

Characteristic	Exosome	Microvesicle	Apoptotic body
Size, nm	50–150	100–1000	500–2000*
Morphology	Cup-shaped	Heterogeneous	Heterogeneous
Origin	Multivesicular body (MVB)	Plasma membrane	Plasma membrane
Formation mechanisms	Exocytosis of MVB	Budding from plasma membrane	Budding from plasma membrane
Pathways	ESCRT-dependent Tetraspanin-dependent Ceramide-dependent	Ca ²⁺ dependent Stimuli- and cell-dependent (various pathways)	Apoptosis-related pathways
Timing of release	Ten minutes or more	A few tenths of a second	
Enriched protein marker	CD81, CD63, Alix, Tsg101	Selectins, integrin, CD40	Caspase 3, histones
Composition	Protein, lipids, coding RNA, noncoding RNA, DNA*	Protein, lipids, cell organelles, coding RNA, noncoding RNA, DNA*	Cell organelles, proteins, nuclear fractions, coding RNA, noncoding RNA, DNA

ESCRT indicates Endosomal Sorting Complexes Required for Transport; MVB, multivesicular body.

*Data that are controversial in the literature.

2.6.1. Role of EVs in liver diseases

The role of EVs to act as mediators of cell communication to modulate molecular pathways in the recipient cells by carrying and transferring proteins, DNA, and RNA, such as mRNA, miRNA, and lncRNA is rapidly interested. EVs are known to represent their cell origin, localization, and mechanism of secretion (7). The functions of the contents within EVs depend on various factors, including the cellular origin and physiological and pathological states. EVs have the capability to directly shuttle RNAs and transcription factors; indeed, they transmit a diverse array of miRNAs to regulate gene expression in recipient cells. For these reasons, EVs may serve as promising biomarkers of disease progression or therapeutic response.

2.6.2. Role of EVs as biomarkers

To identify specific proteins of hepatocyte-derived EVs as biomarkers for NAFLD/NASH diagnosis, EVs proteins from serum samples of healthy individuals, patients with pre-cirrhotic NASH, and patients with cirrhotic NASH were analyzed (52). It was found that the number of hepatocyte-specific markers in circulating EVs based on the asialoglycoprotein receptor 1 (ASGPR1), were significantly higher in patients with cirrhotic NASH who have the hepatic venous pressure gradient (HVPG) ≥ 10 mmHg than patients with HVPG less than 10 mmHg. This suggested that hepatocyte-specific EVs strongly correlate with clinical variables of NASH severity. The proteome profiles were examined using SOMAscan protein array revealed that the top seven most expressed circulating EV proteins, Wnt1-inducible signaling pathway protein-1 (WISP1), aminoacyl-tRNA synthetase interacting multifunctional protein 1 (AIMP1), interleukin-27RA (IL27RA), intercellular cell adhesion molecule 2 (ICAM2), interleukin-1 β (IL1 β), serine/threonine protein kinase (STK16), and repulsive guidance molecule A precursor (RGMA) were increased in pre-cirrhotic NASH samples versus healthy controls, cirrhotic NASH versus healthy controls, and

pre-cirrhotic NASH versus NASH. The results demonstrated that protein EV-based profiles may contribute to NASH diagnosis.

2.6.3. Role of EV-derived miRNAs as biomarkers

Several studies have demonstrated that EVs control the physiological phenotype of target cells through their ability to incorporate and transfer functional RNA, including miRNAs. miRNAs, short non-coding RNAs of approximately 21-22 nucleotides, are recognized as critical regulators of gene expression. Most miRNAs function by turning off gene expression or degrading mRNAs through binding to the 3' untranslated region (UTR) (53). Encapsulated miRNAs within EVs exhibit greater stability and long-term storage capabilities than free extracellular miRNAs, as they are protected from plasma ribonucleases by the EV membrane (54). The miRNAs incorporated in EVs not only reflect the status of parental cells but also signify the progression of diseases (55). In comparison to miRNAs extracted from the complex biofluid of blood, which contains molecules from various cell types, miRNAs derived from EVs are more specific and sensitive in targeting recipient cells. This specificity arises from EVs carrying cell-specific transmembrane proteins (47). Due to the reduced environmental complexity when compared to circulating miRNA and the enrichment of miRNA within EVs, miRNAs from EVs offer heightened sensitivity in detecting low-abundance molecules (56, 57). Thus, owing to these potential advantages, miRNAs derived from EVs are increasingly being considered as potential diagnostic, therapeutic, and prognostic factors for numerous diseases, as reviewed elsewhere (58, 59).

Previous studies have reported dysregulation of miRNAs in EVs in various diseases such as cardiovascular disease, cancers, lung diseases, and diseases of the kidney and liver. In the context of liver diseases, miRNAs in EVs have been widely investigated as non-invasive biomarkers. The specific changes in the expression levels of various miRNA species hold the potential to use in the detection, prediction of treatment response, and molecular monitoring of chronic liver

diseases and liver cancers. These miRNAs can access the early stages of the disease and correlate with clinical parameters such as tumor size, disease staging, overall survival, and disease recurrence. In recent years, there has been significant interest in the functional role of EV in liver physiology and pathology. Clear evidence has reported the EV-associated components in HCC from various factors including viral hepatitis, liver fibrosis, and alcoholic liver disease, as previously reviewed (60, 61). Regarding EVs as biomarkers in HCC, miRNAs emerge as the most promising molecule for the diagnosis and prognosis. For instance, miR-224 in EVs from the serum of HCC patients caused by HBV infection showed significantly higher than healthy controls, with an area under the ROC curve of 0.910 (62). Consistent with correlations with tumor size and stage, higher levels of miR-224 in serum EVs were found in HCC tumors with the size > 3 cm compared to those < 3 cm and the in stage III/IV compared to stage I/II patients. Increased expression of miR-224 in HCC patients was associated with a decrease in overall survival. To understand the mechanism of miRNA-224 in EVs in the development of HCC, two liver cancer cell lines, HepG2 and SKHEP1, were evaluated. After incubation of the cells with miR-224 mimic, higher cell proliferation compared to the control group was observed, whereas the lower cell proliferation was occurred upon adding miR-224 inhibitor. The work also demonstrated that miR-224 targeted glycine N-methyltransferase (GNMT) to promote the proliferation and invasion of liver cancer cells.

Recently, EV miRNA profiling panels have been identified as biomarkers for HCC. By selection of differentially expressed miRs in HCC tissue from previous published, EV miR panels capable of distinguishing among patients with HCC, liver cirrhosis (LC), and chronic hepatitis B (CHB) have been elucidated (63). Specifically, miR-18a, miR-221, miR-222, and miR-224 were significantly upregulated in patients with HCC compared to those with CHB or LC. Conversely,

miR-101, miR-106b, miR-122, and miR-195 were downregulated in HCC compared to CHB, with no significant difference in the levels of miR-21 and miR-93 among the three studied cohorts. The miRNA sequencing was used for profiling of miRNAs derived from EVs of fast- and slow-migrated HCC patient groups. The expression level of five miRNAs including miR-140-3p, miR-30d-5p, miR-29b-3p, miR-130b-3p, and miR-330-5p) was significantly higher, while one miRNA, miR-296-3p, was significantly lower in the fast-migrated group compared to the slow-migrated group. Further pathway analysis indicated that the ‘focal adhesion’ pathway was the target genes of the differentially expressed miRNAs, contributing to tumor metastasis. Additionally, three miRNAs, miR-30d, miR-140, and miR-29b, were significantly correlated with patient survival.

2.6.4. Role of EV in cellular communication in NAFLD

Since NAFLD may progress to NASH if liver injury and inflammation occurred, so the immune response plays a crucial role in this process. Neutrophil infiltration is important for the progression of NASH by producing reactive oxygen species and proinflammatory cytokines. miR-223 is highly expressed in neutrophils. A recent study exhibited both in *intro* and in high fat diet (HFD)-fed mice that miR-223 was transferred from neutrophils to hepatocytes through APOE on EV membrane and low-density lipoprotein receptor (LDLR), which abundance present on the hepatocyte surfaces (64). In *ldlr*-knock out mice hepatocytes with HFD-feeding, hepatic miR-223 was lower but the serum miR-223 and EV levels were significantly higher in these mice than in WT mice. More recently, a report showed that serum IL-6 and miR-223 in NAFLD or NASH were higher than in the healthy control serums. *In vivo*, *Il6* knockout (KO) and *Il6* receptor A (*Il6ra*) conditional KO mice that received HFD displayed a decrease in miR-223 expression as well as poor liver injury and fibrosis as determined by a higher level of fibrotic markers than wild-type mice. To mechanistically explain, myeloid-specific *Il6ra* KO mice have been shown to be decreased in miR-223 and increased in liver fibrosis in the HFD-fed group. RAW264.7 mouse

macrophages and human THP-1 monocytes were treated with IL-6 upon induction to fibrosis with or without palmitic acid (PA) and the level of miR-223 in EVs was measured. It was shown that the IL-6 and PA treatment groups exhibited the highest miR-223 in EVs compared to the others, resulting in the reduction of profibrotic in hepatocytes by inhibiting TAZ expression. This study suggested that IL-6 promoted macrophages to produce miR-223 via EVs to reduce fibrosis in hepatocytes.

2.6.4.1. Lipotoxicity and inflammation in NAFLD development

Lipotoxicity plays a critical role in the development of NAFLD. The excess release of free fatty acids (FFAs), which results from the overtransportation of FFAs from dysfunctional adipose tissue to the liver, leads to lipotoxicity. Also, NAFLD progression is driven by liver inflammation, and immune cells infiltration play an importance role in response of the pathophysiology of the disease. Nonetheless, the mediators of crosstalk linking these two scenarios remain elusive.

Since free fatty acid, which in turn metabolize to lysophosphatidylcholine (LPC) mediates lipotoxicity in hepatocytes. a saturated free fatty acid, palmitic acid (PA) (C16:0) have been widely used to induce lipid droplet accumulation resulting in lipotoxicity in NAFLD model (65). PA has been demonstrated to stimulate lipotoxic ER stress, resulting in the activation of sterol regulatory element-binding transcription factor 2 (SREBP2) and proprotein convertase subtilisin/kexin type 9 (PCSK9), a natural LDLR inhibitor (66-68). The elevation in PCSK9 levels resulted in the degradation of cell-surface LDLR in hepatocytes, leading to a reduction in LDL uptake and facilitating the development of NAFLD (68). Not only does palmitic acid (PA) stimulate lipid storage, but it also promotes the release of EVs from hepatocytes by triggering ER stress through the inositol-requiring protein 1a (IRE1a) pathway. PA induces the production of EVs enriched with C16:0 ceramide by activating IRE1 α , thereby stimulating the ceramide metabolite

sphingosine-1-phosphate (S1P). This activation results in the recruitment of macrophages to the liver in the presence of lipotoxic conditions. Also, elevated levels of C16:0 ceramide were observed in plasma EVs from patients with non-alcoholic steatohepatitis (NASH)(69). Additionally, in another study, PA was found to promote the release of EVs from hepatocytes by activating death receptor 5 (DR5), consequently fostering an inflammatory phenotype in macrophages (70).

NAFLD progression is driven by liver inflammation, and immune cells infiltration play an importance role in response of the pathophysiology of the disease. The majority of liver macrophages including liver-resident phagocytes, or Kupffer cells (KCs), and bone marrow-derived recruited monocytes. Kupffer cells (KCs) primarily control the macrophage population, serving as a "sentinel function" to control liver homeostasis. However, during acute or chronic injury, monocyte-derived macrophages become the predominant players, acting as the "emergency response team.", which trigger in both inflammatory and anti-inflammatory response depend on cellular stimuli (71-73). This shift presents an opportunity for innovative therapeutic strategies in liver disease. The depletion of macrophages had adverse effects on the resolution of liver disease, suggesting the role in tissue repair during liver injury (74, 75). Macrophages were found to transfer miRNAs, including miR-223, to HCC cell lines, inhibiting cell proliferation (76), and to have an impact on naive monocyte differentiation, as well as exhibiting functional activity in target cells, such as monocytes, endothelial cells, epithelial cells, and fibroblasts (77). The inhibition of liver fibrosis in NAFLD can be achieved through myeloid-specific IL-6 signaling, which stimulates the transfer of anti-fibrotic miR-223 from macrophages via EVs to hepatocytes (78).

2.6.4.2. EV receptor

To facilitate the effects of the molecules carried within EVs on the recipient's phenotype, EVs must fuse with target cell membranes. This fusion can occur either by directly merging with

the plasma membrane or through internalization into the cell via endocytosis. Various endocytic pathways are involved, including clathrin/caveolin-mediated endocytosis, macropinocytosis, phagocytosis, and lipid raft-regulated uptake. Different EVs may enter cells through multiple routes, potentially depending on the surface proteins present on both the vesicle and the target cell (79). In recipient cells, these specific mechanisms can vary based on the cell type. For example, neurons may employ clathrin-dependent endocytosis (80), epithelial cells may utilize caveolin-dependent endocytosis (81), and tumor cells may rely on lipid raft-dependent endocytosis (82). In the context of lipotoxic hepatocytes, a previous study in mice demonstrated that the selective uptake of miR-223-enriched EVs derived from neutrophils partially involves the low-density lipoprotein receptor (LDLR) (64).

LDLR is primarily expressed in the liver and plays a crucial role in the endocytosis of cholesterol-enriched LDL, contributing to the elimination of approximately 70% of circulating LDL. The receptor is bound by proprotein convertase subtilisin/kexin type-9 (PCSK9), which then directs lysosomal degradation of the receptor in cells, resulting in increases blood cholesterol. Importantly, PCSK9 is also abundantly produced by hepatocytes. By inhibiting the degradation of LDLR, PCSK9 inhibitors such as alirocumab can effectively reduce circulating LDL cholesterol levels (83, 84).

CHAPTER 3

MATERIALS AND METHODS

3.1. Research subjects and participant consent

Blood samples for the assessment of EV-miRNAs were obtained from patients with NBNC-HCC who were followed-up at King Chulalongkorn Memorial Hospital (Bangkok, Thailand). All patients enrolled in this study were seronegative for HBsAg and anti-HCV, had no significant alcohol consumption (defined as > 20 g ethanol/day in males and >10 g ethanol/day in females) and no coexisting causes of other chronic liver disease such as autoimmune hepatitis, primary biliary cholangitis and Wilson's disease. HCC was diagnosed on the basis of typical findings on imaging studies and/or histopathology according to the American Association for the Study of Liver Diseases (AASLD) guideline (85). Briefly, diagnostic criteria with dynamic imaging were established by findings of focal lesions with hyper-attenuation at the arterial phase and hypo-attenuation at the portal phase. Liver biopsy or fine needle aspiration was performed in case of uncertain diagnosis by the imaging studies. Baseline clinical parameters were recorded, including tumor staging classified by the Barcelona Clinic Liver Cancer staging system (BCLC) (86). Blood and tissue samples were collected from patients prior to any HCC therapy, including liver resection, radiofrequency ablation (RFA) and transarterial chemoembolization (TACE). Moreover, the overall survival (OS) of patients with NBNC-HCC defined by the interval between initial assessment and death or the last follow-up visit was documented.

Patients with NAFLD, who had no evidence of HCC, as well as other liver disease, and seronegative for both HBsAg and anti-HCV, were included as a control group. The diagnosis of NAFLD was according to the American Association for the Study of Liver (AASLD) criteria as determined by controlled attenuation parameter (CAP) using FibroScan device (Echosens, Paris,

France), with the cut-off >248 dB/m (36, 87). Among this group of patients, current and past daily alcohol intake was less than 20 g/week and none of the patients received any steatogenic medication. Additionally, individuals who had no underlying disorders and had normal vibration-controlled transient elastography (VCTE) and CAP values were served as healthy controls. The study was conducted according to the Declaration of Helsinki. The protocol was approved by the Institutional Review Board (IRB) of Faculty of Medicine, Chulalongkorn University and all participants signed informed consent before collecting the samples.

3.2. Blood collection and plasma processing

Blood samples obtained from each subject were processed by centrifugation at 12,000 x g for 30 min at 4°C and then stored at -80°C until analysis for miRNA profile in the discovery cohort by NanoString® nCounter miRNA Expression Assay (NanoString Technologies, WA, USA) and the validation of miRNAs by quantitative Real-Time PCR (qRT-PCR, Applied Biosystems, MA, USA) technique.

3.3. Cell culture and differentiation

Human hepatoma cell line, Huh7, was cultured in Dulbecco's Modified Eagle Medium (DMEM) (Gibco) with 10% heat-inactivated fetal bovine serum (FBS) (Gibco), 100 U/mL penicillin-streptomycin (Gibco), 2 mM L-glutamine (Gibco) at 37°C in 5% CO₂. Macrophages were differentiated from human peripheral blood mononuclear cells (PBMCs) using macrophage colony-stimulating factor (M-CSF). PBMCs were isolated from human blood using Ficoll and differentiated into macrophages in the RPMI basal medium containing 20% human serum (GeminiBio, CA, USA), 50 µg/ml M-CSF (PeproTech, NJ, USA), 100 U/mL penicillin, 100 µg/mL streptomycin, 2 mM L-glutamine, 10 mM HEPES buffer, 0.1 mM pyruvate, for 7 days with half-change media on day 4. On day 8, the differentiated cells were transfected with Cy3-labeled

miRNA-223 mimic (Horizon, Cambridge, UK) using lipofectamine RNAiMAX reagent (ThermoFisher Scientific). Cy3-labeled miR Negative Control (ThermoFisher Scientific, MA, USA), Cy3 dye-only, Cy3-labeled miRNA-223 mimic without lipofectamine RNAiMAX, and Cy3 dye without lipofectamine RNAiMAX were served as controls. After 12 hours of transfection, the cells were washed twice with PBS and cultured in medium containing exosome-depleted FBS (Gibco, ThermoFisher Scientific, MA, USA) for 24 hours. Cy3 red fluorescence on macrophages was visualized under a fluorescence microscope, and miR-223 expression in the cells and EVs was measured by qPCR.

3.4. EV isolation

From plasma samples, EVs were extracted using the ExoQuick™ Exosome Isolation Kit (SBI, System Biosciences, CA, USA) according to the manufacturer's protocol. Briefly, for collecting the clear supernatant of plasma, 1 mL of the samples were incubated for 5 min with 8 μ L of thrombin (final concentration of 5U/mL) before centrifugation at 10,000 rpm for 5 min at 4°C. Next, 250 μ L of ExoQuick™ was added and incubated at 4°C for 30 min. The mixture of ExoQuick™-plasma samples were centrifuged to precipitate EVs at 1,500 \times g for 30 min. The pellet was then resuspended in 0.22 μ m-filtered 1x PBS and stored at -80°C until further use. For the validation, 200 μ L of plasma samples were used.

From conditioned medium of macrophages, EVs were separated following a previously described protocol (88). Briefly, the medium was centrifugation at 2000 \times g for 20 min at 4°C to remove cell debris. The medium was then concentrated for 15-20 min at 4000 \times g using Amicon 15 Ultra RC 10 kDa filters (Millipore Sigma, Darmstadt, Germany). The concentrate was loaded onto a qEVoriginal 70 nm size-exclusion chromatography (SEC) column (Izon, MA, USA) and eluted with Dulbecco's phosphate buffered saline (DPBS) (Gibco). After discarding the void

volume, 0.5 mL fractions were collected. Fractions 1–4, which were enriched in EVs, were pooled and concentrated once more using Amicon 2 Ultra RC 10 kDa filters (Millipore Sigma).

3.5. EV characterization

3.5.1. Nanoparticle tracking analysis (NTA)

To characterize EVs from plasma, the quantity and size distribution of EVs in plasma samples were carried out using the NTA (NanoSight NS300, ATA Scientific, Taren Point NSW 2229, Australia). EVs were diluted 1000-fold for detecting between 50 and 100 particles per frame. Three 40-s videos were recorded with screen gain 3 and camera level 9 followed by an analysis of the data using NanoSight software (NTA 3.4 Build 3.4.003) with screen gain 9 and detection threshold 3.

3.5.2 Nano flow cytometry measurement (NFCM)

Particle distribution, concentration, and size of EVs were determined using NFCM Flow NanoAnalyzer (NanoFCM, China) according to the manufacturer's instructions and as previously described (89). Briefly, laser calibration was employed for particle concentration using fluorescent 250 nm silica nanoparticles at a concentration of 2.19×10^{10} (NanoFCM) and for size using a premixed silica nanosphere cocktail containing monodisperse nanoparticle populations of 68 nm, 91 nm, 113 nm, and 155 nm in diameter (NanoFCM). The blank for background correction was DPBS. EV samples were diluted in DPBS to obtain an event rate between 1,500 and 10,000 events/min. The resulting side-scattering signal was then quantified using the NanoFCM Professional Suite V2.0 software.

3.5.3. Transmission electron microscopy (TEM)

To characterize the morphology and size of EVs, 5 μ L drop of the suspension was loaded onto a 400 mesh formvar/carbon-coated grid (Electron Microscopy Sciences, USA). To enhance the contrast between EVs and background, grids were negatively stained with 2.5% uranyl acetate

for 5 min. The excessive stain was blotted, and the grid was dried. Images were visualized under a transmission electron microscope using JEM-1400plus TEM (JEOL, Tokyo, Japan) at 80 kV.

3.5.4. Immunoblotting analysis

To detect EV protein markers by immunoblotting, EV samples were lysed using RIPA buffer with Proteinase and Phosphatase Inhibitor Cocktail (Merck, NJ, USA). The lysates were sonicated with 7 sets of 3-s pulses using Sonics Vibra-Cell™ (Sonics & Materials, CT, USA). EV proteins (10 µg) were measured using Pierce™ BCA Protein Assay Kit (ThermoFisher Scientific, MA, USA) and loaded onto sodium dodecyl polyacrylamide gel electrophoresis (SDS-PAGE). The proteins were then transferred to nitrocellulose membranes, blocked for 1 hour with 5% BSA, and incubated at 4°C overnight with primary antibodies against TSG101 (1:1,000) (Ab83, 4A10) (Abcam, MA, USA), HSP70 (1:1,000) (4876, D69, Cell signaling), CD63 (1:2,000) (Ab193349, MX-49.129.5, Abcam), CD9 (1:1000, #312102, Biolegend), CD63 (1:1000, #556016, BD Biosciences); or calnexin (1:1000, ab22595, Abcam).. To identify hepatocyte-specific marker, ASGPR1 (1:1,000) (SC-52623, 8D7, Santa Cruz) was used (47, 52). Following this process, the membrane was stained with HRP-conjugated secondary antibodies mouse-IgGk-BP-HRP (sc-516102, SantaCruz) or mouse-anti-rabbit-IgG-HRP (sc-2357, SantaCruz) (1:10,000) for 1 hour at RT. Antigen-antibody reactions were visualized with an enhanced chemiluminescence detection reagent and images were acquired using a ChemiDoc Imaging System (Bio-Rad Laboratories, CA, USA).

3.6. Co-culture between lipotoxic hepatocytes and macrophages

A 0.4 µm polycarbonate transwell plate (Corning) was used for co-culture between macrophages and lipotoxic Huh7 hepatocytes. Macrophages were differentiated on the transwell insert and Huh7 cells were seeded on the lower well. Before co-culture, macrophages were

transfected with Cy3-miR-223 mimic for 12 hours and Huh7 cells were pretreated with 400 μM PA for 24 hours. The co-culture was then performed for another 12 hours.

To inhibit EV secretion, 20 μM GW4869 (Sigma) was used. Macrophages were pretreated with GW4869 for 24 hr, followed by co-culture with Huh7 cells in the continued presence of GW4869 for an additional 12 hours.

3.7. Induction of lipotoxicity in hepatocytes

Palmitic acid (PA) was used as a source of free fatty acids to induce lipotoxicity condition in hepatocytes. PA was prepared from sodium palmitate (Sigma, NJ, USA) and conjugated with bovine serum albumin (BSA) according to a previously described protocol. (88). Huh7 hepatocytes were treated with 400 μM PA for 24 hours, as this concentration corresponds to the range of fasting total free fatty acid plasma concentrations found in NASH patients (90). Stored lipid droplet in the cells was stained with the fluorescent neutral lipid dye 4,4-difluoro-1,3,5,7,8-pentamethyl-4-bora-3a,4a-diaza-s-indacene (BODIPY) and evaluated under a fluorescence microscope.

3.8. NanoString miRNA expression analysis

Before applying to NanoString analysis, miRNA was concentrated and minimized contamination using an Amicon Ultra YM-3 filter (Merck Millipore, NJ, USA). Briefly, 320 μL of RNase-free water was added to the isolated miRNA, loaded onto the filter, and centrifuged at 14,000 $\times g$ at 25 $^{\circ}\text{C}$ for 90 min. Three μL of the concentrated miRNAs were subjected to human NanoString nCounter miRNA expression assay (NanoString Technologies, WA, USA) using the nCounter Human miRNA Panel v3 that evaluated 800 miRNAs according to the manufacturer's instructions. In brief, miRNAs were hybridized to capture and reporter probes at 65 $^{\circ}\text{C}$ for 18 hours, followed by purification and quantification on the nCounter Prep Station and Digital Analyzer.

The resulting data were analyzed by the nSolver 4.0 software to obtain the count of individual miRNA. The miRNA data were calculated by normalization to the top 100 miRNA counts in each sample.

3.9. EV and tissue miRNA extraction

To extract miRNA from EVs, isolated EVs from the above-mentioned method was extracted using miRNeasy Serum/Plasma Kit (Qiagen, Hilden, Germany). For miRNA extraction from tissues, approximately 30 µg of the liver tissue were used and the miRNAs were extracted using RNeasy Fibrous Tissue Kit (Qiagen), according to the manufacturer's recommendations. The quantity and quality of miRNA were measured using the DeNovix DS-11 Spectrophotometer (DeNovix, DE, USA).

3.10. Real-Time Quantitative Reverse Transcription PCR (qRT-PCR)

The miRNAs were reverse transcribed to complementary DNA (cDNA) by SL-poly (A) sequence: GTCGTATCCAGTGCAGGGTCCGAGGTATTTCGCACTGGATACGACAAAAAAAAAAAAAAAAAAVN using RevertAid First Strand cDNA Synthesis Kit (ThermoFisher Scientific). qRT-PCR were performed in duplicate using the QPCR Green Master Mix HRox 4x (Biotechrabbit, Hennigsdorf, Germany). The reactions were detected by a QuantStudio 5 Real-Time PCR System (Applied Biosystems, MA, USA). Reaction with no cDNA template was run as a negative control on every plate for each assay. Thermal cycling parameters were started with activation step at 95°C for 10 min, followed by 40 cycles of denaturation at 95°C for 15 s, and extension at 72°C for 20 s with optimal annealing temperatures of each gene for 15 s. Primer sequences are listed in Table 2.

Four internal control miRNAs including U6, miR-26a-5p, miR-3144-3p and miR-302d-3p from NanoString data were used to normalize the miRNA expressions. The results indicated that in the validation set of samples (n=10 for healthy controls, n=10 for NAFLD, and n =9 for NBNC-HCC), all four miRNAs showed a similar Ct value, 29.92±1.10, 28.06±1.21, 31.987±1.03, and

29.46±1.17 for U6, miR-26a-5p, miR-3144-3p, and miR-302d-3p, respectively (Figure 4). However, miR-3144-3p and U6 exhibited the lowest % cv of 3.23 and 3.69 compared to miR-26a-5p, and miR-302d-3p (4.30 and 3.98, respectively). In this respect, it was suggested that the expression of miR-3144-3p and U6 were the most constant in our sample set. Thus, these miRNAs were suitable for normalization in the validated samples and data were calculated by the $2^{-\Delta\Delta CT}$ method.

3.11. EV uptake assay

The isolated EVs from macrophages were labeled with 200 nM MemGlow 488 fluorescence dye at room temperature (RT) for 30 minutes. PBS incubated with MemGlow 488 was used as a control. Excess dye was removed using Amicon 2 Ultra RC 10 kDa filters. MemGlow 488-labeled EVs were then monitored for MemGlow 488 positive EVs and concentration using nanoflow. A concentration of 4×10^8 particles/mL of MemGlow 488-labeled EVs was used. For EV lysis, the same concentration of EVs were treated with 0.5% Triton X-100 at RT for 15 min. The labeled-EVs were incubated with lipotoxic hepatocytes for 45 minutes at 37°C. The cells were subsequently washed twice with PBS and fixed with 4% paraformaldehyde in PBS for 20 minutes at RT. Nuclei were stained with DAPI, and images were acquired using a confocal microscope.

3.12. Immunofluorescence staining

Cells were first fixed with 4% paraformaldehyde for 15 min at RT, then permeabilized with 0.1% Triton X-100 for 5 min and blocked with 3% BSA for 1 hour at RT. Following this, the cells were subjected to staining with a primary antibody against LDLR (diluted at 1:200, ab30532, Abcam) overnight at 4°C. After thorough washing, Alexa Fluor-conjugated antibody (Goat anti-Rabbit IgG (H+L) Alexa Fluor Plus 555, 1:2000, A32732, Thermo Fisher Scientific), was applied for 1

hour at RT in the dark. Nuclei were counterstained using DAPI (Thermo Fisher Scientific), and fluorescence images were captured using a confocal microscope.

3.13. Flow cytometry

Cells were resuspended in a 100 μ L of cell staining buffer (BioLegend) and stained with a fluorescently conjugated primary antibody: LDLR-APC (1:10, FAB2148A, R and D System), and LIVE/DEAD™ Fixable Near-IR Dead Cell Stain Kit (1:1000, Thermo Fisher Scientific) was added to assess cell viability. The mixture was incubated for 30 min at 4°C followed by washing with cell staining buffer. The stained cells were then directly measured using a BD LSR Fortessa flow cytometer and analyzed using the FlowJo V10.8 Software.

3.14. Statistical analysis

Data were analyzed by SPSS statistics version 22 (SPSS Inc., Chicago, IL) and graph visualizations were constructed using GraphPad Prism 8.0 (GraphPad Software, CA, USA). To compare between groups, Chi's square or Fisher's exact test were applied for categorical variables and Student's t-test or one-way ANOVA were used for quantitative variables. The diagnostic performance was evaluated using receiver operating characteristic (ROC) curve and the area under the curve (AUC) with sensitivity and specificity analysis. The Kaplan-Meier analysis and log-rank test were calculated for the survival analysis. In addition, the Cox regression was applied for identifying independent factors associated with overall survival of patients with NBNC-HCC. A P -value<0.05 was considered statistically significant.

Table 2 Sequences of primers used for qRT-PCR analysis

Sequence	Sequence 5'-3'	Tm (°C)
miR-451a	AAACCGTTACCATTACTGAGTT	52
miR-223-3p	TGTCAGTTTGTCAAATACCCCA	55
miR-19-3p	TGTGCAAATCCATGCAAACTGA	57
miR-16-5p	TAGCAGCACGTAAATATTGGCG	57
miR-30d-5p	TGTAAACATCCCCGACTGGAAG	58
miR-216b-5p	AAATCTCTGCAGGCAAATGTGA	56
miR-765	TGGAGGAGAAGGAAGGTGATG	57
miR-105-5p	TCAAATGCTCAGACTCCTGTGGT	60
miR-608	AGGGGTGGTGTGGGACAGCTCCGT	71
U6	CTCGCTTCGGCAGCACA	58
miR-3144-3p	ATATACCTGTTCGGTCTCTTA	51
miR-302d-3p	TAAGTGCTTCCATGTTTGAGTGT	55
miR-26a-5p	TTCAAGTAATCCAGGATAGGCT	54

CHAPTER 4

RESULTS

4.1. Part I Circulating extracellular vesicle-derived microRNAs as novel diagnostic and prognostic biomarkers for non-viral-related hepatocellular carcinoma

4.1.1. Characteristics of the participants

To construct miRNA profiling in the discovery set, 9 plasma samples per group of NBNC-HCC, NAFLD and healthy controls were analyzed by the NanoString miRNA assay. Moreover, the quantitative levels of candidate miRNAs were validated by qRT-PCR in the plasma samples of 35 healthy controls, 70 patients with NAFLD, and 70 patients with NBNC-HCC. Baseline characteristics of the participants in the validated cohort are shown in Table 3.

4.1.2. Characterization of EVs

To characterize EVs isolated from plasma samples (Figure 5a), the size and concentration of EVs were first determined by nanoparticle tracking analysis (NTA). As expected, the average size of particles in overall samples was 162.9 ± 22.1 nm in diameter (Figure 5b-c). The concentrations of isolated EVs from healthy controls were similar to the NAFLD group ($5.40 \times 10^{11} \pm 2.39 \times 10^{11}$ and $6.12 \times 10^{11} \pm 3.59 \times 10^{11}$ particles/mL, respectively; Figure 5d), whereas the lowest concentration of EVs ($3.41 \times 10^{11} \pm 2.15 \times 10^{11}$ particles/mL) was found in samples from patients with NBNC-HCC. To verify the EV markers, Western blot analysis was then performed. Our results showed that the EV-enriched proteins, including CD63, HSP70, and TSG101 were expressed in isolated EV samples. Hepatocyte-specific receptor or asialoglycoprotein receptor 1 (ASGPR1) was also identified to verify that the isolated EVs were partially hepatocyte-derived EVs (Figure 5e). In addition, the particle diameter and the morphology were confirmed and visualized by

transmission electron microscopy (TEM). These vesicles were less than 200 nm in size, with a lipid bilayer, indicating that they were EVs as described previously (91) (Figure 5f). We next evaluated whether the isolated EVs provided intra-vesicular miRNAs. Our results were in line with previous data demonstrating that there was no statistically significant difference between C_t values of miRNAs (such as miR-26a-5p, miR-223-3p, and let-7a-5p) in EVs treated with RNase and without RNase-A (Figure 6a-c) (92, 93). Together, these results indicated that our protocol could specifically identify EV-miRNAs, in accordance with previous data (91), thus we did not perform RNase-A treatment for the subsequent experiments.

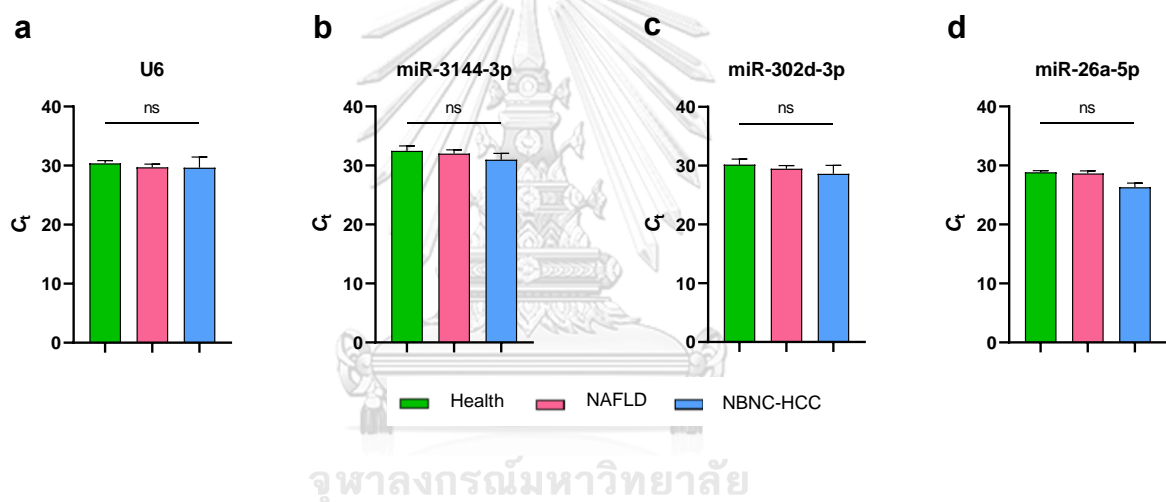


Figure 4 qRT-PCR analysis of candidate internal controls in the study cohort. Plasma EVs of healthy controls (n = 10), NAFLD (n = 10), and NBNC-HCC (n = 9). Data are presented as means \pm S.D.; ns = not significant.

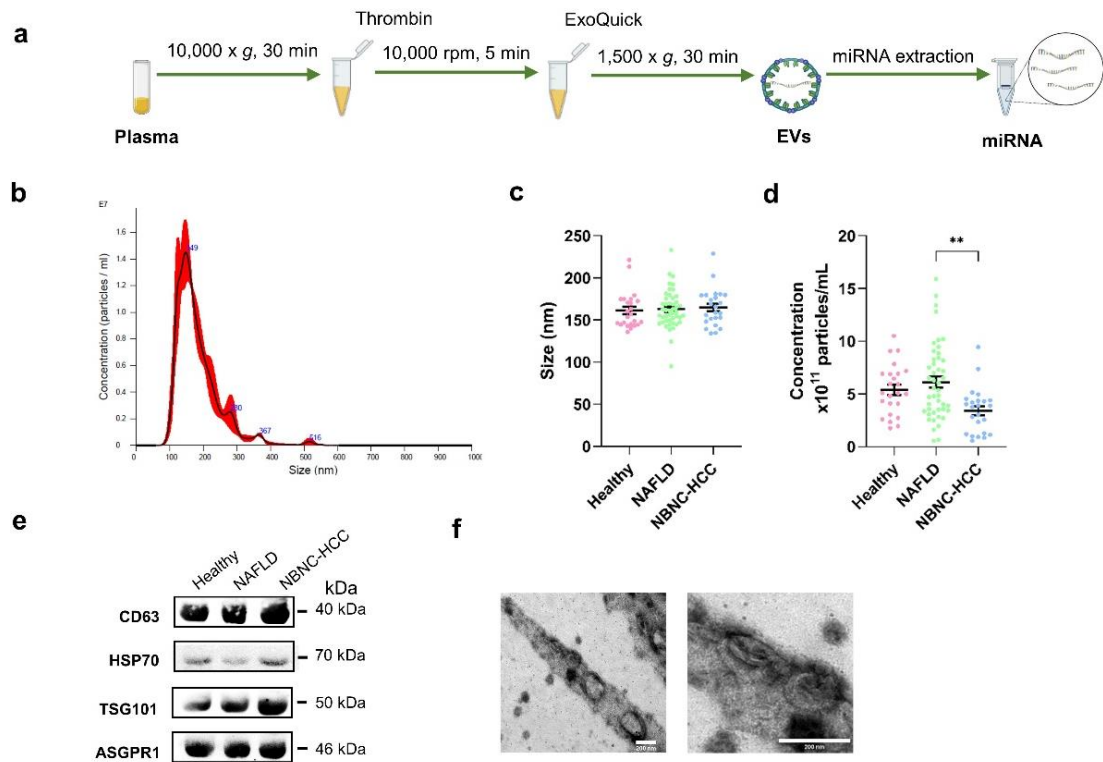


Figure 5 Schematic diagram of the study protocol and characterization of EVs derived from plasma. (a) Diagram of plasma EV isolation protocol. (b) Representative nanoparticle tracking plot for size distribution from a sample. (c) Quantification of particle size diameter (nm) and (d) concentration (particles/ml) of plasma EVs from the healthy controls, NAFLD, and NBNC-HCC groups. (e) Expression of EV markers, CD63, HSP70, and TSG101, and hepatocyte-specific receptor, ASGPR1 by Western blotting. (f) Transmission electron microscopy images of EVs from a sample. Scale bars, 200 μm . Data are presented as means \pm S.E.M, **P < 0.01.

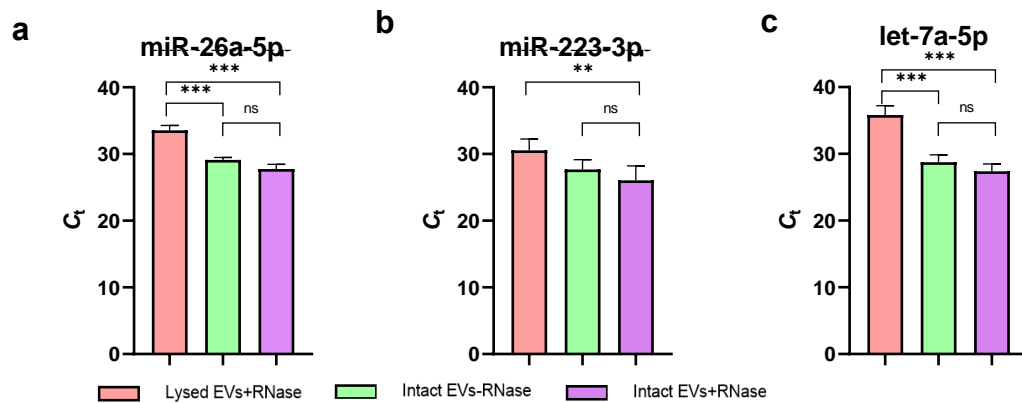


Figure 6 qRT-PCR analysis of EV miRNAs. (a) miR-26a-5p, (b) miR-223-3p, and (c) let-7a-5p upon RNase A treatment of lysed EVs and intact EVs with or without RNase A. Data are presented as means \pm S.E.M of 5 independent samples; ns = not significant, ** $P < 0.01$, and *** $P < 0.001$.

4.1.3. Profiling of EV-derived microRNAs

To explore the profiles of EV-miRNAs, we performed the expression of 800 miRNAs using NanoString platform (nCounter Human v3 miRNA expression assay) on the discovery set of patients with NBNC-HCC, NAFLD, and healthy controls. Raw and normalized NanoString microarray data were submitted to the Gene Expression Omnibus (GEO) (accession number: GSE244605, <https://www.ncbi.nlm.nih.gov/geo/query/acc.cgi?acc=GSE244605>).

Based on differentially expressed miRNAs between groups (\log_2 -fold change (FC) and $P < 0.05$), we found 66 significant differentially-expressed miRNAs (DEmiRNAs) in patients with NBNC-HCC vs. NAFLD, which included 39 up- and 27 downregulated miRNAs (Figure 7a), 73 DEmiRNAs between patients with NBNC-HCC vs. healthy controls, including 36 up- and 36 downregulated miRNAs (Figure 7b). The data of DEmiRNAs between patients with NAFLD and healthy controls are available in Figure 7c. Among the significantly upregulated miRNAs, Venn diagram showed that five miRNAs, including miR-19-3p, miR-16-5p, miR-223-3p, miR-30d-5p, and miR-451a overlapped

between NBNC-HCC vs. NAFLD and NBNC-HCC vs. healthy controls (Figure 8). Accordingly, these five upregulated miRNAs were subsequently selected for further validation.

4.1.4. Functional gene annotation and pathway enrichment analysis

Gene Ontology (GO) and gProfiler analysis were performed to reveal enrichment of potential target genes of the significantly expressed miRNAs. The top 10 GO categories for the differentially upregulated miRNAs and downregulated miRNAs are demonstrated in Figure 9 and Figure 10 ($P < 0.05$), respectively. These significantly up-regulated and downregulated miRNAs were involved in several biological processes, such as protein targeting and transport, nuclear transport, and cell cycle. Regarding molecular function analysis, these miRNAs were found to be

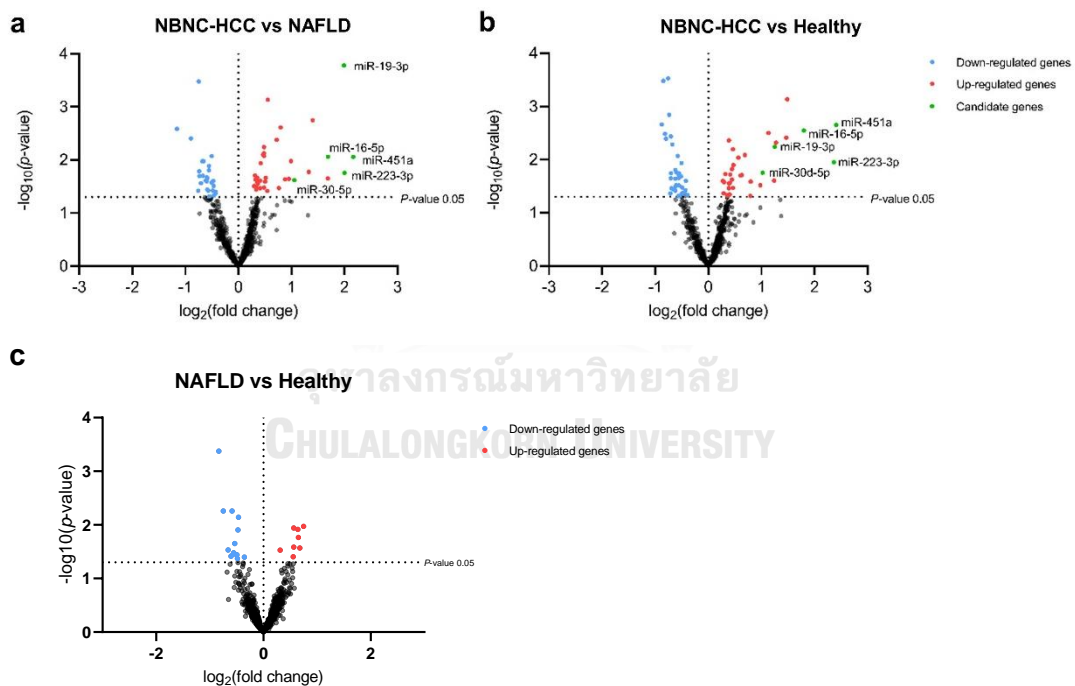


Figure 7 Transcriptome profiling of miRNAs from plasma EVs using NanoString microarray.(a) Volcano plot of all differentially expressed miRNAs in the NBNC-HCC samples compared with the NAFLD samples and (b) the NBNC-HCC samples compared with healthy controls. The significantly up-regulated and down-regulated miRNAs are marked in red and blue dots, respectively.

Table 3 Baseline characteristic of the validation cohort in this study

Baseline Characteristics	Healthy	Patients with	Patients with NBNC-	<i>P</i>
	controls (n=35)	NAFLD (n=70)	HCC (n=70)	
Age (years)	53.2±5.3	50.7±9.5	68.8±11.4	<0.001
Gender (Male)	4 (11.4)	30 (42.9)	54 (77.1)	<0.001
Body mass index (kg/m ²)	22.8±2.6	26.9±4.1	24.3±4.2	<0.001
Presence of metabolic syndrome		33 (47.1)	50 (71.4)	0.006
Total bilirubin (mg/dL)		0.7±0.6	0.8±0.5	0.845
Serum albumin (g/dL)		4.0±0.7	3.6±0.5	<0.001*
Aspartate aminotransferase (IU/L)		24.5±6.8	34.5±17.9	<0.001*
Alanine aminotransferase (IU/L)		42.9±42.8	60.8±79.0	0.134
Alkaline phosphatase (IU/L)		81.4±45.2	146.7±171.3	<0.001*
Platelet count (10 ⁹ /L)		225.4±92.3	216.0±104.7	0.157
Alpha fetoprotein (ng/mL)		3.0±2.9	3423.3±12469.8	0.025*
Controlled attenuation parameter (dB/m)	196.5±23.6	304.0±42.9	-	<0.001*
Transient Elastography (kPa)	3.8±0.8	6.1±1.7	-	<0.001*
BCLC stage (0-A/B/C)		-	25(35.7)/27(38.6)/18(25.7)	-

Data shown as mean ± SD, BCLC; Barcelona Clinic Liver Cancer, **P* < 0.05

enriched in nucleotide, ATP, and enzyme binding. Furthermore, Kyoto Encyclopedia of Genes and Genomes (KEGG) pathways indicated that the significantly upregulated miRNAs participated in pathways in cancer, similar to those with downregulated miRNAs.

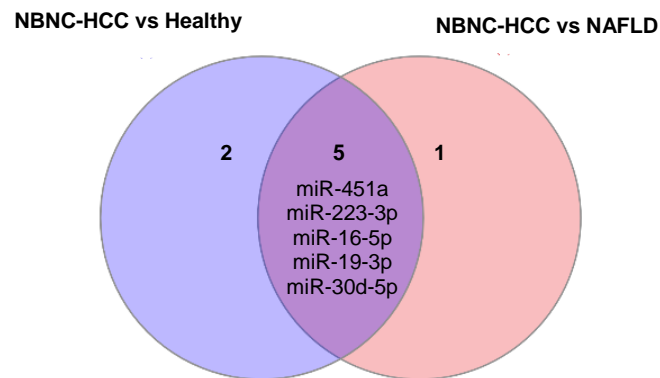


Figure 8 Venn diagram of intersect genes of miRNA profiling. miRNAs with fold change values more than 2.0 and showed a significant increase ($P < 0.05$) when pairwise comparison between NBNC-HCC and NAFLD, and NBNC-HCC and healthy controls were shown.

4.1.5. Plasma EV-miRNA expression in the validation set

To validate the above-mentioned five upregulated candidate miRNAs, plasma EV-miRNAs from a total of 175 participants, including 35 healthy controls, 70 patients with NAFLD and 70 patients with NBNC-HCC were evaluated by qRT-PCR using miR-3144-3p normalization. The results showed that all miR-19-3p, miR-16-5p, miR-223-3p, miR-30d-5p, and miR-451a expression levels were significantly higher in patients with NBNC-HCC compared with healthy controls (Figure 11a-e). When compared with the NAFLD group, the expression levels of miR-19-3p, miR-16-5p, miR-30d-5p, and miR-451a were significantly increased in the NBNC-HCC group (Figure 11a-e). Moreover, similar results of miRNA expression levels were found upon normalization with U6 (Figure 12a-e), suggesting the consistent results of the validated miRNAs across various internal controls. Overall, these findings indicated that plasma EV-miRNAs could effectively distinguish the NBNC-HCC from non-HCC groups.



Figure 9 Gene Ontology (GO) analysis of the differentially upregulated EV miRNAs. Top 10 significantly enriched GO terms of biological process, molecular function, and KEGG pathways ($P < 0.05$).

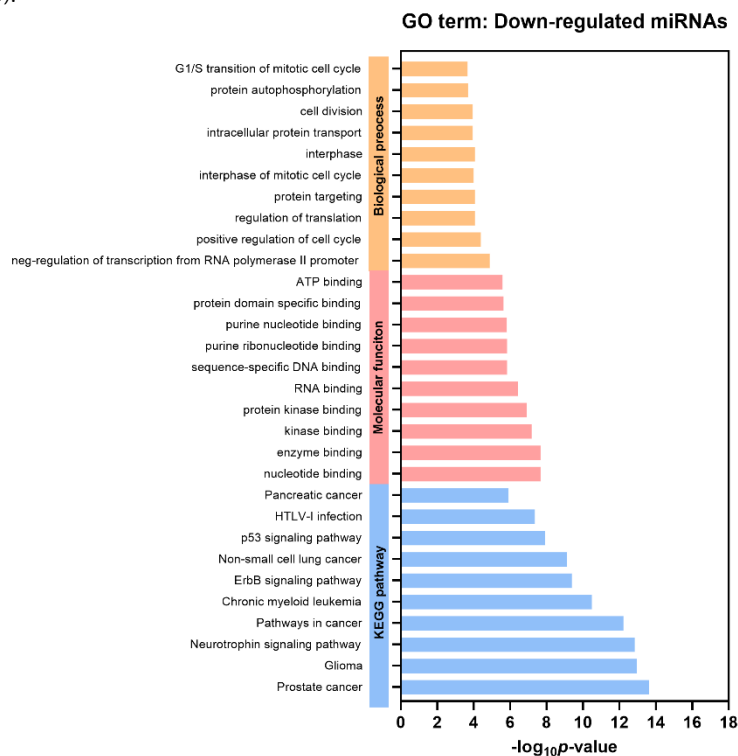


Figure 10 Gene Ontology (GO) analysis of the differentially downregulated EV miRNAs. Top 10 significantly enriched GO terms of biological process, molecular function, and KEGG pathways ($P < 0.05$).

To access the concordance expression of EV miRNAs in plasma and tissues. Besides plasma EVs, we also investigated their expression levels in paired tumors tissues and adjacent tissues (n=11 pairs of tissues) using qRT-PCR. Among candidate miRNAs, only miR-19-3p differed significantly between the HCC tumor tissue and adjacent tissue samples, 18.76 ± 33.31 vs 1.00 ± 0.94 ($P = 0.042$) (Figure 13a). While there was no significant difference in the levels of miR-16-5p (0.63 ± 0.54 vs. 1.00 ± 0.91 , $P = 0.700$), miR-223-3p (1.05 ± 1.31 vs. 1.00 ± 0.79 , $P = 0.465$), miR-30d-5p (0.62 ± 1.26 vs. 1.00 ± 1.49 , $P = 0.175$), and miR-451a (0.31 ± 0.46 vs. 1.00 ± 1.35 , $P = 0.148$) (Figure 13b-e). In summary, these findings suggested that the expression of plasma miR-19-3p was related with its expression in paired-tumor tissue.

4.1.6. Diagnostic role of plasma EV-miRNAs

To evaluate the diagnostic performance of biomarkers in distinguishing between the NBNC-HCC and non-HCC groups, the ROC curves were analyzed (Figure 14a). The area under the curve (AUC) was 0.82 (95 % confidence interval (CI); 0.75-0.88, $P < 0.001$) for miR-19-3p, 0.74 (95 % CI; 0.67-0.82, $P < 0.001$) for miR-16-5p, 0.65 (95 % CI; 0.56-0.73, $P = 0.001$) for miR-223-3p, 0.72 (95 % CI; 0.64-0.80, $P < 0.001$) for miR-30d-5p, 0.70 (95 % CI; 0.61-0.78, $P < 0.001$) for miR451a and 0.83 (95 % CI; 0.76-0.89, $P < 0.001$) for AFP.

In addition, the ROC curve for combination of all EV-miRNAs were also examined. Our results showed that multiple miRNAs did not provide a better AUC than miR-19-3p alone. However, combined miR-19-3p and AFP increased the performance for the diagnosis of HCC compared with miR-19-3p alone. The cut-off value and diagnostic performance of each EV-miRNAs, AFP, and the combination of miR-19-3p and AFP is shown in Figure 14b.

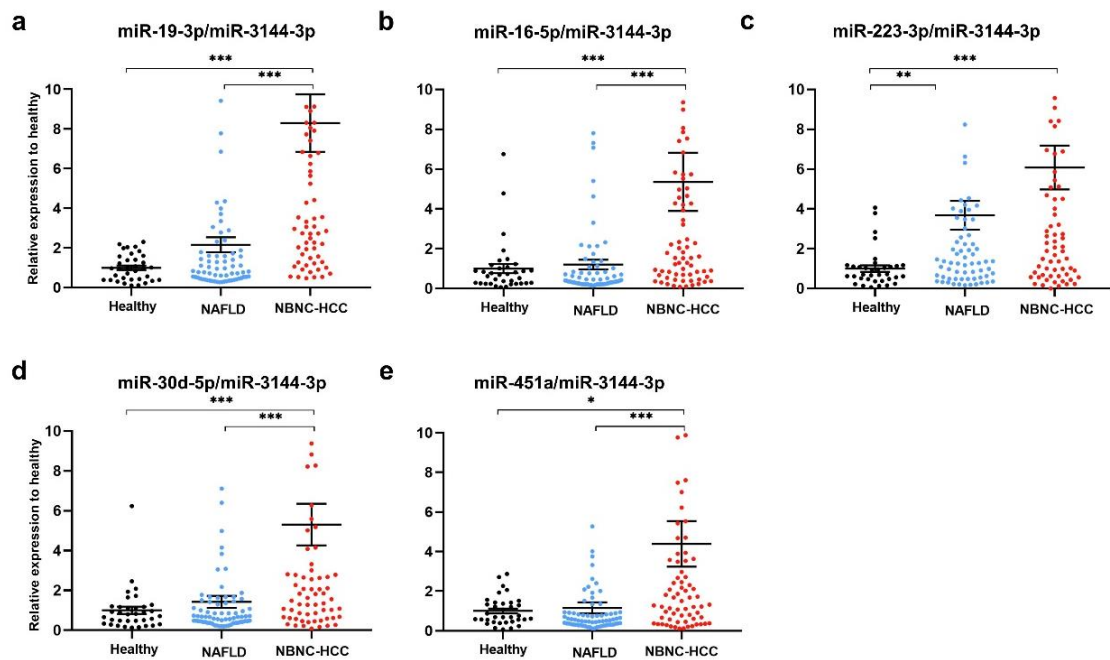


Figure 11 Validation of candidate miRNAs in plasma EV using qRT-PCR. The relative expressions of (a) miR-19-3p, (b) miR-16-5p, (c) miR-223-3p, (d) miR-30d-5p and (e) miR-451a in plasma EVs of healthy controls (n = 35), patients with NAFLD (n = 70), and patients with NBNC-HCC (n = 70). Data are presented as mean \pm S.E.M., normalized with a reference miRNA, miR-3144-3p, and expressed relative to those of healthy controls. * P < 0.05, **P < 0.01 and *** P < 0.001.

If categorized based on the normal upper limit of AFP (20 ng/mL), there were 39 (55.7%) and 31(44.3%) HCC patients with AFP-negative and AFP-positive, respectively. In the AFP-negative group, 76.9% (30/39) of HCC patients had elevated circulating miR-19-3p level (≥ 1.9), while the AFP-positive group, high expression of miR-19-3p was found in 71.0% (22/31). Among early HCC cases (BCLC stage 0 and A), we found that 36.0% (9/25) patients had elevated AFP level, while 80.0% (20/25) patients had high miR-19-3p expression. Together, these results might indicate that circulating EV-miR-19-3p was a promising biomarker for detecting AFP-negative HCC and early HCC, as well as a complementary to AFP in diagnosis of NBNC-HCC in our cohort.

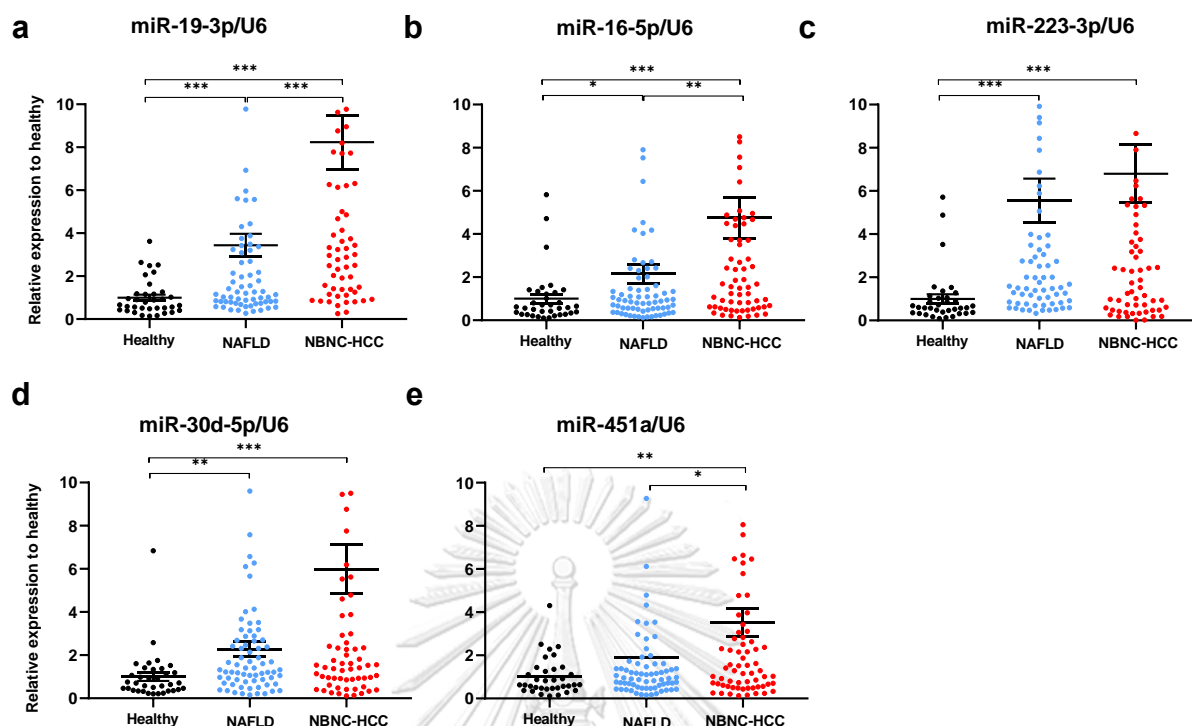


Figure 12 Validation of candidate miRNAs in plasma EV using qRT-PCR. The relative expressions of (a) miR-19-3p, (b) miR-16-5p, (c) miR-223-3p, (d) miR-30d-5p and (e) miR-451a in plasma EVs of healthy controls (n = 35), patients with NAFLD (n = 70), and patients with NBNC-HCC (n = 70). Data are presented as mean ± S.E.M., normalized with a reference gene, U6, and expressed relative to those of healthy controls. * P < 0.05, **P < 0.01 and *** P < 0.001.

4.1.7. Prognostic role of plasma EV-miRNAs regarding overall survival

Apart from its diagnostic value, we further examined the potential prognostic role of plasma EV-miR-19-3p in patients with NBNC-HCC. Using the median value as the cut-off level (3.5), the median overall survival of patients with miR-19-3p <3.5 and ≥3.5 were 38.2 and 22.3 months, respectively (P = 0.05 by log rank test) (Figure 15a). For plasma EV- miR-16-5p, the median overall survival of HCC patients with low (<1.9) was significantly better than that of patients whose levels were elevated (35.7 vs. 23.1 months, P = 0.026) (Figure 15b). However, there was no significant difference in overall survival regarding the circulating levels of other EV-miRNAs, including miR-223-3p, miR-30d-5p, and miR-451a.

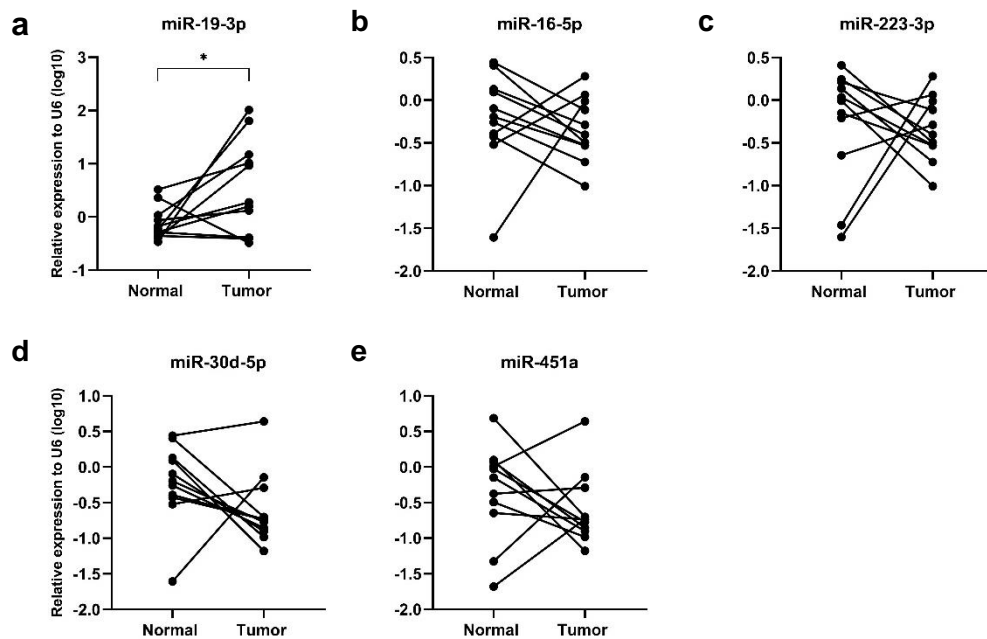


Figure 13 Expression of candidate miRNAs in tumor and adjacent non-tumor liver tissue samples using qRT-PCR. The expressions of (a) miR-19-3p, (b) miR-16-5p, (c) miR-223-3p, (d) miR-30d-5p, and (e) miR-451a in paired tumor tissue samples ($n = 11$ pairs), normalized with a reference gene, U6. Data were analyzed using paired Student's t-test.

All 5 plasma EV-miRNAs were entered into the multivariate analysis together with other parameters that could influence overall survival of patients with NBNC-HCC. These variables included age, gender, serum TB, albumin, AST, ALT, platelet counts, AFP level, tumor size and BCLC stage. The multivariate analysis based on the Cox regression analysis demonstrated that miR-19-3p, AFP and BCLC stage were independent predictive factors for overall survival. However, miR-16-5p was not selected as a parameter associated with overall survival (Table 4).

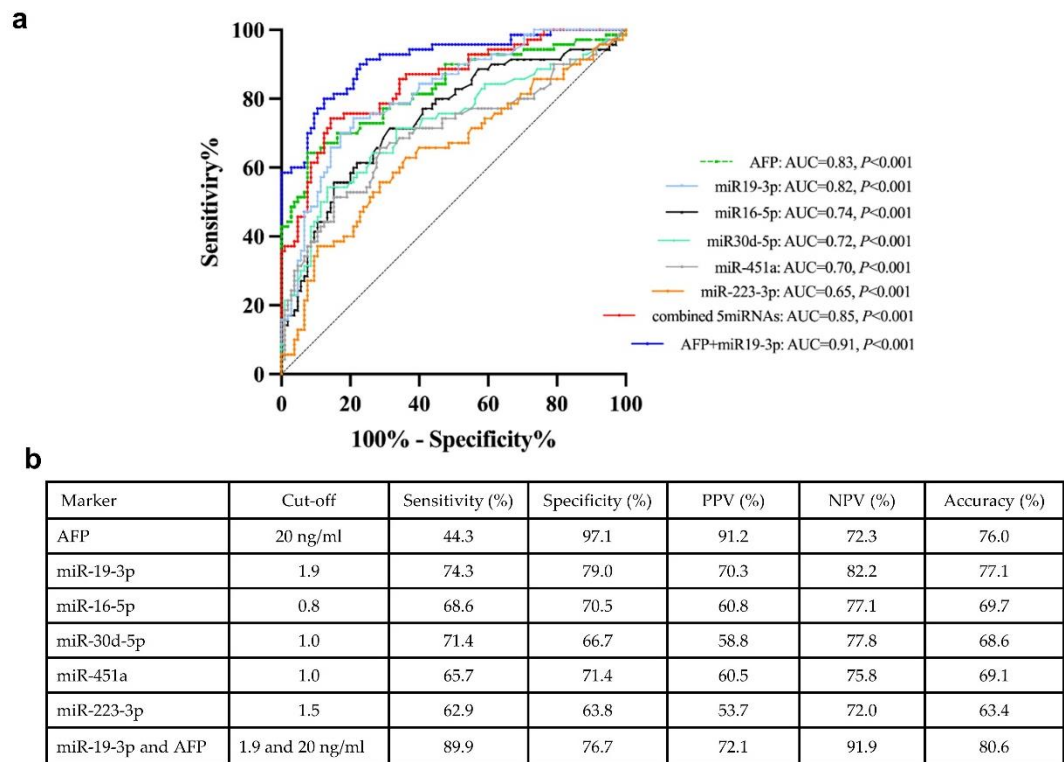


Figure 14 Receiver operating characteristic (ROC) curves of the candidate miRNAs for distinguishing between NBNC-HCC and non-HCC. (a) The area under the curve (AUC) and (b) the cut-off value and the discriminatory performance of each EV-miRNAs.

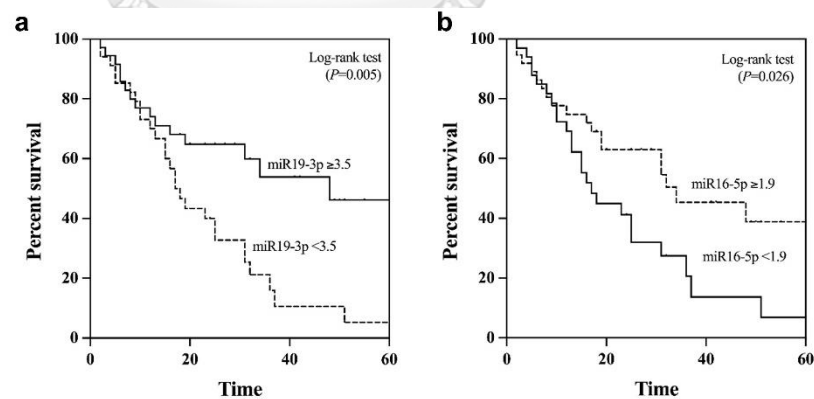
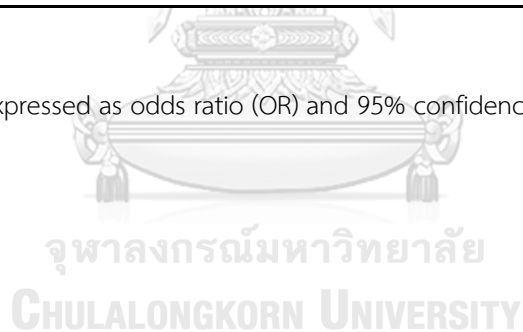


Figure 15 Kaplan–Meier survival curves for overall survival analysis of patients with NBNC-HCC. (a) plasma EV-miR-19-3p and (b) plasma EV-miR-16-5p.

Table 4 Variables associated with overall survival in patients with HCC.

Variables	Category	Overall survival			
		Univariate analysis		Multivariate analysis	
		OR (95%CI)	P	OR (95%CI)	P
Age (years)	< 60 vs. ≥ 60	0.62 (0.28-1.41)	0.254		
Gender	Male vs. Female	0.67 (0.32-1.42)	0.295		
Total bilirubin (mg/dL)	< 1.2 vs. ≥ 1.2	0.77 (0.49-1.27)	0.303		
Serum albumin (g/dL)	< 3.5 vs. ≥ 3.5	0.97 (0.46-2.04)	0.931		
Aspartate aminotransferase (IU/L)	< 55 vs. ≥ 55	1.64 (1.83-3.23)	0.153		
Alanine aminotransferase (IU/L)	< 50 vs. ≥ 50	1.00 (0.42-2.39)	0.998		
Platelet count (10 ⁹ /L)	≥ 100 vs. <100	1.05 (0.37-2.97)	0.927		
Alpha fetoprotein (ng/mL)	< 100 vs. ≥ 100	2.09 (1.08-4.08)	0.029*	2.04 (1.01-4.13)	0.048*
Tumor size (cm.)	< 5.0 vs. ≥ 5.0	1.63 (0.88-3.04)	0.123		
BCLC stage	0-A vs. B vs. C	2.15 (1.38-3.36)	0.001*	2.07 (1.29-3.32)	0.002*
EV-miR-19-3p	< 3.5 vs. ≥ 3.5	2.39 (1.26-4.52)	0.008*	2.71 (1.19-6.19)	0.018*
EV-miR-16-5p	< 1.9 vs. ≥ 1.9	1.98 (1.07-3.69)	0.030*	0.97 (0.44-2.13)	0.944
EV-miR-30d-5p	< 2.0 vs. ≥ 2.0	1.56 (0.83-2.93)	0.171		
EV-miR-451a	< 1.7 vs. ≥ 1.7	1.74 (0.94-3.23)	0.078		
EV-miR-223-3p	< 2.5 vs. ≥ 2.5	1.71 (0.92-3.19)	0.091		

Data were expressed as odds ratio (OR) and 95% confidence intervals (CI). * $P < 0.05$



4.2. Part II Macrophages release miRNA-enriched extracellular vesicles that are taken up by lipotoxic hepatocytes

4.2.1 miR-223 expression in transfected macrophages

Macrophages are cells of greatest interest in liver injury since they are recruited to the liver during lipotoxicity (94). Moreover, suppression of macrophage activation, recruitment, or accumulation in the liver resulting in elevation of steatohepatitis (88). In our study, we differentiated PBMCs to macrophages using human serum and M-CSF and observed the typical "fried egg" morphology of granulocyte-macrophage colony stimulating factor (GM-CSF) type macrophages (Figure 16) (95). Base on previous studies demonstrated that hepatocytes do not basically expressed miR-223 but the cells receive miR-223 from immune cells (96). We examined the expression of miR-223 in macrophages and Huh7 cells. The result revealed a prominent level of miR-223 expression in macrophages but not in Huh7 cells (Figure 17). We hypothesized that miR-223 are carried by EVs from macrophages to hepatocytes. To evaluate possible transfer of macrophage EVs containing miR-223 to hepatocytes, we transfected macrophages with a Cy3-miR-223 mimic conjugated with Cy3 fluorescence dye. As shown in Figure 18a, we found Cy3 fluorescence dye in macrophages after transfection with Cy3-miR-223 mimic but not in controls. We quantified the expression of miR-223 in the transfected macrophage cells using qPCR, revealing a dose-dependent increase in miR-223 levels. (Figure 18b).

4.2.2. miR-223 in macrophage-derived EVs.

To investigate whether Cy3-miR-223 mimic transfected macrophages release EVs containing the mimic, we subjected the conditioned media to EV isolation using size exclusion chromatography. Twelve fractions were collected and pooled to combined EV fraction (F1-4),

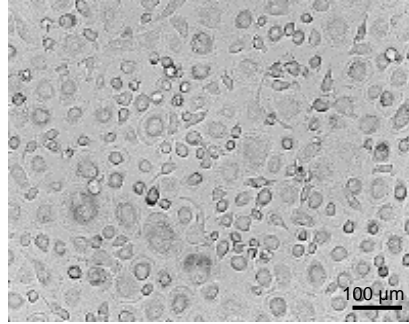


Figure 16 Differentiated macrophages from PBMCs. Phase-contrast image shows the morphology of macrophages after differentiation of PBMCs using M-CSF for 7 days. Bar = 100 μm .

intermediate fraction (F5-8), and non-EV fraction (F9-12). These fractions were characterized by several methods to meet the MISEV criteria (46). To elucidate EV markers, Western blot for CD63, CD9, and a cellular marker, calnexin was conducted (Figure 19a). The EV markers, CD63 and CD9 were mainly detected in the EV fraction, with no presence in the intermediate and non-EV fractions. A small calnexin protein band was observed in the combined EV fraction (F1-4), indicating minimal contamination from other cellular compartments. Nanoflow cytometry was employed to analyze the combined EV fraction (F1-4) to determine particle distribution (Figure 19b), concentration (Figure 19c), and diameter (Figure 19d). The concentration of EVs varied between conditions, ranging from 1×10^8 to 1×10^9 particles/mL, while the average diameter remained consistent at 70 nm. To observe the morphology of EVs, transmission electron microscopy (TEM) was used (Figure 19e). As expected, a cup-shaped EV population with a size of less than 100 nm was predominantly found in the combined EV fraction.

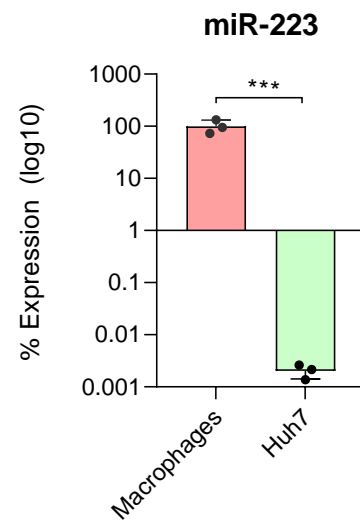


Figure 17 miR-223 in macrophages and Huh7 hepatocyte cell line by qRT-PCR.

To ascertain the presence of Cy3-miR-223 within the isolated fraction, miR-223 in EVs and non-EV fractions was measured by qPCR (Figure 20). The highest miR-223 expression level was found in EV fraction, some levels in the intermediate fraction, and undetectable in non-EV fraction, indicating miR-223 are mainly carried by EVs.

4.2.3. miR-223 in lipotoxic hepatocytes after co-culture with macrophages

To investigate the delivery of miR-223 mimic from macrophages to NAFLD hepatocytes, several experiments were conducted. First, Huh7 hepatocytes were induced to lipotoxicity, a hallmark of NAFLD, using free fatty acid, palmitic acid (PA). The stored lipid droplets were subsequently stained with the fluorescent neutral lipid dye 4,4-difluoro-1,3,5,7,8-pentamethyl-4-bora-3a,4a-diaza-s-indacene (BODIPY) (Figure 21). Then, the co-culture between Cy3-miR-223 mimic transfected macrophages and lipotoxic hepatocytes was performed using a transwell system by differentiation of PBMCs to macrophages on the transwell insert. Huh7 cells were seeded on the lower well and pretreated with 400 μ M PA for 24 hours before being co-cultured with transfected macrophages for another 24 hours. Second, Cy3 red fluorescence in Huh7 was observed under a fluorescence microscope, indicating the transfected macrophages transferred

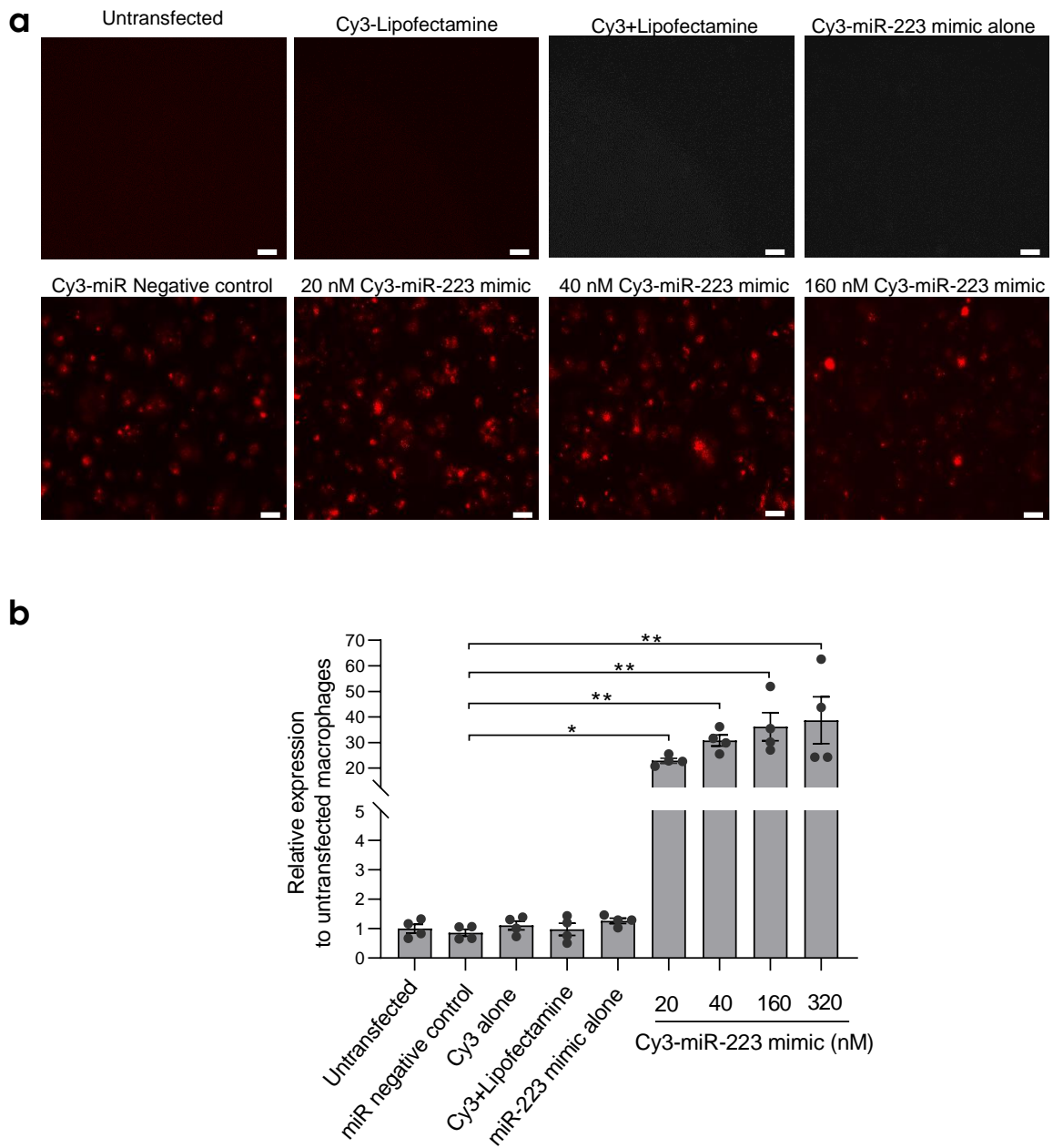


Figure 18 Cy3 fluorescence dye in macrophages after transfection with Cy3-miR-223 mimic. (a) Representative immunofluorescence image of Cy3 and (b) expression of miR-223 in transfected macrophages by qRT-PCR. Scale bars, 100 μ m. Data are presented as means \pm SEM.

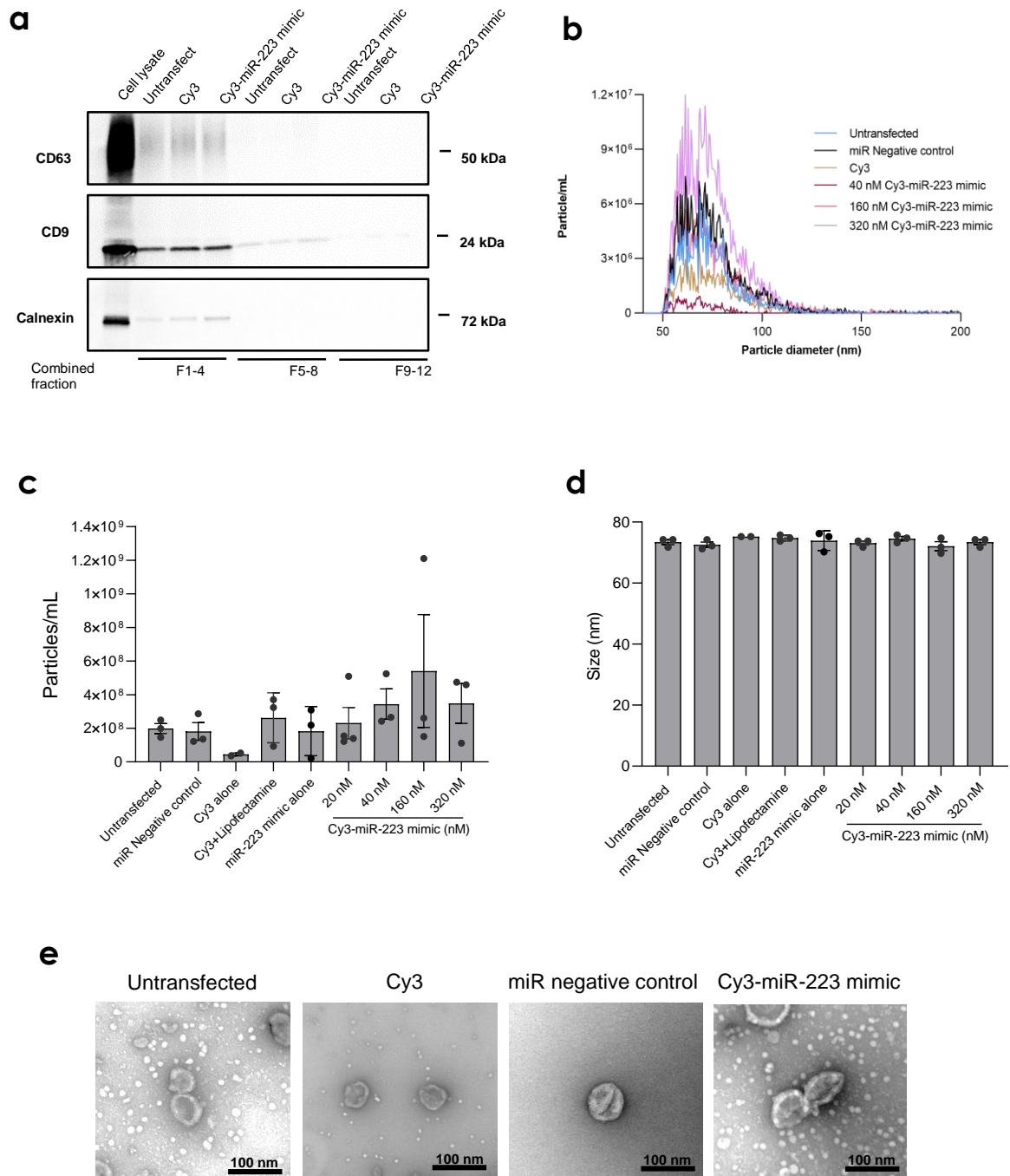


Figure 19 Characterization of EVs from Cy3-miR-223 mimic transfected macrophages. EVs from conditioned medium of Cy3-miR-223 mimic transfected macrophages were isolated using size exclusion chromatography and fractions. (a) Western blot for EV markers CD63, CD9, and a cellular marker, calnexin. (b) EV size distribution, (c) concentration, and (d) size measured by NFCM. (e) Electron micrograph of EVs. Scale bars, 100 μ m. Data are presented as means \pm SEM.

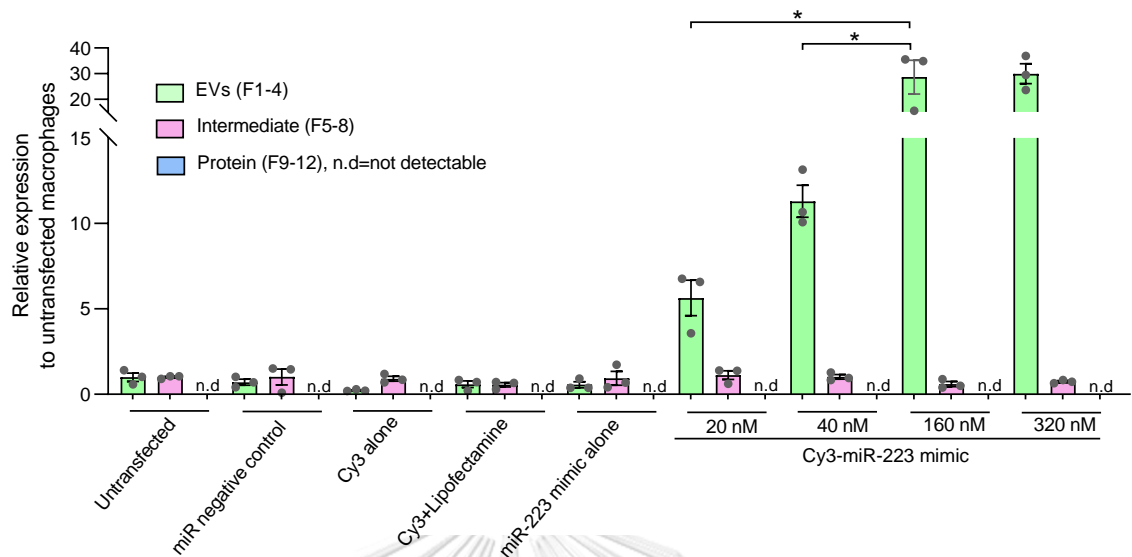


Figure 20 miR-223 in EVs from Cy3-miR-223 transfected macrophages. Expression of miR-223 was measured by qRT-PCR in combined EV fraction (F1-4), intermediate fraction (F5-8), and non-EV fraction (F9-12). Data are presented as means \pm SEM. n.d.=not detectable.

macrophages transferred Cy3-miR-223 mimic to the recipient cells, Huh7, on the lower wells (Figure 22). Third, Huh7 were collected for analysis of miR-223 by qRT-PCR. The expression of miR-223 in Huh7 cells upon co-culture with Cy3-miR-223 mimic transfected macrophages was increased compared to controls including no co-culture cells, Huh7 cells co-culture with untransfected macrophages, and Huh7 co-culture with macrophages transfected with negative miR (Figure 23a). Interestingly, we found that, when comparing Huh7 cells co-culture with Cy3-miR-223 mimic transfected macrophages, the vehicle-pretreated Huh7 had higher levels of miR-223 than PA-pretreated cells. To confirm whether miR-223 was internalized into Huh7 cells, miR-223 target genes were examined. Based on miRNA target database, Targetscan (www.targetscan.org) and previous studies, we selected two direct targets of miR-223, Forkhead Box O3 (FOXO3) (97, 98) and the transcriptional coactivator with PDZ-binding motif (TAZ; encoded by WW domain-containing transcription regulator 1 (99)) (100). As shown in Figure 23b-c.

both PA-treated and untreated Huh7 cells co-cultured with Cy3-miR-223 mimic transfected macrophages showed lower levels of *FOXO3* and *TAZ* compared to those levels in controls. However, only *FOXO3* exhibited a significant decrease, while *TAZ* did not. These results were as expected since miR-223 binds to the conserved position of *FOXO3* at the beginning of its 3' UTR, whereas miR-223 binds to the poorly conserved position located in the middle and late regions of its 3' UTR, as shown by TargetScan miRNA target analysis.

In addition, an EV secretion inhibitor, GW4869, was added to the macrophages before co-culture with Huh7 cells. Prior to co-culture, macrophage EVs were isolated. In macrophages treated with GW4869, both the concentration of EVs and the level of miR-223 in EVs were reduced (Figure 24a-b), whereas the expression of miR-223 in the cells increased (Figure 24c). After co-culturing GW4869-treated macrophages with Huh7 cells, miR-223 expression in Huh7 decreased (Figure 24d). These results suggest that blocking EV secretion from macrophages with

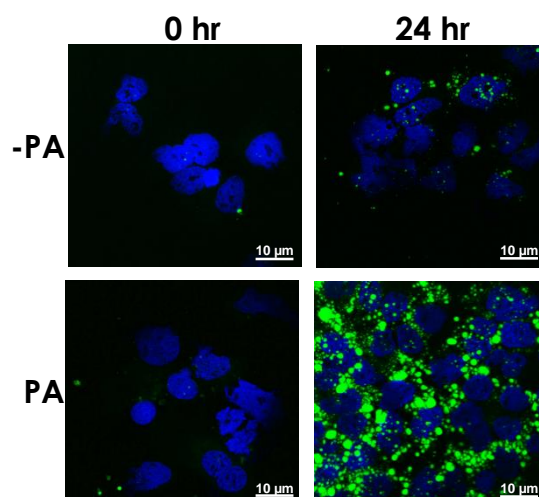


Figure 21 Induction of lipotoxicity in hepatocytes using palmitic acid. Huh7 cells were induced by 400 μ M PA for 24 hours and lipid droplets were stained with the fluorescent neutral lipid dye 4,4-difluoro-1,3,5,7,8-pentamethyl-4-bora-3a,4a-diaza-s-indacene (BODIPY). Nuclei were stained with DAPI (blue). Scale bars, 10 μ m.

GW4869 led to reduced transfer of miR-223 to Huh7 recipient cells and miR-223 is mainly packed into EVs.

4.2.4. Lipotoxic hepatocytes take up macrophage EVs

To demonstrate the lipotoxic effects on Huh7 hepatocytes and their uptake of macrophage-derived EV, we conducted an EV uptake assay using PA-treated Huh7 cells. Initially, we labeled the EVs isolated from macrophages with an EV-staining dye called MemGlow 488. Separated EVs from macrophages were labeled with EV-staining dye, MemGlow 488. PBS stained with MemGlow 488 was used as a control. After removing of the excess dye, MemGlow 488-labeled EVs were measured by nanoflow, and we found that approximately 98% of the population was positive for MemGlow 488 (Figure 25a). Next, we incubated the MemGlow 488-labeled EVs with Huh7 cells that had been treated with 400 μ M PA. We then imaged the green fluorescence of MemGlow 488 and quantified its intensity.

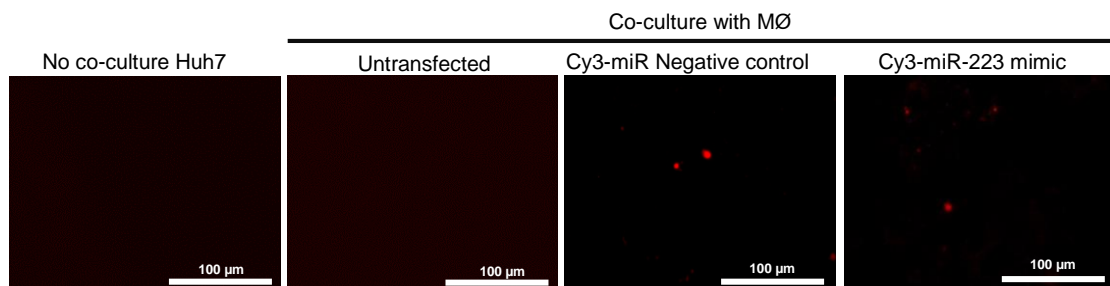


Figure 22 Cy3 fluorescence dye in hepatocytes after co-culture with Cy3-miR-223 mimic transfected macrophages. Representative images of Cy3 red fluorescence in Huh7 upon co-culture with Cy3-miR-223 mimic transfected MØ in a 0.4 μ m transwell plate. Scale bars, 100 μ m.

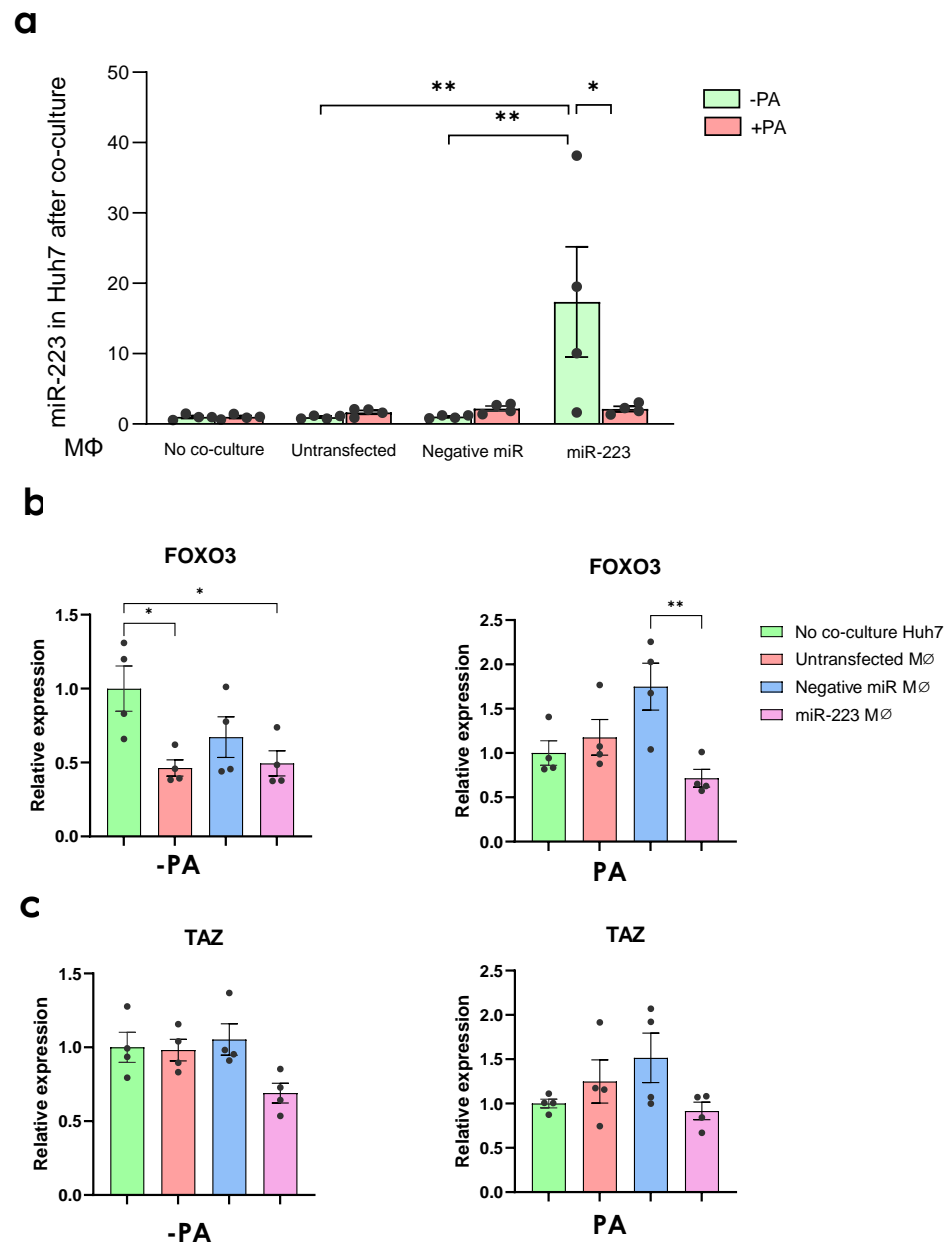


Figure 23 miR-223 in lipotoxic hepatocytes after co-culture with Cy3-miR-223 mimic transfected macrophages. Huh7 cells were pretreated with 400 μ M PA for 24 hours and co-culture with Cy3-miR-223 mimic transfected M Φ for another 24 hours. (a) Expression levels of miR-223 and its target genes (b) FOXO3 and (c) TAZ in lipotoxic hepatocytes induced by palmitic acid (PA) were determined by qRT-PCR. Data are presented as means \pm SEM.

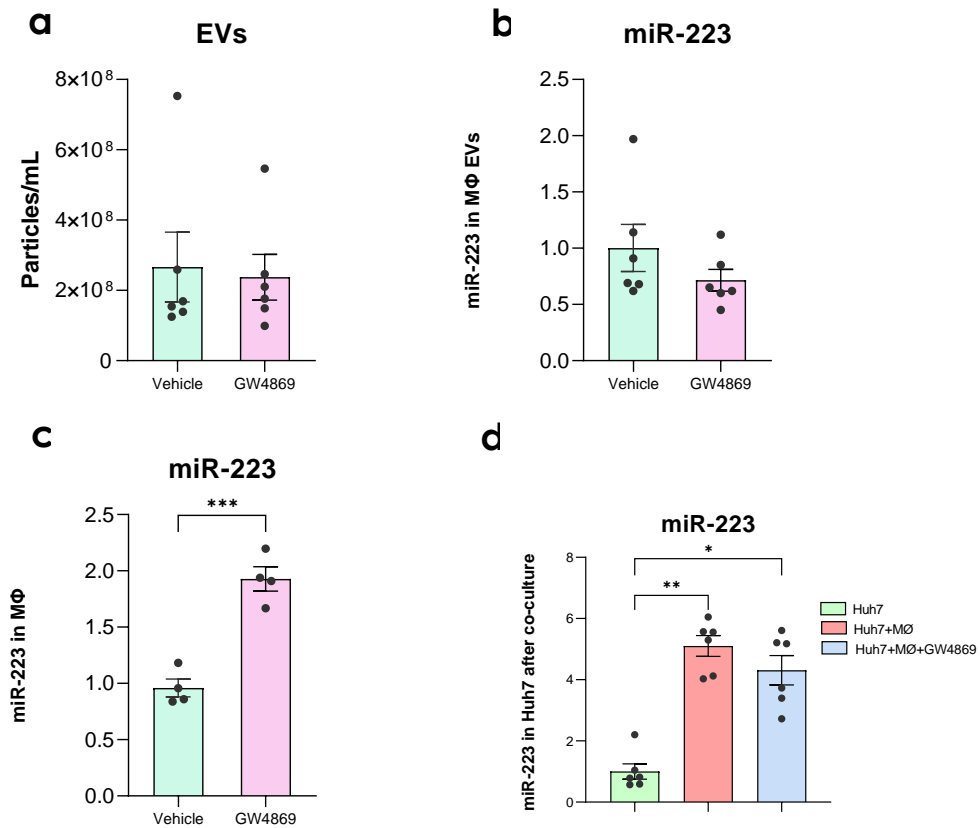


Figure 24 Effects of the EV secretion inhibitor GW4689 on miRNA delivery from macrophages into hepatocyte recipient cells. (a) Before co-culture, macrophages were pretreated with 20 μ M GW4689 concentration of EVs was measured by NFCM. (b) miR-223 levels in EVs from macrophages and (c) macrophages were determined by qRT-PCR. (d) After co-culture between macrophages and hepatocytes in the presence of GW4689, miR-223 levels in Huh7 cells were measured.

In accordance with the level of miR-223 in Huh7, we observed that vehicle-treated Huh7 cells exhibited higher MemGlow 488 fluorescence compared to PA-treated cells. (Figure 25b). Thus, the results suggested that induction of lipotoxic condition in Huh7 by PA results in reduced uptake of macrophage-derived EVs.

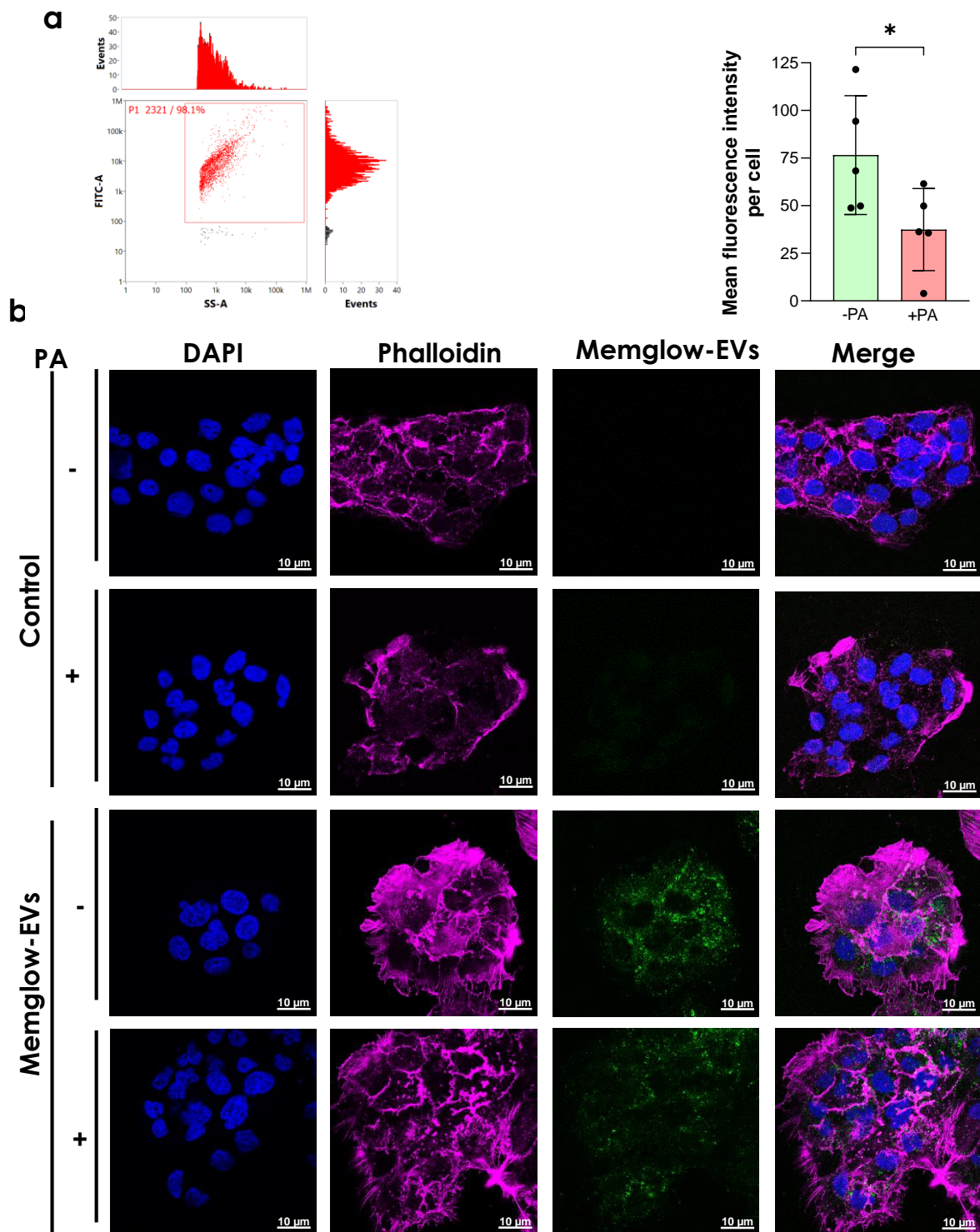


Figure 25 Lipotoxic hepatocytes take up macrophage EVs. After pretreatment with vehicle or 400 μ M PA for 24 hours, hepatocytes were incubated with MemGlow 488- labeled macrophage-derived EVs followed by immunofluorescence staining. (a) NFCM analysis of MemGlow 488-labeled macrophage-derived EVs. (b) Representative images of MemGlow 488 (green), Phalloidin (pink), and nuclei (DAPI, blue). Scale bars, 10 μ m.

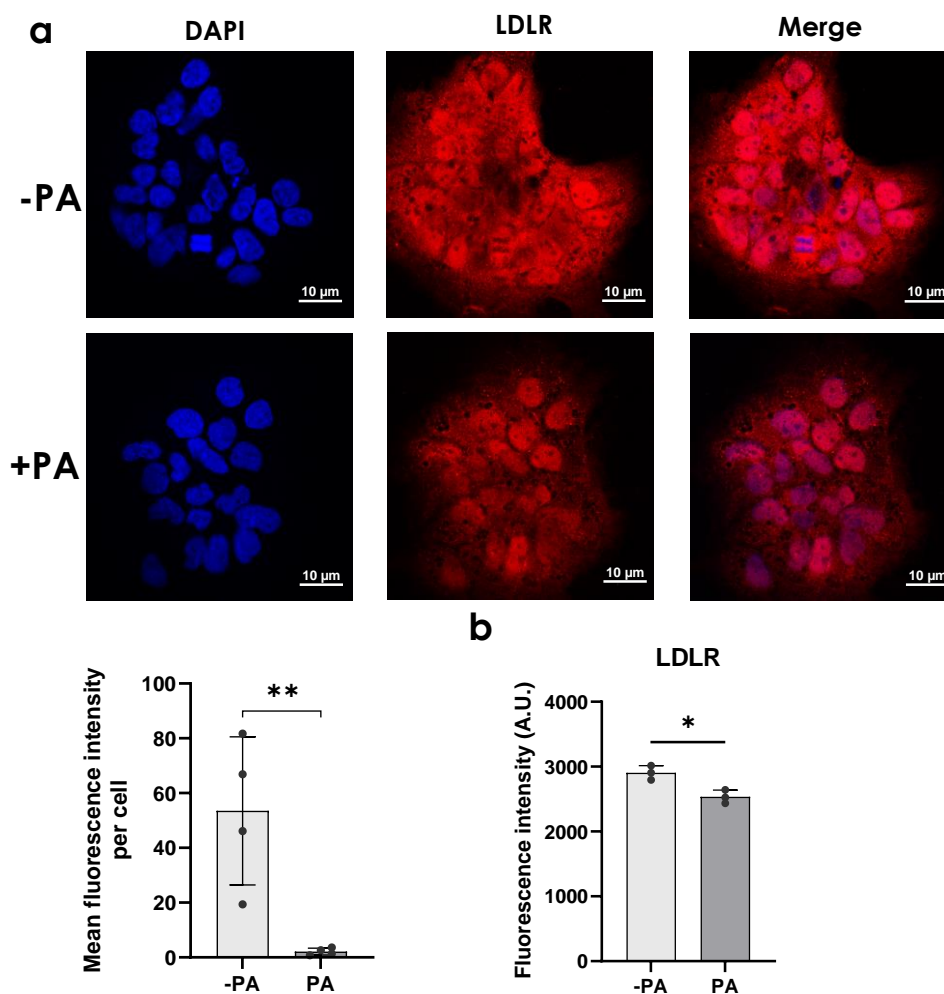


Figure 26 Lipotoxic hepatocytes take up macrophage EVs partially via LDLR. Huh7 cells were induced by 400 μM PA for 24 hours and LDLR expression was analyzed by immunofluorescence staining and flow cytometry. (a) Immunofluorescence staining of LDLR and mean fluorescence intensity per cells was quantified. Nuclei were stained with DAPI (blue). Scale bars, 10 μm . (b) Flow cytometry analysis of LDLR expression in PA-treated Huh7 cells.

We further investigate how PA effect EV uptake in Huh7 recipient cells. Since a previous study demonstrated that upon PA induction, low-density lipoprotein receptor (LDLR) is partially responsible for EV uptake in hepatocytes (64). In this study, we found that after PA treatment, LDLR expression in the cells was decreased as shown by immunofluorescence staining (Figure 26a) and flow cytometry (Figure 26b). All of these findings suggest that the uptake of EVs in lipotoxic hepatocytes is partially dependent on LDLR.

CHAPTER 5

DISCUSSION

The detection of HCC at early-stage cancer is an unmet clinical need because only 20-30% of patients are eligible for curative therapy mainly due to the lack of early-detection biomarkers. At present, serum AFP remains the most commonly used serum biomarker despite its insufficient performance in early detection for HCC. Overall, the sensitivity and specificity of AFP are approximately 60% and 80%, respectively, and its sensitivity decreases significantly in patients with early HCC (101). Moreover, AFP levels remain normal (AFP level <20 ng/ml) in up to 30% of advanced cancer stage but are elevated in some individuals without HCC, leading to high negative and false-positive rates. In this report, our data demonstrated that only 36% of early NBNC-HCC were AFP-positive (AFP level \geq 20 ng/ml). Thus, additional novel biomarkers that could be used individually or in complementary with AFP for better accurate detection of HCC are required.

In recent years, the potential role of EV-based liquid biopsy in the management of liver disease is of great interest. Emerging evidence highlights the significance of EV-miRNAs in various chronic liver diseases, including viral hepatitis, NAFLD, alcohol-related liver disease and HCC (61). For instance, circulating EV-miRNA profiles could be non-invasive biomarkers for the assessment of severity in patients with NAFLD (102, 103). Regarding HCC, previous studies demonstrated that either single or panels of EV-miRNAs are potentially specific and sensitive biomarkers for the diagnosis of viral-related HCC (104, 105). However, data regarding the role of EV-miRNAs as novel biomarkers of NBNC-HCC are still missing. In this study, we initially characterized microtranscriptome to examine circulating EV-miRNA profiles in patients with NBNC-HCC by comparison with those of patients with NAFLD and healthy controls. In this discovery set, several

differential expression profiles of EV-miRNAs between the HCC and control groups were revealed. In the validation set by qRT-PCR, plasma-derived EV-miRNAs, including miR-19-3p, miR-16-5p, miR-223-3p, miR-30d-5p, and miR-451a were significantly elevated in NBNC-HCC compared with the control groups. Also, the data based on bioinformatics identified up- and downregulated miRNAs associated with various biological processes, including protein targeting and transport, nuclear transport, and cell cycle. Moreover, the enriched KEGG pathways of DEGs were found to participate in several cancer-related signaling pathways.

In our report, we demonstrate for the first time that EV-miR-19-3p could be used as a promising biomarker for NBNC-HCC. We showed that EV-miR-19-3p had a high diagnostic ability for detecting AFP-negative cases. Additionally, the combined use of EV-miR-19-3p and AFP increased the diagnostic accuracy of NBNC-HCC. These findings suggest the potential use of EV-miR-19-3p as a sensitive biomarker for early HCC and a complementary biomarker with AFP-negative HCC. Of note, it was recently shown that circulating EV-miR-19a-3p was identified as a novel biomarker among other miRNAs for early and non-invasive diagnosis of pancreatic cancer (106). Moreover, a recent study showed that EV-miR-19a-3p was highly upregulated in the advanced stage of prostate cancer tissue specimens, particularly after androgen stimulation (107).

Regarding its predictive role, Kaplan-Meier analysis also showed that high circulating EV-miR-19-3p was positively correlated with poor overall survival in patients with NBNC-HCC. Moreover, multivariate analysis verified that an increased EV-miR-19-3p level was an independently unfavorable predictor of overall survival. Collectively, our results provide evidence supporting a novel role of EV-miR-19-3p in early detection and prognostic value of NBNC-HCC.

Dysregulated expression of miR-19 has been shown to be involved in several types of solid tumors and represents one of the most investigated miRNAs in human cancer (108). Many studies have demonstrated that miR-19 plays a significant role in regulating and maintaining homeostasis of tissue function and immune regulation. Additionally, its dysregulation has been implicated in the pathogenesis and progression of tissue inflammation and fibrosis, as well as tumorigenesis (109). For example, previous data reported that serum miR-19a, could be a biomarker for early detection of colorectal cancer (110) and breast cancer (111). Among studies related to HCC, most previous reports examined the expression of miR-19 in HCC cell lines or liver tissue specimens (112-117), with limited available data on blood-based samples (118). For instance, miR-19 was shown to be upregulated in tissue specimens and cell lines through the PTEN/Akt pathway in promoting HCC metastasis and chemoresistance (115, 118). In contrast, the expression level of miR-19a in human cancer specimens was significantly lower than that found in adjacent non-cancerous tissue, which might play an inhibitory role for HCC progression by targeting Cyclin D1 (114). This discrepancy might be due to several factors such as the etiologies and the heterogeneity of HCC, as well as different studied HCC cell lines. Although miR-19 expression levels in HCC were rather inconsistent, a recent systematic review and meta-analysis revealed that upregulated miR-19 expression was detected in HCC compared with non-malignant controls in most reports, indicative of its crucial role in the diagnosis and prognosis of HCC (119). Further studies are therefore required to elucidate the mechanism by which EV-miR-19-3p plays a crucial role in the development and progression of NBNC-HCC.

Regarding the function of miR-19 carried by EVs, in accordance with the role of miR-19 in HCC metastasis as mentioned above, EV miR-19a promotes osteoclastogenesis by targeting the PTEN/AKT pathway, as reported in bone metastasis in breast cancer. It was found that EVs from

bone-metastatic breast cancer cells, MCF7BoM2, are taken up by osteoclast precursor cells, RAW264.7, which play critical roles in bone metastasis. It is proposed that miR-19a, when internalized via EVs, suppresses PTEN expression, leading to the activation of the NF- κ B and AKT pathways, ultimately promoting osteoclast cell activity (120).

In order to validate the potential of miRNA-containing EVs as promising biomarkers in NAFLD-related HCC, we demonstrated a mechanistic basis for the delivery of EVs in a NAFLD model. Our study elucidates the transportation of miR-223 from macrophages to lipotoxic hepatocytes via EVs. To examine the possible transfer of EVs from macrophages, which carry miR-223, to hepatocytes, we conducted a transfection of macrophages with a miR-223 mimic, followed by a subsequent co-culturing with hepatocytes. The main findings can be summarized as follows: i) Cy3-miR-223 mimic transfected macrophages release miR-223 to recipient cells, lipotoxic hepatocytes; ii) hepatocytes might use LDLR for partial uptake of EVs from macrophages; and PA-treated hepatocytes had a reduction of LDLR resulting in less EV uptake.

In this study, we used monocyte-derived macrophages (MDM) as a model for tissue macrophages by differentiation of PBMCs into macrophages using M-CSF, following established protocols (95, 121). The macrophage population has been obtained based on various stimuli and growth factors. Generally, for macrophage polarization, monocytes need to be activated to M1 and M2 states by IFN- γ \pm LPS or IL-4 and IL-13, respectively (122, 123). When human monocytes are treated with cytokines, cells treated with GM-CSF are identified as GM-CSF macrophages, characterized by proinflammatory cytokines and some features of M1 cells. On the other hand, M-CSF generates M-CSF macrophages with anti-inflammatory cytokines and some features of M2 macrophages. However, transcriptomic analysis revealed an overlap in gene expression between these cytokine-treated cells (124). In our differentiated macrophages, we observed a "fried egg"

morphology, consistent with a previous study describing GM-CSF macrophages (95). It's important to note that in our experiment, we did not measure phenotypic markers.

The rationale for selecting miR-223 for demonstration is its specificity to myeloid cells, which regulate inflammation in many diseases including liver diseases (125). The expression levels are high in neutrophils and macrophages, but they are low in hepatocytes. (126). In NAFLD or NASH, several target genes of miR-223 have been reported. miR-223 binds to the transcriptional coactivator with PDZ-binding motif (TAZ; encoded by WW domain-containing transcription regulator 1, (C-X-C motif) chemokine 10 (Cxcl10), and NOD-, LRR- and pyrin domain-containing protein 3 (Nlrp3) to reduce NASH in high fat diet (HFD)-induced NASH development mice model (99, 127, 128). The oncogenic role of TAZ has been well described (129). Moreover, TAZ is involved in liver fibrosis. He et al. showed that in NASH mice, TAZ activates Indian hedgehog (Ihh), a secretory factor that activates fibrogenic genes in hepatic stellate cells, via TAZ/TEA domain (TEAD) (130). Inhibition of hepatocyte-specific TAZ can reverse hepatic inflammation and fibrosis in NASH mice (131). The CXCL10 is one crucial pro-inflammatory cytokine linked to lipotoxicity, which draws inflammatory cells to the site of tissue damage (132). Also, CXCL10 was found to mediate macrophage recruitment to the liver. CXCL10-null mice have a decrease in hepatic proinflammatory (M1 polarized) macrophage, resulting in liver inflammation and subsequent liver injury and fibrosis (133). Moreover, miR-223 from neutrophils was shown to suppress NLRP3 inflammasome in proinflammatory macrophages and trigger their alternative activation into a restorative phenotype, thereby preventing the activation of HSCs and collagen synthesis and reducing fibrogenesis. (134). It is crucial to note that the miR-223 target genes were tested in a NASH mice model, in which miR-223 binds to different genes in humans. As suggested by the TargetScan miRNA database and demonstrated by our results in Figure 23, TAZ did not

significantly decrease, but FOXO3 did in the hepatocyte recipient cells. This is because TAZ is a miR-223 target gene in mice hepatocytes, while FOXO3 is its target gene in human hepatocytes.

Previous studies have also been investigated the role of miR-223 carried by EVs in facilitating cellular crosstalk. Macrophages transferred Cy3-labeled miR-223 mimic to 3T3-L1 adipocytes (135). Neutrophils deliver EV miR-223 to hepatocytes, and this selective transfer relies on the presence of LDLR on hepatocytes and APOE on neutrophil-derived EVs (64). The mechanism of hepatocytes communicating to macrophages via EVs have been demonstrated. In hepatocytes, lipotoxicity activates mixed lineage kinase 3 (MLK3) to promote the release of EVs containing (C-X-C motif) ligand 10 (CXCL10) for mediating macrophage chemotaxis (136). Lipotoxic hepatocytes also trigger the activation of the proapoptotic signaling cascade through death receptor 5 (DR5), which, in turn, stimulates rho-associated, coiled-coil-containing protein kinase 1 (ROCK1) to promote EVs containing TRAIL. These EVs then initiate the activation of macrophages through a non-canonical and non-apoptotic signaling pathway involving DR5, depending on receptor-interacting protein kinase 1 (RIP1) (137). And as aforementioned above, macrophages transfer EVs containing miRNA-223 to hepatocytes, including *in vitro* HCC cell lines, to restrict their proliferative growth (76), and *in vivo* mice model, to suppress liver fibrosis (78). Here, we focus on the transfer of EV miR-223 from macrophages to hepatocytes in human cell setting with comprehensive studied in mechanistically EV transfer.

In the context of lipotoxic hepatocytes, a previous study in mice demonstrated that the selective uptake of miR-223-enriched EVs derived from neutrophils partially involves the LDLR. This was observed following the induction of a lipotoxic condition through palmitic acid (PA) treatment, which led to an increase in LDLR expression, enabling enhanced EV uptake from neutrophils (64). However, this contradicts our findings, where PA treatment in human hepatocytes resulted in decreased LDLR expression and subsequently reduced EV uptake from

macrophages. As mentioned above, PA has been shown to stimulate lipotoxic ER stress, which activates PCSK9, a natural inhibitor of LDLR. This activation, in turn, reduces LDL uptake and contributes to the development of NAFLD (68). This finding may provide an explanation for our results, suggesting that PA-treated hepatocytes exhibit a reduction in LDLR. However, further experiments are required to elucidate and describe this phenomenon.

Our work had some limitations as the sample size was relatively small, and thus additional studies from multi-centers are required to confirm our findings. Secondly, although there are several potential etiologies for NBNC-HCC, the majority of our cases could likely be related to NAFLD as other major causes of HCC including significant alcohol consumption were already excluded at the initial enrollment. Moreover, most cases of NBNC-HCC in our cohort had coexisting metabolic syndrome that was linked to NAFLD as reported in most studies (138). Thirdly, liver biopsy was not performed in patients with NAFLD. Although liver biopsy is currently the gold standard for diagnosis of NAFLD, this invasive method has limitations including sampling error, risk of complications and being not feasible to perform in all patients. Instead, we used transient elastography, which is considered to be an accurate non-invasive tool to determine the severity of fibrosis and steatosis. Forth, longitudinal studies to investigate the dynamics of the candidate EV-miRNAs should be further explored. Furthermore, the major challenges in using EV miRNAs as diagnostic biomarkers are the lack of standardization in the EV isolation method (139, 140). According to the literature, the preparation of EVs using polymer-based precipitation, which involves a small sample volume, has been shown to provide a high yield of EVs while remaining time- and cost-effective. To support clinical application practices and overcome the limitations related to the restricted sample volumes in our study, we selected Exoquick™ solution to enrich EVs from plasma (61, 141, 142). However, this method comes with the drawback of being non-selective and yielding low purity. Despite these limitations, our results demonstrated that

circulating EV-miR-19-3p was a reliable biomarker to differentiate between the NBNC-HCC and non-HCC groups. Apart from its diagnostic role, plasma EV-miR-19-3p also displayed a good prognostic indicator for NBNC-HCC. Together, this novel circulating biomarker might serve as a promising tool for the diagnosis and prognosis prediction of NBNC-HCC.

Additionally, our NAFLD model has same limitations, including, we did not identify phenotype markers of the differentiated macrophages. The experiments to confirm the involvement of LDLR in EV uptake have not yet been demonstrated. Moreover, the molecular regulation of LDLR expression after palmitic acid treatment is required. Additionally, the study is limited by the need for further investigation into the ligand produced by macrophage-derived EVs in order to obtain a more thorough understanding of the process of EV uptake in hepatocytes.



CHAPTER 6

CONCLUSION

In summary, our study aimed to assess the potential of plasma EV-derived miRNAs as biomarkers for non-hepatitis B, non-hepatitis C-related hepatocellular carcinoma (NBNC-HCC). We identified five specific plasma EV-miRNAs - miR-19-3p, miR-16-5p, miR-223-3p, miR-30d-5p, and miR-451a - that were significantly elevated in NBNC-HCC. Among these, miR-19-3p exhibited the most promising diagnostic performance, demonstrating high sensitivity in detecting AFP-negative HCC and early-stage HCC. This indicates that EV-miR-19-3p could serve as a novel circulating biomarker for the diagnosis and prognosis of NBNC-HCC. Furthermore, we investigated the role of EVs in mediating communication between macrophages and lipotoxic hepatocytes in an NAFLD model. Co-culturing Cy3-miR-223 mimic-transfected macrophages with lipotoxic hepatocytes induced by palmitic acid revealed that hepatocyte recipient cells exhibited Cy3 fluorescence, increased miR-223 levels, and reduced levels of miR-223 target genes. Importantly, our results suggested that the low-density lipoprotein receptor (LDLR) played a partial role in facilitating EV uptake by lipotoxic hepatocytes. In conclusion, the results indicate that the miRNA within carried by EVs has the potential to function as an innovative circulating biomarker for diagnosis and prognosis of NBNC-HCC and macrophages can transfer miRNA to lipotoxic hepatocytes. Our findings provide fundamental evidence to support the role of EV-derived miRNAs as potential predictors of NBNC-HCC and may be applicable in the development of novel therapeutic strategies for NBNC-HCC treatment.

Future experiments should aim to confirm the involvement of LDLR in EV uptake by conducting an EV uptake assay in LDLR-overexpressing and knockdown hepatocytes. Further

research is necessary to elucidate the molecular regulation of LDLR expression following palmitic acid treatment, providing a more comprehensive understanding of the pathway of EV internalization in lipotoxic hepatocytes. Additionally, the ligand produced by macrophage-derived EVs, which is expected to be responsible for EV uptake in hepatocytes, for example, a high-affinity ligand for LDLR; apolipoprotein E (ApoE), should be determined to achieve a more comprehensive understanding of this process.





APPENDIX

จุฬาลงกรณ์มหาวิทยาลัย
CHULALONGKORN UNIVERSITY



Article

Circulating Extracellular Vesicle-Derived microRNAs as Novel Diagnostic and Prognostic Biomarkers for Non-Viral-Related Hepatocellular Carcinoma

Bootsakorn Boonkaew ¹, Nantawat Satthawiwat ¹, Nutcha Pinjaroen ², Natthaya Chuaypen ^{1,*} and Pisit Tangkijvanich ^{1,*}

¹ Center of Excellence in Hepatitis and Liver Cancer, Department of Biochemistry, Faculty of Medicine, Chulalongkorn University, Bangkok 10330, Thailand; bootsakorn.b@gmail.com (B.B.); 6371007030@student.chula.ac.th (N.S.)

² Department of Radiology, Faculty of Medicine, Chulalongkorn University, Bangkok 10330, Thailand; nutcha.p@chula.ac.th

* Correspondence: natthaya.c@chula.ac.th (N.C.); pisitkvn@yahoo.com (P.T.); Tel.: +66-2-256-4482 (N.C.)

Abstract: Extracellular vesicle-derived microRNAs (EV-miRNAs) are promising circulating biomarkers for chronic liver disease. In this study, we explored the potential significance of plasma EV-miRNAs in non-hepatitis B-, non-hepatitis C-related HCC (NBNC-HCC). We compared, using the NanoString method, plasma EV-miRNA profiles between NBNC-HCC and control groups including patients with non-alcoholic fatty liver disease (NAFLD) and healthy controls. The differentially expressed EV-miRNAs were validated in another set of plasma samples by qRT-PCR. A total of 66 significantly differentially expressed EV-miRNAs between the HCC and the control groups were identified in the discovery set. In the validation cohort, including plasma samples of 70 NBNC-HCC patients, 70 NAFLD patients, and 35 healthy controls, 5 plasma EV-miRNAs were significantly elevated in HCC, which included miR-19-3p, miR-16-5p, miR-223-3p, miR-30d-5p, and miR-451a. These miRNAs were found to participate in several cancer-related signaling pathways based on bioinformatic analysis. Among them, EV-miR-19-3p exhibited the best diagnostic performance and displayed a high sensitivity for detecting alpha-fetoprotein-negative HCC and early-stage HCC. In multivariate analysis, a high EV-miR-19-3p level was demonstrated as an independently unfavorable predictor of overall survival in patients with NBNC-HCC. In conclusion, our data have indicated, for the first time, that EV-miR-19-3p could serve as a novel circulating biomarker for the diagnosis and prognosis of NBNC-HCC.

Keywords: extracellular vesicles; nonalcoholic fatty liver disease; hepatocellular carcinoma; microRNAs; biomarker



Citation: Boonkaew, B.; Satthawiwat, N.; Pinjaroen, N.; Chuaypen, N.; Tangkijvanich, P. Circulating Extracellular Vesicle-Derived microRNAs as Novel Diagnostic and Prognostic Biomarkers for Non-Viral-Related Hepatocellular Carcinoma. *Int. J. Mol. Sci.* **2023**, *24*, 16043. <https://doi.org/10.3390/ijms242216043>

Academic Editors: Giuliano Ramadori and Nam Deuk Kim

Received: 16 August 2023

Revised: 1 November 2023

Accepted: 2 November 2023

Published: 7 November 2023



Copyright: © 2023 by the authors. Licensee MDPI, Basel, Switzerland. This article is an open access article distributed under the terms and conditions of the Creative Commons Attribution (CC BY) license (<https://creativecommons.org/licenses/by/4.0/>).

1. Introduction

Hepatocellular carcinoma (HCC) is a heterogeneous tumor with the majority of cases occurring in the setting of underlying chronic liver disease (CLD) [1]. Although chronic viral hepatitis has been the major risk factor for HCC, an increasing proportion of patient disease is attributable to non-hepatitis B-, non-hepatitis C-related HCC (NBNC-HCC) as a result of the growing burden of non-alcoholic fatty liver disease (NAFLD) [1]. Currently, NAFLD is considered to be a leading cause of HCC in most Western countries. In Asian populations, the prevalence of NAFLD is also becoming an important public health concern that potentially leads to progressive liver disease including cirrhosis and HCC [2]. Early detection of HCC enhances the likelihood of curative treatment by surgical resection, liver transplantation, or local ablation. However, the overall prognosis of HCC remains unsatisfactory because of the biologic aggressiveness of the tumor and high rates of recurrence after therapies [3]. Moreover, NBNC-HCC tends to be detected at a late tumor stage,

which could lead to worse prognosis in comparison to virus-related HCC [4]. A recent multicenter study demonstrated that there was no survival improvement among patients with NBNC-HCC over the past two decades while the survival rate of viral-related HCC considerably increased [5]. Therefore, reliable circulating biomarkers for early diagnosis and prognostic prediction are urgently required to improve the clinical outcomes of patients with NBNC-HCC.

In recent years, 'liquid biopsy' has emerged as a novel method for the characterization of circulating cancer components, and provides a strong basis for precision oncology in terms of early diagnosis, therapeutic monitoring, and prognostication [6]. Among various liquid-biopsy based techniques, extracellular vesicles (EVs) are promising circulating biomarkers for HCC [6]. EVs are membrane-bound organelles produced by cells that are classified based on size and biogenesis process. Exosomes (50–150 nm) originate from multivesicular bodies, microvesicles (100–1000 nm) produce directly from membrane bubbling, and apoptotic bodies (500–2000 nm) generate from apoptotic process [7]. EVs serve as cargoes to mediate intercellular communication and are involved in various biological functions and disease progression by actively carrying proteins, lipids, and nucleic acids. Among them, microRNAs (miRNAs), small non-coding RNAs of 20–22 nucleotides, have attracted more attention because of their regulatory roles in a number of key pathophysiological processes [8]. Additionally, circulating enriched EV-derived miRNAs (EV-miRNAs) appear to be more stable and homogeneous than free miRNAs in serum/plasma [9]. Thus, EV-miRNAs, as opposed to free miRNAs, are considered to be more specific and better candidates as cancer biomarkers [10]. Although several 'free-circulating' miRNAs have been shown to be useful in distinguishing HCC from non-HCC, available data regarding the role of EV-miRNAs are limited, particularly in NBNC-HCC.

In the present study, we aimed to explore the potential clinical significance of EV-miRNAs in patients with NBNC-HCC. First, we compared the profiles of plasma EV-miRNAs of the NBNC-HCC and non-cancerous groups, including patients with NAFLD and healthy controls using the NanoString technique. Additionally, the differentially expressed EV-miRNAs were validated in another set of plasma samples by quantitative Real-Time PCR (qRT-PCR) to identify novel biomarkers for NBNC-HCC. Finally, the diagnostic and prognostic roles of these potential biomarkers were analyzed.

2. Results

2.1. Characteristics of the Participants

To construct miRNA profiling in the discovery set, 9 plasma samples per group of patients with NBNC-HCC, NAFLD, versus healthy controls were analyzed by the NanoString miRNA assay. Moreover, the quantitative levels of candidate miRNAs were validated by qRT-PCR in the plasma samples of 35 healthy controls, 70 patients with NAFLD, and 70 patients with NBNC-HCC. Baseline characteristics of the participants in the validated cohort are shown in Table 1.

2.2. Characterization of EVs

To characterize EVs isolated from plasma samples (Figure 1a), the size and concentration of EVs were first determined by nanoparticle tracking analysis (NTA). As expected, the average size of particles in overall samples was 162.9 ± 22.1 nm in diameter (Figure 1b,c). The concentrations of isolated EVs from healthy controls were similar to the NAFLD group ($5.40 \times 10^{11} \pm 2.39 \times 10^{11}$ and $6.12 \times 10^{11} \pm 3.59 \times 10^{11}$ particles/mL, respectively; Figure 1d), whereas the lowest concentration of EVs ($3.41 \times 10^{11} \pm 2.15 \times 10^{11}$ particles/mL) was found in samples from patients with NBNC-HCC. To verify the EV markers, Western blot analysis was then performed. Our results showed that the EV-enriched proteins, including CD63, heat shock protein 70 (HSP70), and the tumor-susceptibility gene 101 (TSG101), were expressed in isolated EV samples. A hepatocyte-specific receptor or asialoglycoprotein receptor 1 (ASGPR1) was also identified to verify that the isolated EVs were partially hepatocyte-derived EVs (Figure 1e). In addition, the particle diameter

and the morphology were confirmed and visualized by transmission electron microscopy (TEM). These vesicles were less than 200 nm in size, with a lipid bilayer, indicating that they were EVs as described previously [11] (Figure 1f). We next evaluated whether the isolated EVs provided intra-vesicular miRNAs. Our results were in line with previous data demonstrating that there was no statistically significant difference between C_t values of miRNAs (such as miR-26a-5p, miR-223-3p, and let-7a-5p) in EVs treated with RNase and without RNase-A (Figure S1a–c) [12,13]. Together, these results indicated that our protocol could specifically identify EV-miRNAs, in accordance with previous data [11]; thus, we did not perform RNase-A treatment for the subsequent experiments.

Table 1. Baseline characteristic of the validation cohort in this study.

Baseline Characteristics	Healthy Controls (n = 35)	Patients with NAFLD (n = 70)	Patients with NBNC-HCC (n = 70)	p
Age (years)	53.2 ± 5.3	50.7 ± 9.5	68.8 ± 11.4	<0.001
Gender (Male)	4 (11.4)	30 (42.9)	54 (77.1)	<0.001
Body mass index (kg/m ²)	22.8 ± 2.6	26.9 ± 4.1	24.3 ± 4.2	<0.001
Presence of metabolic syndrome		33 (47.1)	50 (71.4)	0.006
Total bilirubin (mg/dL)		0.7 ± 0.6	0.8 ± 0.5	0.845
Serum albumin (g/dL)		4.0 ± 0.7	3.6 ± 0.5	<0.001 *
Aspartate aminotransferase (IU/L)		24.5 ± 6.8	34.5 ± 17.9	<0.001 *
Alanine aminotransferase (IU/L)		42.9 ± 42.8	60.8 ± 79.0	0.134
Alkaline phosphatase (IU/L)		81.4 ± 45.2	146.7 ± 171.3	<0.001 *
Platelet count (10 ⁹ /L)		225.4 ± 92.3	216.0 ± 104.7	0.157
Alpha fetoprotein (ng/mL)		3.0 ± 2.9	3423.3 ± 12,469.8	0.025 *
Controlled attenuation parameter (dB/m)	196.5 ± 23.6	304.0 ± 42.9	-	<0.001 *
Transient Elastography (kPa)	3.8 ± 0.8	6.1 ± 1.7	-	<0.001 *
BCLC stage (0-A/B/C)		-	25(35.7)/27(38.6)/18(25.7)	-

Data shown as mean ± SD, BCLC; Barcelona Clinic Liver Cancer, * p < 0.05.

2.3. Profiling of EV-Derived microRNAs

To explore the profiles of EV-miRNAs, we performed the expression of 800 miRNAs using NanoString platform (nCounter Human v3 miRNA expression assay) on the discovery set of patients with NBNC-HCC, NAFLD, and healthy controls. Raw data and normalized data outputs from nSolver 4.0 Software are available in Supplementary S1 File.

Based on differentially expressed miRNAs between groups (\log_2 -fold change (FC) and $p < 0.05$), we found 66 significant differentially expressed miRNAs (DEmiRNAs) in patients with NBNC-HCC vs. NAFLD, which included 39 up- and 27 down-regulated miRNAs (Figure 2a), and 73 DEmiRNAs between patients with NBNC-HCC vs. healthy controls, including 36 up- and 36 down-regulated miRNAs (Figure 2b). Among the significantly up-regulated miRNAs, a Venn diagram showed that five miRNAs, including miR-19-3p, miR-16-5p, miR-223-3p, miR-30d-5p, and miR-451a, overlapped between NBNC-HCC vs. NAFLD and NBNC-HCC vs. healthy controls (Figure S2). Accordingly, these five up-regulated miRNAs were subsequently selected for further validation. The data for DEmiRNAs between patients with NAFLD and healthy controls are available in Figure S3.

2.4. Functional Gene Annotation and Pathway Enrichment Analysis

Gene Ontology (GO) and gProfiler analysis were performed to reveal enrichment of potential target genes of the significantly expressed miRNAs. The top 10 GO categories for the differentially up-regulated miRNAs and down-regulated miRNAs are demonstrated in Figure 3 and Figure S4 ($p < 0.05$), respectively. These significantly up-regulated and down-regulated miRNAs were involved in several biological processes, such as protein targeting and transport, nuclear transport, and cell cycle. Regarding molecular function analysis, these miRNAs were found to be enriched in nucleotide, ATP, and enzyme binding. Furthermore, Kyoto Encyclopedia of Genes and Genomes (KEGG) pathways indicated that

the significantly up-regulated miRNAs participated in pathways in cancer, similar to those with down-regulated miRNAs.

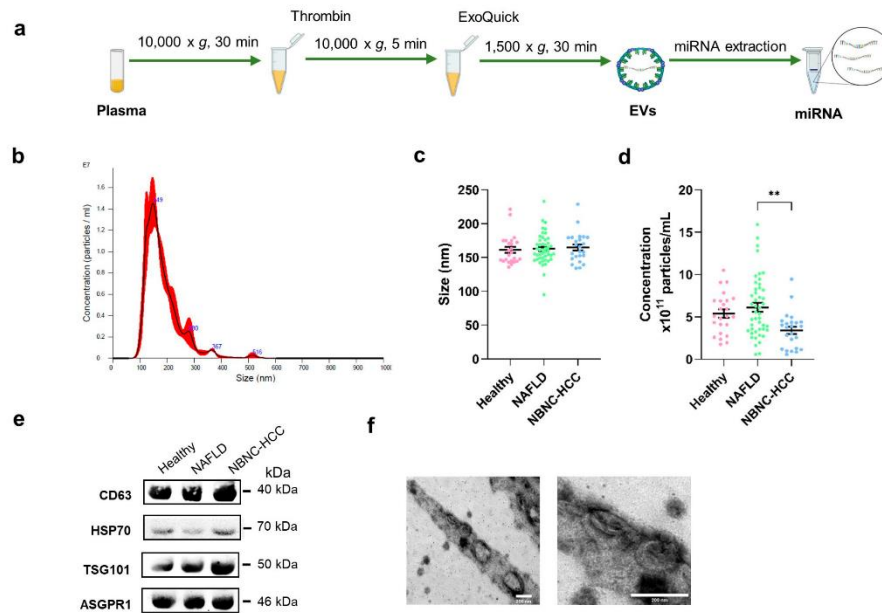


Figure 1. Schematic diagram of the study protocol and characterization of EVs derived from plasma. (a) Diagram of plasma EV isolation protocol, (b) Representative nanoparticle tracking plot for size distribution from a sample, (c) Quantification of particle size diameter (nm), and (d) Concentration (particles/mL) of plasma EVs from the healthy control, NAFLD, and NBNC-HCC groups. (e) Expression of EV markers, CD63, HSP70, and TSG101, and hepatocyte-specific receptor, ASGPR1 by Western blotting. (f) Transmission electron microscopy images of EVs from a sample. Scale bars, 200 μ m. Data are presented as means \pm S.E.M, ** $p < 0.01$.

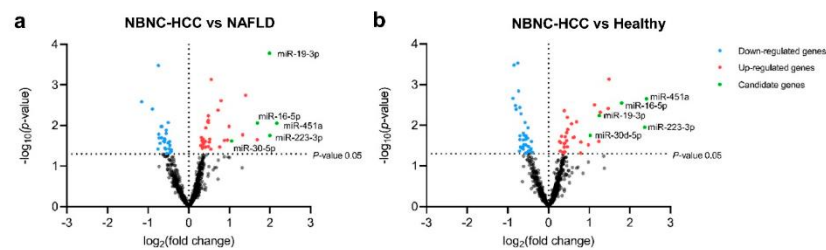


Figure 2. Transcriptome profiling of miRNAs from plasma EVs using NanoString microarray. (a) Volcano plot of all differentially expressed miRNAs in the NBNC-HCC samples compared with the NAFLD samples, and (b) the NBNC-HCC samples compared with healthy controls. The significantly up-regulated and down-regulated miRNAs are denoted as red and blue dots, respectively.

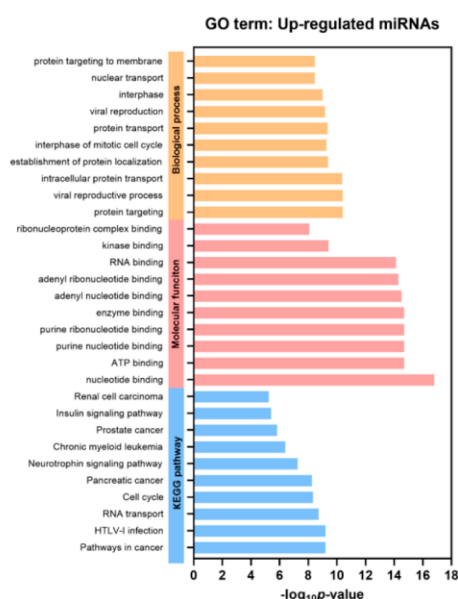


Figure 3. Gene Ontology (GO) analysis of the differentially up-regulated EV miRNAs. Top 10 significantly enriched GO terms of biological process, molecular function, and KEGG pathways ($p < 0.05$).

2.5. Plasma EV-miRNA Expression in the Validation Set

To validate the above-mentioned five up-regulated candidate miRNAs, plasma EV-miRNAs from a total of 175 participants, including 35 healthy controls, 70 patients with NAFLD, and 70 patients with NBNC-HCC were evaluated by qRT-PCR using miR-3144-3p normalization. The results showed that all miR-19-3p, miR-16-5p, miR-223-3p, miR-30d-5p, and miR-451a expression levels were significantly higher in patients with NBNC-HCC compared with healthy controls (Figure 4a–e). When compared with the NAFLD group, the expression levels of miR-19-3p, miR-16-5p, miR-30d-5p, and miR-451a were significantly increased in the NBNC-HCC group (Figure 4a–e). Moreover, similar results of miRNA expression levels were found upon normalization with U6 (Figure S5a–e), suggesting consistent results of validated miRNAs across various internal controls. Overall, these findings indicate that plasma EV-miRNAs could effectively distinguish the NBNC-HCC from non-HCC groups.

Besides plasma EVs, we also investigated the expression levels of candidate miRNAs in both tumor and adjacent non-tumor liver tissue samples obtained from patients with NBNC-HCC ($n = 11$ pairs) using qRT-PCR. Among candidate miRNAs, only miR-19-3p differed significantly between the tumor and adjacent non-tumor samples, 18.76 ± 33.31 vs. 1.00 ± 0.94 ($p = 0.042$) (Figure S6a). There was no significant difference found between the levels of miR-16-5p (0.63 ± 0.54 vs. 1.00 ± 0.91 , $p = 0.700$), miR-223-3p (1.05 ± 1.31 vs. 1.00 ± 0.79 , $p = 0.465$), miR-30d-5p (0.62 ± 1.26 vs. 1.00 ± 1.49 , $p = 0.175$), and miR-451a (0.31 ± 0.46 vs. 1.00 ± 1.35 , $p = 0.148$) (Figure S6b–e).

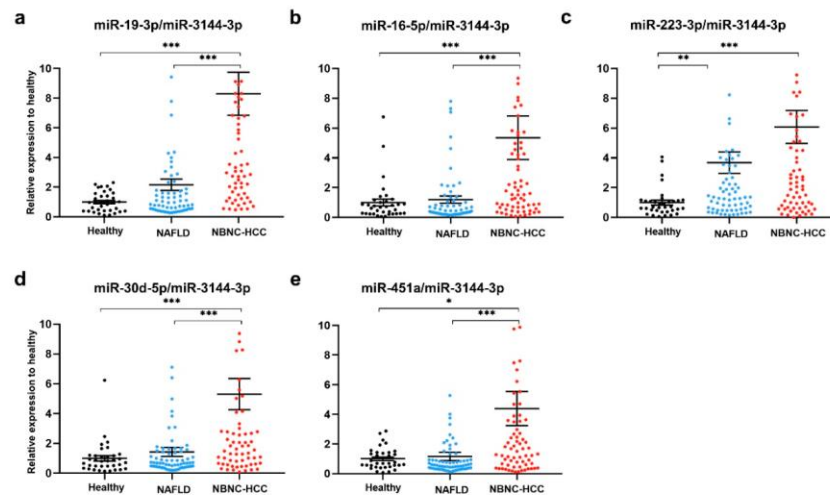


Figure 4. Validation of candidate miRNAs in plasma EV using qRT-PCR. The relative expressions of the following: (a) miR-19-3p, (b) miR-16-5p, (c) miR-223-3p, (d) miR-30d-5p, and (e) miR-451a, in plasma EVs of healthy controls ($n = 35$), patients with NAFLD ($n = 70$), and patients with NBNC-HCC ($n = 70$). Data are presented as mean \pm S.E.M., normalized with a reference miRNA, miR-3144-3p, and expressed relative to those of healthy controls. * $p < 0.05$, ** $p < 0.01$ and *** $p < 0.001$.

2.6. Diagnostic Role of Plasma EV-miRNAs

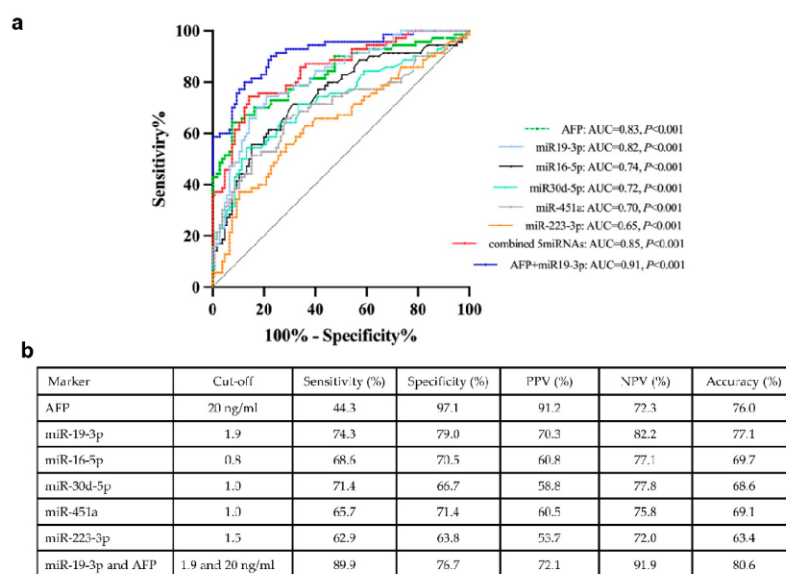
To evaluate the diagnostic performance of biomarkers in distinguishing between the NBNC-HCC and non-HCC groups, receiver operating characteristic (ROC) curves were analyzed (Figure 5a). The area under the curve (AUC) was 0.82 (95% confidence interval (CI); 0.75–0.88, $p < 0.001$) for miR-19-3p, 0.74 (95% CI; 0.67–0.82, $p < 0.001$) for miR-16-5p, 0.65 (95% CI; 0.56–0.73, $p = 0.001$) for miR-223-3p, 0.72 (95% CI; 0.64–0.80, $p < 0.001$) for miR-30d-5p, 0.70 (95% CI; 0.61–0.78, $p < 0.001$) for miR451a, and 0.83 (95% CI; 0.76–0.89, $p < 0.001$) for alpha-fetoprotein (AFP). In addition, the ROC curve for a combination of all EV-miRNAs was also examined. Our results showed that multiple miRNAs did not provide a better AUC than miR-19-3p alone. However, combined miR-19-3p and AFP increased performance for the diagnosis of HCC compared with miR-19-3p alone. The cut-off value and diagnostic performance of each EV-miRNAs, AFP, and the combination of miR-19-3p and AFP is shown in Figure 5b.

If categorized based on the normal upper limit of AFP (20 ng/mL), there were 39 (55.7%) and 31 (44.3%) HCC patients showing AFP-negative and AFP-positive, respectively. In the AFP-negative group, 76.9% (30/39) of HCC patients had elevated circulating miR-19-3p levels (≥ 1.9), while in the AFP-positive group, high expression of miR-19-3p was found in 71.0% (22/31) of patients. Among early HCC cases (BCLC stage 0 and A), we found that 36.0% (9/25) of patients had elevated AFP levels, while 80.0% (20/25) of patients had high miR-19-3p expression. Together, these results might indicate that circulating EV-miR-19-3p was a promising biomarker for detecting AFP-negative HCC and early HCC, as well as a complementary to AFP in diagnosis of NBNC-HCC in our cohort.

2.7. Prognostic Role of Plasma EV-miRNAs Regarding Overall Survival

Apart from its diagnostic value, we further examined the potential prognostic role of plasma EV-miR-19-3p in patients with NBNC-HCC. Using the median value as the cut-off level (3.5), the median overall survival of patients with miR-19-3p < 3.5 and ≥ 3.5

were 38.2 and 22.3 months, respectively ($p = 0.05$ by log rank test) (Figure 6a). For plasma EV-miR-16-5p, the median overall survival of HCC patients with low (<1.9) levels was significantly better than that of patients whose levels were elevated (35.7 vs. 23.1 months, $p = 0.026$) (Figure 6b). However, there was no significant difference in overall survival associated with the circulating levels of other EV-miRNAs, including miR-223-3p, miR-30d-5p, and miR-451a.



AFP; alpha-fetoprotein, NPV; negative predictive value, PPV; positive predictive value

Figure 5. Receiver operating characteristic (ROC) curves of the candidate miRNAs for distinguishing between NBNC-HCC and non-HCC. (a) The area under the curve (AUC), and (b) the cut-off value and the discriminatory performance of each EV-miRNAs.

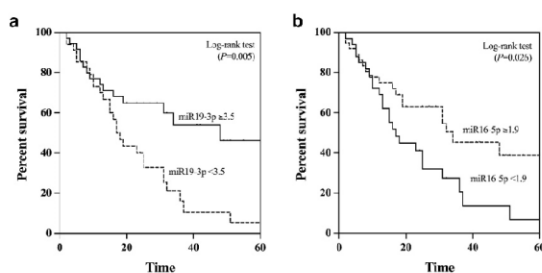


Figure 6. Kaplan-Meier survival curves for overall survival analysis of patients with NBNC-HCC (a) plasma EV-miR-19-3p, and (b) plasma EV-miR-16-5p.

All 5 plasma EV-miRNAs were entered into the multivariate analysis together with other parameters that could influence overall survival of patients with NBNC-HCC. These variables included age, gender, serum TB, albumin, AST, ALT, platelet counts, AFP level, tumor size, and BCLC stage. The multivariate analysis based on the Cox regression analysis

demonstrated that miR-19-3p, AFP, and BCLC stage were independent predictive factors for overall survival. However, miR-16-5p was not a parameter associated with overall survival (Table 2).

Table 2. Variables associated with overall survival in patients with HCC.

Variables	Category	Overall Survival			
		Univariate Analysis		Multivariate Analysis	
		OR (95%CI)	<i>p</i>	OR (95%CI)	<i>p</i>
Age (years)	<60 vs. ≥60	0.62 (0.28–1.41)	0.254		
Gender	Male vs. Female	0.67 (0.32–1.42)	0.295		
Total bilirubin (mg/dL)	<1.2 vs. ≥1.2	0.77 (0.49–1.27)	0.303		
Serum albumin (g/dL)	<3.5 vs. ≥3.5	0.97 (0.46–2.04)	0.931		
Aspartate aminotransferase (IU/L)	<55 vs. ≥55	1.64 (1.83–3.23)	0.153		
Alanine aminotransferase (IU/L)	<50 vs. ≥50	1.00 (0.42–2.39)	0.998		
Platelet count (10 ⁹ /L)	≥100 vs. <100	1.05 (0.37–2.97)	0.927		
Alpha fetoprotein (ng/mL)	<100 vs. ≥100	2.09 (1.08–4.08)	0.029 *	2.04 (1.01–4.13)	0.048 *
Tumor size (cm.)	<5.0 vs. ≥5.0	1.63 (0.88–3.04)	0.123		
BCLC stage	0-A vs. B vs. C	2.15 (1.38–3.36)	0.001 *	2.07 (1.29–3.32)	0.002 *
EV-miR-19-3p	<3.5 vs. ≥3.5	2.39 (1.26–4.52)	0.008 *	2.71 (1.19–6.19)	0.018 *
EV-miR-16-5p	<1.9 vs. ≥1.9	1.98 (1.07–3.69)	0.030 *	0.97 (0.44–2.13)	0.944
EV-miR-30d-5p	<2.0 vs. ≥2.0	1.56 (0.83–2.93)	0.171		
EV-miR-451a	<1.7 vs. ≥1.7	1.74 (0.94–3.23)	0.078		
EV-miR-223-3p	<2.5 vs. ≥2.5	1.71 (0.92–3.19)	0.091		

Data were expressed as odds ratio (OR) and 95% confidence intervals (CI). BCLC; Barcelona Clinic Liver Cancer. * *p* < 0.05.

3. Discussion

The detection of HCC in early-stage cancer is an unmet clinical need; only 20–30% of patients are eligible for curative therapy mainly because of the lack of early-detection biomarkers. At present, serum AFP remains the most commonly used serum biomarker despite its insufficient performance in early detection of HCC. Overall, the sensitivity and specificity of AFP are approximately 60% and 80%, respectively, and its sensitivity decreases significantly in patients with early HCC [14]. Moreover, AFP levels remain normal (AFP level < 20 ng/mL) in up to 30% of advanced cancer cases but are elevated in some individuals without HCC, leading to high negative and false-positive rates. In this report, our data demonstrated that only 36% of early NBNC-HCC were AFP-positive (AFP level ≥ 20 ng/mL). Thus, additional novel biomarkers that could be used individually or in complement to AFP for better, more accurate detection of HCC are required.

In recent years, the potential role of EV-based liquid biopsy in the management of liver disease has been of great interest. Emerging evidence highlights the significance of EV-miRNAs in various chronic liver diseases, including viral hepatitis, NAFLD, alcohol-related liver disease, and HCC [15]. For instance, circulating EV-miRNA profiles could constitute non-invasive biomarkers for the assessment of severity in patients with NAFLD [16,17]. Regarding HCC, previous studies demonstrated that either single samples or panels of EV-miRNAs are potentially specific and sensitive biomarkers for the diagnosis of viral-related HCC [18,19]. However, data regarding the role of EV-miRNAs as novel biomarkers of NBNC-HCC are still needed. In this study, we initially characterized microtranscriptome to examine circulating EV-miRNA profiles in patients with NBNC-HCC by comparing with those of patients with NAFLD and healthy controls. In this discovery set, several differential expression profiles of EV-miRNAs between the HCC and control groups were revealed. In the validation set by qRT-PCR, plasma-derived EV-miRNAs, including miR-19-3p, miR-16-5p, miR-223-3p, miR-30d-5p, and miR-451a were significantly elevated in NBNC-HCC patients compared with the control group. Also, the data based on bioinformatics identified up- and down-regulated miRNAs associated with various biological processes, including protein targeting and transport, nuclear transport, and cell cycle. Moreover, the

enriched KEGG pathways of DEGs were found to participate in several cancer-related signaling pathways.

In our report, we demonstrate for the first time that EV-miR-19-3p could be used as a promising biomarker for NBNC-HCC detection. We showed that EV-miR-19-3p had a high diagnostic ability in detecting AFP-negative cases. Additionally, the combined use of EV-miR-19-3p and AFP increased the diagnostic accuracy for NBNC-HCC. These findings suggest the potential use of EV-miR-19-3p as a sensitive biomarker for early HCC and a complementary biomarker for AFP-negative HCC. The clinical significance of the miR-19 family has been studied in various diseases. Of note, circulating EV-miR-19a-3p was recently identified as a novel biomarker among other miRNAs for early and non-invasive diagnosis of pancreatic cancer [20]. Moreover, a recent study showed that EV-miR-19a-3p was highly up-regulated in prostate cancer tissue specimens at the advanced stage, particularly after androgen stimulation [21]. Regarding its predictive role, Kaplan–Meier analysis also showed that high circulating EV-miR-19-3p was positively correlated with poor overall survival in patients with NBNC-HCC. Moreover, multivariate analysis verified that an increased EV-miR-19-3p level was an independently unfavorable predictor of overall survival. Collectively, our results provide evidence supporting a novel role of EV-miR-19-3p in the early detection and prognosis of NBNC-HCC patients.

Dysregulated expression of miR-19 has been shown to be involved in several types of solid tumors and represents one of the most investigated miRNAs in human cancer research [22]. Many studies have demonstrated that miR-19 plays a significant role in regulating and maintaining homeostasis of tissue function and immune regulation. Additionally, its dysregulation has been implicated in the pathogenesis and progression of tissue inflammation and fibrosis, as well as tumorigenesis [23]. For example, previous data suggests that serum miR-19a could be a biomarker for the early detection of colorectal cancer [24] and breast cancer [25]. Among studies related to HCC, most previous reports examine the expression of miR-19 in HCC cell lines or liver tissue specimens [26–31], with limited available data on blood-based samples [32]. For instance, miR-19 was shown to be up-regulated in tissue specimens and cell lines through the PTEN/Akt pathway in promoting HCC metastasis and chemoresistance [29,32]. In contrast, the expression level of miR-19a in human cancer specimens was significantly lower than that found in adjacent non-cancerous tissue, which might play an inhibitory role for HCC progression by targeting cyclin D1 [28]. This discrepancy might be due to several factors such as the etiologies and the heterogeneity of HCC, as well as differences in the studied HCC cell lines. Although miR-19 expression levels in HCC were rather inconsistent, a recent systematic review and meta-analysis revealed that up-regulated miR-19 expression was detected in HCC patients compared with non-malignant controls in most reports, indicating its crucial role in the diagnosis and prognosis of HCC [33]. Further studies are therefore required to elucidate the mechanism by which EV-miR-19-3p plays a crucial role in the development and progression of NBNC-HCC.

Our work had some limitations. The sample size was relatively small, and, thus, additional studies from multi-centers are required to confirm our findings. Secondly, although there are several potential etiologies for NBNC-HCC, the majority of our cases could likely be related to NAFLD, as other major causes of HCC including significant alcohol consumption were excluded at the initial enrollment. Moreover, most NBNC-HCC patients in our cohort had coexisting metabolic syndrome that was linked to NAFLD, as reported in most studies [34]. Thirdly, liver biopsy was not performed in patients with NAFLD. Although liver biopsy is currently the gold standard for diagnosis of NAFLD, this invasive method has limitations including sampling error, risk of complications, and is not feasible to perform in all patients. Instead, we used transient elastography, which is considered an accurate non-invasive tool to determine the severity of fibrosis and steatosis. Fourthly, this report was a cross-sectional cohort, and longitudinal studies to investigate the dynamic changes of the candidate EV-miRNAs should be further explored. Finally, one of the major challenges in applying EV miRNAs as diagnostic biomarkers is the lack of a

standardized method for EV isolation [35]. In this study, we selected Exoquick™ solution to enrich EVs from plasma. Compared with other techniques, this method is considered fast and easier to perform, and might be a better alternative for processing a large number of plasma samples in clinical setting. However, the potential drawback of this method is that it is non-selective and might yield low purity [15,36]. Despite these limitations, our results demonstrate that circulating EV-miR-19-3p is a reliable biomarker to differentiate between NBNC-HCC and non-HCC groups. Apart from its diagnostic role, plasma EV-miR-19-3p also serves as a good prognostic indicator for NBNC-HCC. This novel circulating biomarker might serve as a promising tool for the diagnosis and prognosis prediction of NBNC-HCC.

4. Materials and Methods

4.1. Research Subjects and Participant Consent

Blood samples for the assessment of EV-miRNAs were obtained from patients with NBNC-HCC who were followed-up at King Chulalongkorn Memorial Hospital (Bangkok, Thailand). All patients enrolled in this study were seronegative for HBsAg and anti-HCV, had no significant alcohol consumption (defined as >20 g ethanol/day in males and >10 g ethanol/day in females), and no coexisting causes of other chronic liver diseases such as autoimmune hepatitis, primary biliary cholangitis, or Wilson's disease. HCC was diagnosed on the basis of typical findings on imaging studies and/or histopathology according to the American Association for the Study of Liver Diseases (AASLD) guideline [37]. Briefly, diagnostic criteria with dynamic imaging were established by findings of focal lesions with hyper-attenuation at the arterial phase and hypo-attenuation at the portal phase. Liver biopsy or fine needle aspiration was performed in case of uncertain diagnosis after imaging studies. Baseline clinical parameters were recorded, including tumor staging classified by the BCLC staging system [38]. Blood and tissue samples were collected from patients prior to any HCC therapy, including liver resection, radiofrequency ablation and transarterial chemoembolization. Moreover, the OS of patients with NBNC-HCC defined by the interval between initial assessment and death or the last follow-up visit was documented.

Patients with NAFLD, who had no evidence of HCC, as well as other liver disease, and who were seronegative for both HBsAg and anti-HCV, were included as a control group. The diagnosis of NAFLD was according to the AASLD criteria as determined by the controlled attenuation parameter (CAP) using a FibroScan device (Echosens, Paris, France), with the cut-off >248 dB/m [39,40]. Among this group of patients, current and past daily alcohol intake was less than 20 g/week and none of the patients received any steatogenic medication. Additionally, individuals who had no underlying disorders and had normal vibration-controlled transient elastography and CAP values served as healthy controls. The study was conducted according to the Declaration of Helsinki. The protocol was approved by the Institutional Review Board (IRB) of the Faculty of Medicine, Chulalongkorn University, and all participants signed informed consent forms before collection of the samples.

4.2. Blood Collection and Plasma Processing

Blood samples obtained from each subject were processed by centrifugation at $12,000 \times g$ for 30 min at 4 °C and then stored at -80 °C until analysis for miRNA profiles in the discovery cohort using NanoString® nCounter miRNA Expression Assay (NanoString Technologies, Seattle, WA, USA) and the validation of miRNAs using the qRT-PCR technique (Applied Biosystems, Waltham, MA, USA).

4.3. EV Isolation

EVs were extracted from plasma samples using the ExoQuick™ Exosome Isolation Kit (SBI, System Biosciences, Palo Alto, CA, USA) according to the manufacturer's protocol. Briefly, for collecting the clear supernatant of plasma, 1 mL of the samples were incubated for 5 min with 8 μ L of thrombin (final concentration of 5 U/mL) before centrifugation at $10,000 \times g$ for 5 min at 4 °C. Next, 250 μ L of ExoQuick™ was added and incubated at 4 °C

for 30 min. The mixture of ExoQuick™-plasma samples were centrifuged to precipitate EVs at $1500\times g$ for 30 min. The pellet was then resuspended in $0.22\ \mu\text{m}$ -filtered $1\times$ PBS and stored at $-80\ ^\circ\text{C}$ until further use. For validation, $200\ \mu\text{L}$ of plasma samples were used.

4.4. EV Characterization

4.4.1. NTA

To characterize EVs from plasma, the quantity and size distribution of EVs in plasma samples were carried out using the NTA (Malvern Instruments, Malvern, UK). EVs were diluted 1000-fold for detecting between 50 and 100 particles per frame. Three 40-s videos were recorded with screen gain 3 and camera level 9 followed by an analysis of the data using NanoSight software (NTA 3.4 Build 3.4.003) with screen gain 9 and detection threshold 3.

4.4.2. TEM

To characterize the morphology and size of EVs, a $5\ \mu\text{L}$ drop of the suspension was loaded onto a 400 mesh formvar/carbon-coated grid (Electron Microscopy Sciences, Hatfield, PA, USA). To enhance the contrast between EVs and the background, grids were negatively stained with 2.5% uranyl acetate for 5 min. The excessive stain was blotted, and the grid was dried. Images were visualized under a transmission electron microscope using JEM-1400plus TEM (JEOL, Tokyo, Japan) at 80 kV.

4.4.3. Western Blotting

To detect EV protein markers by immunoblotting, EV samples were lysed using RIPA buffer with Proteinase and Phosphatase Inhibitor Cocktail (Merck, Rahway, NJ, USA). The lysates were sonicated with 7 sets of 3-s pulses using Sonics Vibra-Cell™ (Sonics & Materials, Newtown, CT, USA). EV proteins ($10\ \mu\text{g}$) were measured using Pierce™ BCA Protein Assay Kit (ThermoFisher Scientific, Waltham, MA, USA.) and loaded onto sodium dodecyl polyacrylamide gel electrophoresis. The proteins were then transferred to nitrocellulose membranes, blocked for 1 h with 5% BSA, and incubated at $4\ ^\circ\text{C}$ overnight with primary antibodies against TSG101 (1:1000) (Ab83, 4A10) (Abcam, Boston, MA, USA), HSP70 (1:1000) (4876, D69, Cell signaling), CD63 (1:2000) (Ab193349, MX-49.129.5, Abcam). To identify hepatocyte-specific markers, ASGPR1 (1:1000) (SC-52623, 8D7, Santa Cruz) was used [41,42]. Following this process, the membrane was stained with horseradish peroxidase-conjugated secondary antibodies for 1 h. Antigen-antibody reactions were visualized with an enhanced chemiluminescence detection reagent and images were acquired using a ChemiDoc Imaging System (Bio-Rad Laboratories, Hercules, CA, USA).

4.5. NanoString miRNA Expression Analysis

To extract miRNA from EVs, isolated EVs from the above-mentioned method was extracted using miRNeasy Serum/Plasma Kit (Qiagen, Hilden, Germany). Before applying to NanoString analysis, miRNA was concentrated and contamination minimized using an Amicon Ultra YM-3 filter (Merck Millipore, Burlington, NJ, USA). Briefly, $320\ \mu\text{L}$ of RNase-free water was added to the isolated miRNA, loaded onto the filter, and centrifuged at $14,000\times g$ at $25\ ^\circ\text{C}$ for 90 min. Three μL of the concentrated miRNAs were subjected to human NanoString nCounter miRNA expression assay (NanoString Technologies, Seattle, WA, USA) using, according to the manufacturer's instructions, the nCounter Human miRNA Panel v3 that evaluated 800 miRNAs. In brief, miRNAs were hybridized to capture and report probes at $65\ ^\circ\text{C}$ for 18 h, followed by purification and quantification on the nCounter Prep Station and Digital Analyzer. The resulting data were analyzed by nSolver 4.0 software to obtain the count of individual miRNA. The miRNA data were calculated by normalization to the top 100 miRNA counts in each sample.

4.6. EV and Tissue miRNA Extraction

To extract miRNA from EVs, isolated EVs from the above-mentioned method were extracted using the miRNeasy Serum/Plasma Kit (Qiagen, Hilden, Germany). For miRNA

extraction from tissues, approximately 30 µg of the liver tissue was used and the miRNAs were extracted using the RNeasy Fibrous Tissue Kit (Qiagen, Hilden, Germany), according to the manufacturer's recommendations. The quantity and quality of miRNA were measured using the DeNovix DS-11 Spectrophotometer (DeNovix, Wilmington, DE, USA).

4.7. Real-Time Quantitative Reverse Transcription PCR (qRT-PCR)

The miRNAs were reverse transcribed to complementary DNA (cDNA) by the SL-poly (A) sequence GTCGTATCCAGTGCAGGGTCCGAGGTATTCCGACTGGATACGA-CAAAAAAAAAAAAAAAAAAAVN using RevertAid First Strand cDNA Synthesis Kit (ThermoFisher Scientific). qRT-PCRs were performed in duplicate using the QPCR Green Master Mix HRox 4x (Biotechrabbit, Hennigsdorf, Germany). The reactions were detected by a QuantStudio 5 Real-Time PCR System (Applied Biosystems, Waltham, MA, USA). Reaction with no cDNA template was run as a negative control on every plate for each assay. Thermal cycling parameters were started with activation step at 95 °C for 10 min, followed by 40 cycles of denaturation at 95 °C for 15 s, and extension at 72 °C for 20 s with optimal annealing temperatures of each gene for 15 s. Primer sequences are listed in Table S1.

Four internal control miRNAs including U6, miR-26a-5p, miR-3144-3p, and miR-302d-3p from NanoString data were used to normalize the miRNA expressions. The results indicated that in the validation set of samples (n = 10 for healthy controls, n = 10 for NAFLD, and n = 9 for NBNC-HCC), all four miRNAs showed a similar Ct value, 29.92 ± 1.10 , 28.06 ± 1.21 , 31.987 ± 1.03 , and 29.46 ± 1.17 for U6, miR-26a-5p, miR-3144-3p, and miR-302d-3p, respectively (Figure S7a–d). However, miR-3144-3p and U6 exhibited the lowest % coefficient of variation of 3.23 and 3.69 compared to miR-26a-5p and miR-302d-3p (4.30 and 3.98, respectively). In this respect, it was suggested that the expression of miR-3144-3p and U6 were the most constant in our sample set. Thus, these miRNAs were suitable for normalization in the validated samples and data were calculated by the $2^{-\Delta\Delta CT}$ method.

4.8. Statistical Analysis

Data were analyzed by SPSS statistics version 22 (SPSS Inc., Chicago, IL, USA) and graph visualizations were constructed using GraphPad Prism 8.0 (GraphPad Software, La Jolla, CA, USA). To compare between groups, Chi's square or Fisher's exact test were applied for categorical variables and Student's *t*-test or one-way ANOVA were used for quantitative variables. The diagnostic performance was evaluated using ROC curve and the AUC with sensitivity and specificity analysis. The Kaplan–Meier analysis and log-rank test were calculated for the survival analysis. In addition, the Cox regression was applied for identifying independent factors associated with overall survival of patients with NBNC-HCC. A *p*-value < 0.05 was considered statistically significant.

Supplementary Materials: The following supporting information can be downloaded at: <https://www.mdpi.com/article/10.3390/ijms242216043/s1>.

Author Contributions: Conceptualization, B.B., N.C. and P.T.; Methodology, B.B., N.S. and N.C.; Software, B.B. and N.C.; Validation, B.B. and N.C.; Formal analysis, B.B. and N.C.; Investigation, B.B.; Resources, P.T. and N.P.; Data curation, P.T. and N.C.; Writing—original draft preparation, B.B.; Writing—review and editing, N.C. and P.T.; Visualization, B.B. and N.C.; Supervision, N.C. and P.T.; Project administration, P.T.; Funding acquisition, N.C. and P.T. All authors have read and agreed to the published version of the manuscript.

Funding: This study was supported by National Research Council of Thailand (NRCT) (N41A640187) and the Second Century Fund (C2F), Chulalongkorn University. This Research was funded by Thailand Science research and Innovation Fund Chulalongkorn University (HEA663000025) (Fundamental Fund 66), Program Management Unit for Human Resources & Institutional Development, Research and Innovation (PMU-B) (B36G660010), and Center of Excellence in Hepatitis and Liver Cancer, Faculty of Medicine, Chulalongkorn University. The funders had no role in study design, data collection and analysis, decision to publish, or preparation of the manuscript.

Institutional Review Board Statement: The study was conducted according to the guidelines of the Declaration of Helsinki, and approved by the IRB of Faculty of Medicine, Chulalongkorn University (IRB No. 909/64, COA No. 0042/2022).

Informed Consent Statement: Informed consent was obtained from all subjects involved in the study.

Data Availability Statement: This published article and the Supplementary Materials contain all of the established data or analyzed data throughout this study. Raw data for quantitative analysis may be provided by corresponding authors upon reasonable inquiry. Raw and normalized NanoString microarray data were submitted to the Gene Expression Omnibus (GEO) (accession number: GSE244605, <https://www.ncbi.nlm.nih.gov/geo/query/acc.cgi?acc=GSE244605>, accessed on 1 November 2023).

Acknowledgments: We would like to thank all of members in Center of Excellence in Hepatitis and Liver Cancer, Faculty of Medicine, Chulalongkorn University for their efforts in conducting the experiments.

Conflicts of Interest: The authors declare no conflict of interest.

References

- Singal, A.G.; Lampertico, P.; Nahon, P. Epidemiology and surveillance for hepatocellular carcinoma: New trends. *J. Hepatol.* **2020**, *72*, 250–261. [[CrossRef](#)] [[PubMed](#)]
- Li, J.; Zou, B.; Yeo, Y.H.; Feng, Y.; Xie, X.; Lee, D.H.; Fujii, H.; Wu, Y.; Kam, L.Y.; Ji, F.; et al. Prevalence, incidence, and outcome of non-alcoholic fatty liver disease in Asia, 1999–2019: A systematic review and meta-analysis. *Lancet Gastroenterol. Hepatol.* **2019**, *4*, 389–398. [[CrossRef](#)] [[PubMed](#)]
- Kulik, L.; El-Serag, H.B. Epidemiology and Management of Hepatocellular Carcinoma. *Gastroenterology* **2019**, *156*, 477–491.e1. [[CrossRef](#)]
- Hsu, P.Y.; Hsu, C.T.; Yeh, M.L.; Huang, C.F.; Huang, C.I.; Liang, P.C.; Lin, Y.H.; Hsieh, M.Y.; Wei, Y.J.; Hsieh, M.H.; et al. Early Fibrosis but Late Tumor Stage and Worse Outcomes in Hepatocellular Carcinoma Patients Without Hepatitis B or Hepatitis C. *Dig. Dis. Sci.* **2020**, *65*, 2120–2129. [[CrossRef](#)]
- Toyoda, H.; Kariyama, K.; Hiraoka, A.; Tsuji, K.; Ishikawa, T.; Hatanaka, T.; Naganuma, A.; Yasuda, S.; Nouse, K.; Kakizaki, S.; et al. Improved survival of viral hepatocellular carcinoma but not non-viral hepatocellular carcinoma from 2000 to 2020: A multi-centre cohort study of 6007 patients from high-volume academic centres in Japan. *Aliment. Pharmacol. Ther.* **2022**, *56*, 694–701. [[CrossRef](#)]
- von Felden, J.; Garcia-Lezana, T.; Schulze, K.; Losic, B.; Villanueva, A. Liquid biopsy in the clinical management of hepatocellular carcinoma. *Gut* **2020**, *69*, 2025–2034. [[CrossRef](#)]
- Cocucci, E.; Meldolesi, J. Exosomes and exosomes: Shedding the confusion between extracellular vesicles. *Trends Cell Biol.* **2015**, *25*, 364–372. [[CrossRef](#)]
- Alexander, M.; Hu, R.; Runtsch, M.C.; Kagele, D.A.; Mosbrugger, T.L.; Tolmachova, T.; Seabra, M.C.; Round, J.L.; Ward, D.M.; O’Connell, R.M. Exosome-delivered microRNAs modulate the inflammatory response to endotoxin. *Nat. Commun.* **2015**, *6*, 7321. [[CrossRef](#)]
- Li, A.; Zhang, T.; Zheng, M.; Liu, Y.; Chen, Z. Exosomal proteins as potential markers of tumor diagnosis. *J. Hematol. Oncol.* **2017**, *10*, 175. [[CrossRef](#)]
- Thind, A.; Wilson, C. Exosomal miRNAs as cancer biomarkers and therapeutic targets. *J. Extracell. Vesicles* **2016**, *5*, 31292. [[CrossRef](#)]
- Amorim, M.G.; Valieris, R.; Drummond, R.D.; Pizzi, M.P.; Freitas, V.M.; Sinigaglia-Coimbra, R.; Calin, G.A.; Pasqualini, R.; Arap, W.; Silva, I.T. A total transcriptome profiling method for plasma-derived extracellular vesicles: Applications for liquid biopsies. *Sci. Rep.* **2017**, *7*, 14395. [[CrossRef](#)] [[PubMed](#)]
- Li, Y.; Xiang, G.M.; Liu, L.L.; Liu, C.; Liu, F.; Jiang, D.N.; Pu, X.Y. Assessment of endogenous reference gene suitability for serum exosomal microRNA expression analysis in liver carcinoma resection studies. *Mol. Med. Rep.* **2015**, *12*, 4683–4691. [[CrossRef](#)] [[PubMed](#)]
- Li, Y.; Zhang, L.; Liu, F.; Xiang, G.; Jiang, D.; Pu, X. Identification of endogenous controls for analyzing serum exosomal miRNA in patients with hepatitis B or hepatocellular carcinoma. *Dis. Markers* **2015**, *2015*, 893594. [[CrossRef](#)]
- Forner, A.; Reig, M.; Bruix, J. α -fetoprotein for hepatocellular carcinoma diagnosis: The demise of a brilliant star. *Gastroenterology* **2009**, *137*, 26–29. [[CrossRef](#)]
- Szabo, G.; Momen-Heravi, F. Extracellular vesicles in liver disease and potential as biomarkers and therapeutic targets. *Nat. Rev. Gastroenterol. Hepatol.* **2017**, *14*, 455–466. [[CrossRef](#)] [[PubMed](#)]
- Vulif, M.; Shunkina, D.; Komar, A.; Bograya, M.; Zatulokin, P.; Kirienkova, E.; Gazatova, N.; Kozlov, I.; Litvinova, L. Analysis of miRNAs profiles in serum of patients with steatosis and steatohepatitis. *Front. Cell Dev. Biol.* **2021**, *9*, 736677. [[CrossRef](#)]
- Newman, L.A.; Useckaite, Z.; Johnson, J.; Sorich, M.J.; Hopkins, A.M.; Rowland, A. Selective isolation of liver-derived extracellular vesicles redefines performance of miRNA biomarkers for non-alcoholic fatty liver disease. *Biomedicines* **2022**, *10*, 195. [[CrossRef](#)]

18. Sorop, A.; Iacob, R.; Iacob, S.; Constantinescu, D.; Chitoiu, L.; Fertig, T.E.; Dinischiotu, A.; Chivu-Economescu, M.; Bacalbasa, N.; Savu, L. Plasma small extracellular vesicles derived miR-21-5p and miR-92a-3p as potential biomarkers for hepatocellular carcinoma screening. *Front. Genet.* **2020**, *11*, 712. [[CrossRef](#)]
19. Lin, J.; Lin, W.; Bai, Y.; Liao, Y.; Lin, Q.; Chen, L.; Wu, Y. Identification of exosomal hsa-miR-483-5p as a potential biomarker for hepatocellular carcinoma via microRNA expression profiling of tumor-derived exosomes. *Exp. Cell Res.* **2022**, *417*, 113232. [[CrossRef](#)]
20. Zou, X.; Wei, J.; Huang, Z.; Zhou, X.; Lu, Z.; Zhu, W.; Miao, Y. Identification of a six-miRNA panel in serum benefiting pancreatic cancer diagnosis. *Cancer Med.* **2019**, *8*, 2810–2822. [[CrossRef](#)]
21. Martens-Uzunova, E.S.; Kusuma, G.D.; Crucitta, S.; Lim, H.K.; Cooper, C.; Riches, J.E.; Azad, A.; Ochiya, T.; Boyle, G.M.; Southey, M.C. Androgens alter the heterogeneity of small extracellular vesicles and the small RNA cargo in prostate cancer. *J. Extracell. Vesicles* **2021**, *10*, e12136. [[CrossRef](#)] [[PubMed](#)]
22. Ardizzone, A.; Calabrese, G.; Campolo, M.; Filippone, A.; Giuffrida, D.; Esposito, F.; Colarossi, C.; Cuzzocrea, S.; Esposito, E.; Patemiti, I. Role of miRNA-19a in cancer diagnosis and poor prognosis. *Int. J. Mol. Sci.* **2021**, *22*, 4697. [[CrossRef](#)] [[PubMed](#)]
23. Li, X.; Teng, C.; Ma, J.; Fu, N.; Wang, L.; Wen, J.; Wang, T.-Y. miR-19 family: A promising biomarker and therapeutic target in heart, vessels and neurons. *Life Sci.* **2019**, *232*, 116651. [[CrossRef](#)] [[PubMed](#)]
24. Zheng, G.; Du, L.; Yang, X.; Zhang, X.; Wang, L.; Yang, Y.; Li, J.; Wang, C. Serum microRNA panel as biomarkers for early diagnosis of colorectal adenocarcinoma. *Br. J. Cancer* **2014**, *111*, 1985–1992. [[CrossRef](#)]
25. Sochor, M.; Basova, P.; Pesta, M.; Dusilkova, N.; Bartos, J.; Burda, P.; Pospisil, V.; Stopka, T. Oncogenic microRNAs: miR-155, miR-19a, miR-181b, and miR-24 enable monitoring of early breast cancer in serum. *BMC Cancer* **2014**, *14*, 448. [[CrossRef](#)]
26. Han, Z.-B.; Zhong, L.; Teng, M.-J.; Fan, J.-W.; Tang, H.-M.; Wu, J.-Y.; Chen, H.-Y.; Wang, Z.-W.; Qiu, G.-Q.; Peng, Z.-H. Identification of recurrence-related microRNAs in hepatocellular carcinoma following liver transplantation. *Mol. Oncol.* **2012**, *6*, 445–457. [[CrossRef](#)]
27. Hung, C.-L.; Yen, C.-S.; Tsai, H.-W.; Su, Y.-C.; Yen, C.-J. Upregulation of MicroRNA-19b predicts good prognosis in patients with hepatocellular carcinoma presenting with vascular invasion or multifocal disease. *BMC Cancer* **2015**, *15*, 665. [[CrossRef](#)]
28. Zhang, Y.; Guo, X.; Li, Z.; Li, B.; Li, Z.; Li, R.; Guo, Q.; Xiong, L.; Yu, L.; Zhao, J. A systematic investigation based on microRNA-mediated gene regulatory network reveals that dysregulation of microRNA-19a/Cyclin D1 axis confers an oncogenic potential and a worse prognosis in human hepatocellular carcinoma. *RNA Biol.* **2015**, *12*, 643–657. [[CrossRef](#)]
29. Jiang, X.-M.; Yu, X.-N.; Liu, T.-T.; Zhu, H.-R.; Shi, X.; Bilegsaikhan, E.; Guo, H.-Y.; Song, G.-Q.; Weng, S.-Q.; Huang, X.-X. microRNA-19a-3p promotes tumor metastasis and chemoresistance through the PTEN/Akt pathway in hepatocellular carcinoma. *Biomol. Pharmacother.* **2018**, *105*, 1147–1154. [[CrossRef](#)]
30. Hu, B.; Tang, W.G.; Fan, J.; Xu, Y.; Sun, H.X. Differentially expressed miRNAs in hepatocellular carcinoma cells under hypoxic conditions are associated with transcription and phosphorylation. *Oncol. Lett.* **2018**, *15*, 467–474. [[CrossRef](#)]
31. Sun, H.-X.; Yang, Z.-F.; Tang, W.-G.; Ke, A.-W.; Liu, W.-R.; Li, Y.; Gao, C.; Hu, B.; Fu, P.-Y.; Yu, M.-C. MicroRNA-19a-3p regulates cell growth through modulation of the PIK3IP1-AKT pathway in hepatocellular carcinoma. *J. Cancer* **2020**, *11*, 2476. [[CrossRef](#)] [[PubMed](#)]
32. Yu, G.; Chen, X.; Chen, S.; Ye, W.; Hou, K.; Liang, M. MiR-19a, miR-122 and miR-223 are differentially regulated by hepatitis B virus X protein and involve in cell proliferation in hepatoma cells. *J. Transl. Med.* **2016**, *14*, 122. [[CrossRef](#)] [[PubMed](#)]
33. Song, X.; Li, W.; Shen, P.; Bai, B.; Cao, L.-L. miR-19 is a potential clinical biomarker for gastrointestinal malignancy: A systematic review and meta-analysis. *BioMed Res. Int.* **2020**, *2020*, 2810150. [[CrossRef](#)]
34. Huang, D.Q.; El-Serag, H.B.; Loomba, R. Global epidemiology of NAFLD-related HCC: Trends, predictions, risk factors and prevention. *Nat. Rev. Gastroenterol. Hepatol.* **2021**, *18*, 223–238. [[CrossRef](#)] [[PubMed](#)]
35. Makler, A.; Asghar, W. Exosomal biomarkers for cancer diagnosis and patient monitoring. *Expert Rev. Mol. Diagn.* **2020**, *20*, 387–400. [[CrossRef](#)] [[PubMed](#)]
36. Tian, Y.; Gong, M.; Hu, Y.; Liu, H.; Zhang, W.; Zhang, M.; Hu, X.; Aubert, D.; Zhu, S.; Wu, L. Quality and efficiency assessment of six extracellular vesicle isolation methods by nano-flow cytometry. *J. Extracell. Vesicles* **2020**, *9*, 1697028. [[CrossRef](#)] [[PubMed](#)]
37. Bruix, J.; Sherman, M. Management of hepatocellular carcinoma: An update. *Hepatology* **2011**, *53*, 1020. [[CrossRef](#)]
38. Llovet, J.M.; Di Bisceglie, A.M.; Bruix, J.; Kramer, B.S.; Lencioni, R.; Zhu, A.X.; Sherman, M.; Schwartz, M.; Lotze, M.; Talwalkar, J. Design and endpoints of clinical trials in hepatocellular carcinoma. *J. Natl. Cancer Inst.* **2008**, *100*, 698–711. [[CrossRef](#)]
39. Karlas, T.; Petroff, D.; Sasso, M.; Fan, J.-G.; Mi, Y.-Q.; de Lédinghen, V.; Kumar, M.; Lupsor-Platon, M.; Han, K.-H.; Cardoso, A.C. Individual patient data meta-analysis of controlled attenuation parameter (CAP) technology for assessing steatosis. *J. Hepatol.* **2017**, *66*, 1022–1030. [[CrossRef](#)]
40. Chalasani, N.; Younossi, Z.; Lavine, J.E.; Charlton, M.; Cusi, K.; Rinella, M.; Harrison, S.A.; Brunt, E.M.; Sanyal, A.J. The diagnosis and management of nonalcoholic fatty liver disease: Practice guidance from the American Association for the Study of Liver Diseases. *Hepatology* **2018**, *67*, 328–357. [[CrossRef](#)]

41. Conde-Vancells, J.; Rodriguez-Suarez, E.; Embade, N.; Gil, D.; Matthiesen, R.; Valle, M.; Elortza, F.; Lu, S.C.; Mato, J.M.; Falcon-Perez, J.M. Characterization and comprehensive proteome profiling of exosomes secreted by hepatocytes. *J. Proteome Res.* **2008**, *7*, 5157–5166. [[CrossRef](#)] [[PubMed](#)]
42. Povero, D.; Yamashita, H.; Ren, W.; Subramanian, M.G.; Myers, R.P.; Eguchi, A.; Simonetto, D.A.; Goodman, Z.D.; Harrison, S.A.; Sanyal, A.J. Characterization and proteome of circulating extracellular vesicles as potential biomarkers for NASH. *Hepatol. Commun.* **2020**, *4*, 1263–1278. [[CrossRef](#)] [[PubMed](#)]

Disclaimer/Publisher's Note: The statements, opinions and data contained in all publications are solely those of the individual author(s) and contributor(s) and not of MDPI and/or the editor(s). MDPI and/or the editor(s) disclaim responsibility for any injury to people or property resulting from any ideas, methods, instructions or products referred to in the content.

REFERENCES

1. Singal AG, Lampertico P, Nahon P. Epidemiology and surveillance for hepatocellular carcinoma: New trends. *J Hepatol.* 2020;72(2):250-61.
2. Li J, Zou B, Yeo YH, Feng Y, Xie X, Lee DH, et al. Prevalence, incidence, and outcome of non-alcoholic fatty liver disease in Asia, 1999-2019: a systematic review and meta-analysis. *Lancet Gastroenterol Hepatol.* 2019;4(5):389-98.
3. Kulik L, El-Serag HB. Epidemiology and Management of Hepatocellular Carcinoma. *Gastroenterology.* 2019;156(2):477-91 e1.
4. Hsu PY, Hsu CT, Yeh ML, Huang CF, Huang CI, Liang PC, et al. Early Fibrosis but Late Tumor Stage and Worse Outcomes in Hepatocellular Carcinoma Patients Without Hepatitis B or Hepatitis C. *Dig Dis Sci.* 2020;65(7):2120-9.
5. von Felden J, Garcia-Lezana T, Schulze K, Losic B, Villanueva A. Liquid biopsy in the clinical management of hepatocellular carcinoma. *Gut.* 2020;69(11):2025-34.
6. Cocucci E, Meldolesi J. Ectosomes and exosomes: shedding the confusion between extracellular vesicles. *Trends in cell biology.* 2015;25(6):364-72.
7. Alexander M, Hu R, Runtsch MC, Kagele DA, Mosbrugger TL, Tolmachova T, et al. Exosome-delivered microRNAs modulate the inflammatory response to endotoxin. *Nature communications.* 2015;6(1):1-16.
8. Li A, Zhang T, Zheng M, Liu Y, Chen Z. Exosomal proteins as potential markers of tumor diagnosis. *Journal of hematology & oncology.* 2017;10(1):1-9.
9. James SL, Abate D, Abate KH, Abay SM, Abbafati C, Abbasi N, et al. Global, regional, and national incidence, prevalence, and years lived with disability for 354 diseases and injuries for 195 countries and territories, 1990–2017: a systematic analysis for the Global Burden of Disease Study 2017. *The Lancet.* 2018;392(10159):1789-858.
10. Younossi ZM, Koenig AB, Abdelatif D, Fazel Y, Henry L, Wymer M. Global epidemiology of nonalcoholic fatty liver disease—meta-analytic assessment of prevalence, incidence, and outcomes. *Hepatology.* 2016;64(1):73-84.
11. Chalasani N, Younossi Z, Lavine JE, Diehl AM, Brunt EM, Cusi K, et al. The diagnosis and management of non-alcoholic fatty liver disease: Practice Guideline by the American Association for the Study of Liver Diseases, American College of Gastroenterology, and the American Gastroenterological Association. *Hepatology.* 2012;55(6):2005-23.
12. Burt AD, Lackner C, Tiniakos DG, editors. *Diagnosis and assessment of NAFLD: definitions and histopathological classification. Seminars in liver disease;* 2015: Thieme Medical Publishers.
13. White DL, Kanwal F, El-Serag HB. Association between nonalcoholic fatty liver disease and risk for hepatocellular cancer, based on systematic review. *Clinical gastroenterology and hepatology.* 2012;10(12):1342-59. e2.
14. Choudhury J, Sanyal AJ. Insulin resistance and the pathogenesis of nonalcoholic fatty liver disease. *Clinics in liver disease.* 2004;8(3):575-94.
15. Lomonaco R, Ortiz-Lopez C, Orsak B, Webb A, Hardies J, Darland C, et al. Effect of adipose tissue insulin resistance on metabolic parameters and liver histology in obese patients with nonalcoholic fatty liver disease. *Hepatology.* 2012;55(5):1389-97.
16. Pal M, Febbraio MA, Lancaster GI. The roles of c-Jun NH2-terminal kinases

- (JNKs) in obesity and insulin resistance. *The Journal of physiology*. 2016;594(2):267-79.
17. Gadd VL, Skoien R, Powell EE, Fagan KJ, Winterford C, Horsfall L, et al. The portal inflammatory infiltrate and ductular reaction in human nonalcoholic fatty liver disease. *Hepatology*. 2014;59(4):1393-405.
 18. Wolf MJ, Adili A, Piotrowitz K, Abdullah Z, Boege Y, Stemmer K, et al. Metabolic activation of intrahepatic CD8+ T cells and NKT cells causes nonalcoholic steatohepatitis and liver cancer via cross-talk with hepatocytes. *Cancer cell*. 2014;26(4):549-64.
 19. Bieghs V, Trautwein C. The innate immune response during liver inflammation and metabolic disease. *Trends in immunology*. 2013;34(9):446-52.
 20. Younossi Z, Anstee QM, Marietti M, Hardy T, Henry L, Eslam M, et al. Global burden of NAFLD and NASH: trends, predictions, risk factors and prevention. *Nature reviews Gastroenterology & hepatology*. 2018;15(1):11-20.
 21. Liu Y-L, Reeves HL, Burt AD, Tiniakos D, McPherson S, Leathart JB, et al. TM6SF2 rs58542926 influences hepatic fibrosis progression in patients with non-alcoholic fatty liver disease. *Nature communications*. 2014;5(1):1-6.
 22. Valenti L, Al-Serri A, Daly AK, Galmozzi E, Rametta R, Dongiovanni P, et al. Homozygosity for the patatin-like phospholipase-3/adiponutrin I148M polymorphism influences liver fibrosis in patients with nonalcoholic fatty liver disease. *Hepatology*. 2010;51(4):1209-17.
 23. Fracanzani AL, Petta S, Lombardi R, Pisano G, Russello M, Consonni D, et al. Liver and cardiovascular damage in patients with lean nonalcoholic fatty liver disease, and association with visceral obesity. *Clinical Gastroenterology and Hepatology*. 2017;15(10):1604-11. e1.
 24. Conus F, Rabasa-Lhoret R, Peronnet F. Characteristics of metabolically obese normal-weight (MONW) subjects. *Applied physiology, nutrition, and metabolism*. 2007;32(1):4-12.
 25. Younossi ZM, Otgonsuren M, Venkatesan C, Mishra A. In patients with non-alcoholic fatty liver disease, metabolically abnormal individuals are at a higher risk for mortality while metabolically normal individuals are not. *Metabolism*. 2013;62(3):352-60.
 26. Gerber L, Otgonsuren M, Mishra A, Escheik C, Biredinc A, Stepanova M, et al. Non-alcoholic fatty liver disease (NAFLD) is associated with low level of physical activity: a population-based study. *Alimentary pharmacology & therapeutics*. 2012;36(8):772-81.
 27. Younossi ZM, Otgonsuren M, Henry L, Venkatesan C, Mishra A, Erario M, et al. Association of nonalcoholic fatty liver disease (NAFLD) with hepatocellular carcinoma (HCC) in the United States from 2004 to 2009. *Hepatology*. 2015;62(6):1723-30.
 28. Piscaglia F, Svegliati-Baroni G, Barchetti A, Pecorelli A, Marinelli S, Tiribelli C, et al. Clinical patterns of hepatocellular carcinoma in nonalcoholic fatty liver disease: a multicenter prospective study. *Hepatology*. 2016;63(3):827-38.
 29. Dyson J, Jaques B, Chattopadhyay D, Lochan R, Graham J, Das D, et al. Hepatocellular cancer: the impact of obesity, type 2 diabetes and a multidisciplinary team. *Journal of hepatology*. 2014;60(1):110-7.
 30. Lindenmeyer CC, McCullough AJ. The natural history of nonalcoholic fatty

- liver disease—an evolving view. *Clinics in liver disease*. 2018;22(1):11-21.
31. Anstee QM, Reeves HL, Kotsiliti E, Govaere O, Heikenwalder M. From NASH to HCC: current concepts and future challenges. *Nature reviews Gastroenterology & hepatology*. 2019;16(7):411-28.
 32. Singh S, Allen AM, Wang Z, Prokop LJ, Murad MH, Loomba R. Fibrosis progression in nonalcoholic fatty liver vs nonalcoholic steatohepatitis: a systematic review and meta-analysis of paired-biopsy studies. *Clinical gastroenterology and hepatology*. 2015;13(4):643-54. e9.
 33. Sherman M, Bruix J. *Biopsy for liver cancer: How to balance research needs with evidence-based clinical practice*. Wiley Online Library; 2015.
 34. Friemel J, Rechsteiner M, Frick L, Böhm F, Struckmann K, Egger M, et al. Intratumor heterogeneity in hepatocellular carcinoma. *Clinical Cancer Research*. 2015;21(8):1951-61.
 35. Dulai PS, Sirlin CB, Loomba R. MRI and MRE for non-invasive quantitative assessment of hepatic steatosis and fibrosis in NAFLD and NASH: clinical trials to clinical practice. *Journal of hepatology*. 2016;65(5):1006-16.
 36. Karlas T, Petroff D, Sasso M, Fan J-G, Mi Y-Q, de Lédinghen V, et al. Individual patient data meta-analysis of controlled attenuation parameter (CAP) technology for assessing steatosis. *Journal of hepatology*. 2017;66(5):1022-30.
 37. Younossi ZM, Loomba R, Anstee QM, Rinella ME, Bugianesi E, Marchesini G, et al. Diagnostic modalities for nonalcoholic fatty liver disease, nonalcoholic steatohepatitis, and associated fibrosis. *Hepatology*. 2018;68(1):349-60.
 38. Feldstein AE, Wieckowska A, Lopez AR, Liu YC, Zein NN, McCullough AJ. Cytokeratin-18 fragment levels as noninvasive biomarkers for nonalcoholic steatohepatitis: a multicenter validation study. *Hepatology*. 2009;50(4):1072-8.
 39. Huang X, Sun L, Wen S, Deng D, Wan F, He X, et al. RNA sequencing of plasma exosomes revealed novel functional long noncoding RNAs in hepatocellular carcinoma. *Cancer science*. 2020;111(9):3338.
 40. Cusi K, Chang Z, Harrison S, Lomonaco R, Bril F, Orsak B, et al. Limited value of plasma cytokeratin-18 as a biomarker for NASH and fibrosis in patients with non-alcoholic fatty liver disease. *Journal of hepatology*. 2014;60(1):167-74.
 41. Vilar-Gomez E, Martinez-Perez Y, Calzadilla-Bertot L, Torres-Gonzalez A, Gra-Oramas B, Gonzalez-Fabian L, et al. Weight loss through lifestyle modification significantly reduces features of nonalcoholic steatohepatitis. *Gastroenterology*. 2015;149(2):367-78. e5.
 42. Llovet JM, Brú C, Bruix J, editors. *Prognosis of hepatocellular carcinoma: the BCLC staging classification*. *Seminars in liver disease*; 1999: © 1999 by Thieme Medical Publishers, Inc.
 43. Llovet JM, Real MI, Montaña X, Planas R, Coll S, Aponte J, et al. Arterial embolisation or chemoembolisation versus symptomatic treatment in patients with unresectable hepatocellular carcinoma: a randomised controlled trial. *The Lancet*. 2002;359(9319):1734-9.
 44. Llovet JM, Ricci S, Mazzaferro V, Hilgard P, Gane E, Blanc J-F, et al. Sorafenib in advanced hepatocellular carcinoma. *New England journal of medicine*. 2008;359(4):378-90.
 45. Friedman SL, Neuschwander-Tetri BA, Rinella M, Sanyal AJ. Mechanisms of NAFLD development and therapeutic strategies. *Nature medicine*. 2018;24(7):908-22.

46. Théry C, Witwer KW, Aikawa E, Alcaraz MJ, Anderson JD, Andriantsitohaina R, et al. Minimal information for studies of extracellular vesicles 2018 (MISEV2018): a position statement of the International Society for Extracellular Vesicles and update of the MISEV2014 guidelines. *Journal of extracellular vesicles*. 2018;7(1):1535750.
47. Conde-Vancells J, Rodriguez-Suarez E, Embade N, Gil D, Matthiesen R, Valle M, et al. Characterization and comprehensive proteome profiling of exosomes secreted by hepatocytes. *Journal of proteome research*. 2008;7(12):5157-66.
48. Colombo M, Raposo G, Théry C. Biogenesis, secretion, and intercellular interactions of exosomes and other extracellular vesicles. *Annual review of cell and developmental biology*. 2014;30:255-89.
49. Yáñez-Mó M, Siljander PR-M, Andreu Z, Bedina Zavec A, Borràs FE, Buzas EI, et al. Biological properties of extracellular vesicles and their physiological functions. *Journal of extracellular vesicles*. 2015;4(1):27066.
50. Szabo G, Momen-Heravi F. Extracellular vesicles in liver disease and potential as biomarkers and therapeutic targets. *Nature reviews Gastroenterology & hepatology*. 2017;14(8):455.
51. Todorova D, Simoncini S, Lacroix R, Sabatier F, Dignat-George F. Extracellular vesicles in angiogenesis. *Circulation research*. 2017;120(10):1658-73.
52. Povero D, Yamashita H, Ren W, Subramanian MG, Myers RP, Eguchi A, et al. Characterization and proteome of circulating extracellular vesicles as potential biomarkers for NASH. *Hepatology communications*. 2020;4(9):1263-78.
53. Goretti E, Wagner DR, Devaux Y. miRNAs as biomarkers of myocardial infarction: a step forward towards personalized medicine? *Trends in molecular medicine*. 2014;20(12):716-25.
54. Johnson TK, Zhao L, Zhu D, Wang Y, Xiao Y, Oguljahan B, et al. Exosomes derived from induced vascular progenitor cells promote angiogenesis in vitro and in an in vivo rat hindlimb ischemia model. *American Journal of Physiology-Heart and Circulatory Physiology*. 2019;317(4):H765-H76.
55. Matsumura T, Sugimachi K, Iinuma H, Takahashi Y, Kurashige J, Sawada G, et al. Exosomal microRNA in serum is a novel biomarker of recurrence in human colorectal cancer. *British journal of cancer*. 2015;113(2):275-81.
56. Momen-Heravi F, Saha B, Kodys K, Catalano D, Satishchandran A, Szabo G. Increased number of circulating exosomes and their microRNA cargos are potential novel biomarkers in alcoholic hepatitis. *Journal of translational medicine*. 2015;13(1):1-13.
57. Xu H, Zhao G, Zhang Y, Jiang H, Wang W, Zhao D, et al. Mesenchymal stem cell-derived exosomal microRNA-133b suppresses glioma progression via Wnt/ β -catenin signaling pathway by targeting EZH2. *Stem cell research & therapy*. 2019;10(1):1-14.
58. Nik Mohamed Kamal NNSB, Shahidan WNS. Non-exosomal and exosomal circulatory microRNAs: Which are more valid as biomarkers? *Frontiers in pharmacology*. 2020;10:1500.
59. Sorop A, Constantinescu D, Cojocaru F, Dinischiotu A, Cucu D, Dima SO. Exosomal microRNAs as Biomarkers and Therapeutic Targets for Hepatocellular Carcinoma. *International Journal of Molecular Sciences*. 2021;22(9):4997.
60. Devhare PB, Ray RB. Extracellular vesicles: Novel mediator for cell to cell communications in liver pathogenesis. *Molecular aspects of medicine*. 2018;60:115-22.

61. Szabo G, Momen-Heravi F. Extracellular vesicles in liver disease and potential as biomarkers and therapeutic targets. *Nature reviews Gastroenterology & hepatology*. 2017;14(8):455-66.
62. Cui Y, Xu H-F, Liu M-Y, Xu Y-J, He J-C, Zhou Y, et al. Mechanism of exosomal microRNA-224 in development of hepatocellular carcinoma and its diagnostic and prognostic value. *World journal of gastroenterology*. 2019;25(15):1890.
63. Sohn W, Kim J, Kang SH, Yang SR, Cho J-Y, Cho HC, et al. Serum exosomal microRNAs as novel biomarkers for hepatocellular carcinoma. *Experimental & molecular medicine*. 2015;47(9):e184-e.
64. He Y, Rodrigues RM, Wang X, Seo W, Ma J, Hwang S, et al. Neutrophil-to-hepatocyte communication via LDLR-dependent miR-223-enriched extracellular vesicle transfer ameliorates nonalcoholic steatohepatitis. *The Journal of clinical investigation*. 2021;131(3).
65. Hirsova P, Gores GJ. Death receptor-mediated cell death and proinflammatory signaling in nonalcoholic steatohepatitis. *Cellular and molecular gastroenterology and hepatology*. 2015;1(1):17-27.
66. Kakazu E, Mauer AS, Yin M, Malhi H. Hepatocytes release ceramide-enriched pro-inflammatory extracellular vesicles in an IRE1 α -dependent manner [S]. *Journal of lipid research*. 2016;57(2):233-45.
67. Martínez L, Torres S, Baulies A, Alarcón-Vila C, Elena M, Fabriàs G, et al. Myristic acid potentiates palmitic acid-induced lipotoxicity and steatohepatitis associated with lipodystrophy by sustaining de novo ceramide synthesis. *Oncotarget*. 2015;6(39):41479.
68. Lebeau PF, Byun JH, Platko K, MacDonald ME, Poon SV, Faiyaz M, et al. Diet-induced hepatic steatosis abrogates cell-surface LDLR by inducing de novo PCSK9 expression in mice. *Journal of Biological Chemistry*. 2019;294(23):9037-47.
69. Kakazu E, Mauer AS, Yin M, Malhi H. Hepatocytes release ceramide-enriched pro-inflammatory extracellular vesicles in an IRE1 α -dependent manner. *J Lipid Res*. 2016;57(2):233-45.
70. Hirsova P, Ibrahim SH, Krishnan A, Verma VK, Bronk SF, Werneburg NW, et al. Lipid-Induced Signaling Causes Release of Inflammatory Extracellular Vesicles From Hepatocytes. *Gastroenterology*. 2016;150(4):956-67.
71. Schuster S, Cabrera D, Arrese M, Feldstein AE. Triggering and resolution of inflammation in NASH. *Nature Reviews Gastroenterology & Hepatology*. 2018;15(6):349-64.
72. Guillot A, Tacke F. Liver Macrophages: Old Dogmas and New Insights. *Hepatol Commun*. 2019;3(6):730-43.
73. McGettigan B, McMahan R, Orlicky D, Burchill M, Danhorn T, Francis P, et al. Dietary Lipids Differentially Shape Nonalcoholic Steatohepatitis Progression and the Transcriptome of Kupffer Cells and Infiltrating Macrophages. *Hepatology*. 2019;70(1):67-83.
74. Ramachandran P, Pellicoro A, Vernon MA, Boulter L, Aucott RL, Ali A, et al. Differential Ly-6C expression identifies the recruited macrophage phenotype, which orchestrates the regression of murine liver fibrosis. *Proceedings of the National Academy of Sciences*. 2012;109(46):E3186-E95.
75. Duffield JS, Forbes SJ, Constandinou CM, Clay S, Partolina M, Vuthoori S, et al. Selective depletion of macrophages reveals distinct, opposing roles during liver

- injury and repair. *The Journal of clinical investigation*. 2005;115(1):56-65.
76. Aucher A, Rudnicka D, Davis DM. MicroRNAs transfer from human macrophages to hepato-carcinoma cells and inhibit proliferation. *J Immunol*. 2013;191(12):6250-60.
77. Ismail N, Wang Y, Dakhllallah D, Moldovan L, Agarwal K, Batte K, et al. Macrophage microvesicles induce macrophage differentiation and miR-223 transfer. *Blood*. 2013;121(6):984-95.
78. Hou X, Yin S, Ren R, Liu S, Yong L, Liu Y, et al. Myeloid cell-specific IL-6 signaling promotes miR-223-enriched exosome production to attenuate NAFLD-associated fibrosis. *Hepatology (Baltimore, Md)*. 2020.
79. Mulcahy LA, Pink RC, Carter DR. Routes and mechanisms of extracellular vesicle uptake. *J Extracell Vesicles*. 2014;3.
80. Murphy DE, de Jong OG, Brouwer M, Wood MJ, Lavieu G, Schiffelers RM, et al. Extracellular vesicle-based therapeutics: natural versus engineered targeting and trafficking. *Experimental & Molecular Medicine*. 2019;51(3):1-12.
81. Nanbo A, Kawanishi E, Yoshida R, Yoshiyama H. Exosomes Derived from Epstein-Barr Virus-Infected Cells Are Internalized via Caveola-Dependent Endocytosis and Promote Phenotypic Modulation in Target Cells. *Journal of Virology*. 2013;87(18):10334-47.
82. Wei F, Ma C, Zhou T, Dong X, Luo Q, Geng L, et al. Exosomes derived from gemcitabine-resistant cells transfer malignant phenotypic traits via delivery of miRNA-222-3p. *Molecular Cancer*. 2017;16(1):132.
83. Lagace TA. PCSK9 and LDLR degradation: regulatory mechanisms in circulation and in cells. *Curr Opin Lipidol*. 2014;25(5):387-93.
84. Weinreich M, Frishman WH. Antihyperlipidemic Therapies Targeting PCSK9. *Cardiology in Review*. 2014;22(3):140-6.
85. Bruix J, Sherman M. Management of hepatocellular carcinoma: an update. *Hepatology (Baltimore, Md)*. 2011;53(3):1020.
86. Llovet JM, Di Bisceglie AM, Bruix J, Kramer BS, Lencioni R, Zhu AX, et al. Design and endpoints of clinical trials in hepatocellular carcinoma. *Journal of the National Cancer Institute*. 2008;100(10):698-711.
87. Chalasani N, Younossi Z, Lavine JE, Charlton M, Cusi K, Rinella M, et al. The diagnosis and management of nonalcoholic fatty liver disease: practice guidance from the American Association for the Study of Liver Diseases. *Hepatology*. 2018;67(1):328-57.
88. Alexander M, Hu R, Runtsch MC, Kagele DA, Mosbrugger TL, Tolmachova T, et al. Exosome-delivered microRNAs modulate the inflammatory response to endotoxin. *Nature communications*. 2015;6(1):7321.
89. Arab T, Mallick ER, Huang Y, Dong L, Liao Z, Zhao Z, et al. Characterization of extracellular vesicles and synthetic nanoparticles with four orthogonal single-particle analysis platforms. *J Extracell Vesicles*. 2021;10(6):e12079.
90. Akazawa Y, Cazanave S, Mott JL, Elmi N, Bronk SF, Kohno S, et al. Palmitoleate attenuates palmitate-induced Bim and PUMA up-regulation and hepatocyte lipoapoptosis. *Journal of hepatology*. 2010;52(4):586-93.
91. Amorim MG, Valieris R, Drummond RD, Pizzi MP, Freitas VM, Sinigaglia-Coimbra R, et al. A total transcriptome profiling method for plasma-derived extracellular vesicles: applications for liquid biopsies. *Scientific reports*. 2017;7(1):1-11.

92. Li Y, Xiang GM, Liu LL, Liu C, Liu F, Jiang DN, et al. Assessment of endogenous reference gene suitability for serum exosomal microRNA expression analysis in liver carcinoma resection studies. *Molecular medicine reports*. 2015;12(3):4683-91.
93. Li Y, Zhang L, Liu F, Xiang G, Jiang D, Pu X. Identification of endogenous controls for analyzing serum exosomal miRNA in patients with hepatitis B or hepatocellular carcinoma. *Disease markers*. 2015;2015.
94. Morinaga H, Mayoral R, Heinrichsdorff J, Osborn O, Franck N, Hah N, et al. Characterization of distinct subpopulations of hepatic macrophages in HFD/obese mice. *Diabetes*. 2015;64(4):1120-30.
95. Jin X, Kruth HS. Culture of macrophage colony-stimulating factor differentiated human monocyte-derived macrophages. *JoVE (Journal of Visualized Experiments)*. 2016(112):e54244.
96. Li M, He Y, Zhou Z, Ramirez T, Gao Y, Gao Y, et al. MicroRNA-223 ameliorates alcoholic liver injury by inhibiting the IL-6-p47phox-oxidative stress pathway in neutrophils. *Gut*. 2017;66(4):705-15.
97. Long C, Cen S, Zhong Z, Zhou C, Zhong G. FOXO3 is targeted by miR-223-3p and promotes osteogenic differentiation of bone marrow mesenchymal stem cells by enhancing autophagy. *Human Cell*. 2021;34:14-27.
98. Zhou Y, Chen E, Tang Y, Mao J, Shen J, Zheng X, et al. miR-223 overexpression inhibits doxorubicin-induced autophagy by targeting FOXO3a and reverses chemoresistance in hepatocellular carcinoma cells. *Cell Death & Disease*. 2019;10(11):843.
99. Wang X, Sommerfeld MR, Jahn-Hofmann K, Cai B, Filliol A, Remotti HE, et al. A Therapeutic Silencing RNA Targeting Hepatocyte TAZ Prevents and Reverses Fibrosis in Nonalcoholic Steatohepatitis in Mice. *Hepatology*. 2019;3(9):1221-34.
100. He Y, Hwang S, Cai Y, Kim SJ, Xu M, Yang D, et al. MicroRNA-223 ameliorates nonalcoholic steatohepatitis and cancer by targeting multiple inflammatory and oncogenic genes in hepatocytes. *Hepatology*. 2019;70(4):1150-67.
101. Forner A, Reig M, Bruix J. α -fetoprotein for hepatocellular carcinoma diagnosis: the demise of a brilliant star. *Gastroenterology*. 2009;137(1):26-9.
102. Vulf M, Shunkina D, Komar A, Bograya M, Zatulokin P, Kirienkova E, et al. Analysis of miRNAs profiles in serum of patients with steatosis and steatohepatitis. *Frontiers in Cell and Developmental Biology*. 2021;9:736677.
103. Newman LA, Useckaite Z, Johnson J, Sorich MJ, Hopkins AM, Rowland A. Selective isolation of liver-derived extracellular vesicles redefines performance of miRNA biomarkers for non-alcoholic fatty liver disease. *Biomedicines*. 2022;10(1):195.
104. Sorop A, Iacob R, Iacob S, Constantinescu D, Chitoiu L, Fertig TE, et al. Plasma small extracellular vesicles derived miR-21-5p and miR-92a-3p as potential biomarkers for hepatocellular carcinoma screening. *Frontiers in Genetics*. 2020;11:712.
105. Lin J, Lin W, Bai Y, Liao Y, Lin Q, Chen L, et al. Identification of exosomal hsa-miR-483-5p as a potential biomarker for hepatocellular carcinoma via microRNA expression profiling of tumor-derived exosomes. *Experimental Cell Research*. 2022;417(2):113232.
106. Zou X, Wei J, Huang Z, Zhou X, Lu Z, Zhu W, et al. Identification of a six-miRNA panel in serum benefiting pancreatic cancer diagnosis. *Cancer medicine*. 2019;8(6):2810-22.

107. Martens-Uzunova ES, Kusuma GD, Crucitta S, Lim HK, Cooper C, Riches JE, et al. Androgens alter the heterogeneity of small extracellular vesicles and the small RNA cargo in prostate cancer. *Journal of Extracellular Vesicles*. 2021;10(10):e12136.
108. Ardizzone A, Calabrese G, Campolo M, Filippone A, Giuffrida D, Esposito F, et al. Role of miRNA-19a in cancer diagnosis and poor prognosis. *International journal of molecular sciences*. 2021;22(9):4697.
109. Li X, Teng C, Ma J, Fu N, Wang L, Wen J, et al. miR-19 family: a promising biomarker and therapeutic target in heart, vessels and neurons. *Life sciences*. 2019;232:116651.
110. Zheng G, Du L, Yang X, Zhang X, Wang L, Yang Y, et al. Serum microRNA panel as biomarkers for early diagnosis of colorectal adenocarcinoma. *British journal of cancer*. 2014;111(10):1985-92.
111. Sochor M, Basova P, Pesta M, Dusilkova N, Bartos J, Burda P, et al. Oncogenic microRNAs: miR-155, miR-19a, miR-181b, and miR-24 enable monitoring of early breast cancer in serum. *BMC cancer*. 2014;14(1):1-7.
112. Han Z-B, Zhong L, Teng M-J, Fan J-W, Tang H-M, Wu J-Y, et al. Identification of recurrence-related microRNAs in hepatocellular carcinoma following liver transplantation. *Molecular oncology*. 2012;6(4):445-57.
113. Hung C-L, Yen C-S, Tsai H-W, Su Y-C, Yen C-J. Upregulation of MicroRNA-19b predicts good prognosis in patients with hepatocellular carcinoma presenting with vascular invasion or multifocal disease. *BMC cancer*. 2015;15(1):1-10.
114. Zhang Y, Guo X, Li Z, Li B, Li Z, Li R, et al. A systematic investigation based on microRNA-mediated gene regulatory network reveals that dysregulation of microRNA-19a/Cyclin D1 axis confers an oncogenic potential and a worse prognosis in human hepatocellular carcinoma. *RNA biology*. 2015;12(6):643-57.
115. Jiang X-M, Yu X-N, Liu T-T, Zhu H-R, Shi X, Bilegsaikhan E, et al. microRNA-19a-3p promotes tumor metastasis and chemoresistance through the PTEN/Akt pathway in hepatocellular carcinoma. *Biomedicine & Pharmacotherapy*. 2018;105:1147-54.
116. Hu B, Tang WG, Fan J, Xu Y, Sun HX. Differentially expressed miRNAs in hepatocellular carcinoma cells under hypoxic conditions are associated with transcription and phosphorylation. *Oncology Letters*. 2018;15(1):467-74.
117. Sun H-X, Yang Z-F, Tang W-G, Ke A-W, Liu W-r, Li Y, et al. MicroRNA-19a-3p regulates cell growth through modulation of the PIK3IP1-AKT pathway in hepatocellular carcinoma. *Journal of Cancer*. 2020;11(9):2476.
118. Yu G, Chen X, Chen S, Ye W, Hou K, Liang M. MiR-19a, miR-122 and miR-223 are differentially regulated by hepatitis B virus X protein and involve in cell proliferation in hepatoma cells. *Journal of translational medicine*. 2016;14:1-13.
119. Song X, Li W, Shen P, Bai B, Cao L-L. miR-19 is a potential clinical biomarker for gastrointestinal malignancy: a systematic review and meta-analysis. *BioMed Research International*. 2020;2020.
120. Wu K, Feng J, Lyu F, Xing F, Sharma S, Liu Y, et al. Exosomal miR-19a and IBSP cooperate to induce osteolytic bone metastasis of estrogen receptor-positive breast cancer. *Nature Communications*. 2021;12(1):5196.
121. Way KJ, Dinh H, Keene MR, White KE, Clanchy FI, Lusby P, et al. The generation and properties of human macrophage populations from hemopoietic stem cells. *Journal of Leucocyte Biology*. 2009;85(5):766-78.

122. Mantovani A, Sozzani S, Locati M, Allavena P, Sica A. Macrophage polarization: tumor-associated macrophages as a paradigm for polarized M2 mononuclear phagocytes. *Trends in immunology*. 2002;23(11):549-55.
123. Mosser DM, Edwards JP. Exploring the full spectrum of macrophage activation. *Nature reviews immunology*. 2008;8(12):958-69.
124. Lacey DC, Achuthan A, Fleetwood AJ, Dinh H, Roiniotis J, Scholz GM, et al. Defining GM-CSF–and macrophage-CSF–dependent macrophage responses by in vitro models. *The Journal of Immunology*. 2012;188(11):5752-65.
125. Ye D, Zhang T, Lou G, Liu Y. Role of miR-223 in the pathophysiology of liver diseases. *Exp Mol Med*. 2018;50(9):1-12.
126. Li M, He Y, Zhou Z, Ramirez T, Gao Y, Gao Y, et al. MicroRNA-223 ameliorates alcoholic liver injury by inhibiting the IL-6-p47(phox)-oxidative stress pathway in neutrophils. *Gut*. 2017;66(4):705-15.
127. He Y, Hwang S, Cai Y, Kim SJ, Xu M, Yang D, et al. MicroRNA-223 Ameliorates Nonalcoholic Steatohepatitis and Cancer by Targeting Multiple Inflammatory and Oncogenic Genes in Hepatocytes. *Hepatology*. 2019;70(4):1150-67.
128. Hou X, Yin S, Ren R, Liu S, Yong L, Liu Y, et al. Myeloid-Cell-Specific IL-6 Signaling Promotes MicroRNA-223-Enriched Exosome Production to Attenuate NAFLD-Associated Fibrosis. *Hepatology*. 2021;74(1):116-32.
129. Hagenbeek TJ, Webster JD, Kljavin NM, Chang MT, Pham T, Lee H-J, et al. The Hippo pathway effector TAZ induces TEAD-dependent liver inflammation and tumors. *Science signaling*. 2018;11(547):eaaj1757.
130. Wang X, Zheng Z, Caviglia JM, Corey KE, Herfel TM, Cai B, et al. Hepatocyte TAZ/WWTR1 promotes inflammation and fibrosis in nonalcoholic steatohepatitis. *Cell metabolism*. 2016;24(6):848-62.
131. Wang X, Sommerfeld MR, Jahn-Hofmann K, Cai B, Filliol A, Remotti HE, et al. A Therapeutic Silencing RNA Targeting Hepatocyte TAZ Prevents and Reverses Fibrosis in Nonalcoholic Steatohepatitis in Mice. *Hepatology Communications*. 2019;3(9):1221-34.
132. Neville LF, Mathiak G, Bagasra O. The immunobiology of interferon-gamma inducible protein 10 kD (IP-10): A novel, pleiotropic member of the C-X-C chemokine superfamily. *Cytokine & Growth Factor Reviews*. 1997;8(3):207-19.
133. Tomita K, Freeman BL, Bronk SF, LeBrasseur NK, White TA, Hirsova P, et al. CXCL10-Mediates Macrophage, but not Other Innate Immune Cells-Associated Inflammation in Murine Nonalcoholic Steatohepatitis. *Scientific Reports*. 2016;6(1):28786.
134. Calvente CJ, Tameda M, Johnson CD, Del Pilar H, Lin YC, Adronikou N, et al. Neutrophils contribute to spontaneous resolution of liver inflammation and fibrosis via microRNA-223. *J Clin Invest*. 2019;129(10):4091-109.
135. Ying W, Riopel M, Bandyopadhyay G, Dong Y, Birmingham A, Seo JB, et al. Adipose tissue macrophage-derived exosomal miRNAs can modulate in vivo and in vitro insulin sensitivity. *Cell*. 2017;171(2):372-84. e12.
136. Ibrahim SH, Hirsova P, Tomita K, Bronk SF, Werneburg NW, Harrison SA, et al. Mixed lineage kinase 3 mediates release of C-X-C motif ligand 10-bearing chemotactic extracellular vesicles from lipotoxic hepatocytes. *Hepatology*. 2016;63(3):731-44.
137. Hirsova P, Ibrahim SH, Krishnan A, Verma VK, Bronk SF, Werneburg NW, et

- al. Lipid-induced signaling causes release of inflammatory extracellular vesicles from hepatocytes. *Gastroenterology*. 2016;150(4):956-67.
138. Huang DQ, El-Serag HB, Loomba R. Global epidemiology of NAFLD-related HCC: trends, predictions, risk factors and prevention. *Nature Reviews Gastroenterology & Hepatology*. 2021;18(4):223-38.
139. Makler A, Asghar W. Exosomal biomarkers for cancer diagnosis and patient monitoring. *Expert review of molecular diagnostics*. 2020;20(4):387-400.
140. Chu YL, Li H, Ng PLA, Kong ST, Zhang H, Lin Y, et al. The potential of circulating exosomal RNA biomarkers in cancer. *Expert Review of Molecular Diagnostics*. 2020;20(7):665-78.
141. Gurunathan S, Kang M-H, Jeyaraj M, Qasim M, Kim J-H. Review of the isolation, characterization, biological function, and multifarious therapeutic approaches of exosomes. *Cells*. 2019;8(4):307.
142. Tian Y, Gong M, Hu Y, Liu H, Zhang W, Zhang M, et al. Quality and efficiency assessment of six extracellular vesicle isolation methods by nano-flow cytometry. *Journal of extracellular vesicles*. 2020;9(1):1697028.





จุฬาลงกรณ์มหาวิทยาลัย
CHULALONGKORN UNIVERSITY

VITA

NAME Bootsakorn Boonkaew

DATE OF BIRTH 2 January 1990

PLACE OF BIRTH Phatthalung, Thailand

INSTITUTIONS ATTENDED Department of Biochemistry,
Faculty of Medicine, Chulalongkorn University

HOME ADDRESS 230 Moo. 10, Phanangtung, Khuankanun, Phatthalung 93150

PUBLICATION

1. Boonkaew, B., Suwanpitak, S., Pattanapanyasat, K., Sermsathanasawadi, N., Wattanapanitch, M. (2022) Efficient generation of endothelial cells from induced pluripotent stem cells derived from a patient with peripheral arterial disease. *Cell Tissue Res*, <https://doi.org/10.1007/s00441-022-03576-2>.
2. Netsrithong, R., Suwanpitak, S., Bootsakorn, B., Trakarnsanga, K., Chang L.J., Tipgomut, C., Vatanashevanopakorn, C., Pattanapanyasat, K., Wattanapanitch, M. (2020) Multilineage differentiation potential of hematoendothelial progenitors derived from human induced pluripotent stem cells. *Stem Cell Res. Ther*, 11:481.
3. Boonkaew, B., Udompaisarn, S., Arthan, D., Somana, J. (2019) Expression and characterization of a recombinant stevioside hydrolyzing β -glycosidase from *Enterococcus casseliflavus*. *Protein Expr Purif*, 163:105449.
4. Netsrithong, R., Promnakhon, N., Boonkaew, B., Vatanashevanopakorn, C., Pattanapanyasat, K., Wattanapanitch, M. (2019) Generation of two induced pluripotent stem cell lines (MUSli011-A and MUSli011-B) from peripheral blood T lymphocytes of a healthy individual. *Stem Cell Res*, 39:101487.
5. Tantarungsee, N., Bostan Ali, Z., Soi-ampornkul, R., Rujitharanawong, C., Subchookul, C., Ritthaphai, A., Boonkaew, B., Wattanapanitch, M., Thanomkitti, K., Triwongwanat, D.,

Vatanashevanopakorn, C., Thuangtong, R. (2019) Generation of an integration-free human induced pluripotent stem cell line MUSli010-A from occipital scalp fibroblasts of a male patient with androgenetic alopecia. *Stem Cell Res*, 38:101486.

6. Boonkaew, B., Tapeng, T., Netsrithong, R., Vatanashevanopakorn, C., Pattanapanyasat, K., Wattanapanitch, M. (2018) Induced pluripotent stem cell line MUSli006-A derived from hair follicle keratinocytes as a non-invasive somatic cell source. *Stem Cell Res*, 31:79-82.

7. Boonkaew, B., Thummavichit, W., Netsrithong, R., Vatanashevanopakorn, C., Pattanapanyasat, K., Wattanapanitch, M. (2018) Establishment of an integration-free induced pluripotent stem cell line (MUSli005-A) from exfoliated renal epithelial cells. *Stem Cell Res*, 30:34-7.

8. Wattanapatnitch, M., Ritthaphai, A., Park, C., Boonkaew, B., Netsrithong, R., Pattanapanyasat, K., Limsiri, P., Vatanashevanopakorn, C. (2018) Generation of a human induced pluripotent stem cell line (MUSli001-A) from caesarean section scar fibroblasts using Sendai viral vectors. *Stem Cell Res*, 27:105-8.

9. Boonkaew, B., Sathawiwat, N., Pinjaroen, N., Chuaypen, N., Tangkijvanich, P. (2023) Circulating extracellular vesicle-derived microRNAs as novel diagnostic and prognostic biomarkers for non-viral-related hepatocellular carcinoma. *Int J Mol Sci*, 24(22).

AWARD RECEIVED

- 2022 Fulbright Junior Research Scholarship Program (JRS-NRCT), Depts of Molecular and Comparative Pathobiology and Neurology, Johns Hopkins University School of Medicine, USA
- Travel Grant and APASL 2022 Scientific Debrief Session (31st Asian Pacific Association for the Study of the Liver (APASL), Seoul, Korea, 2022)
- 2nd Place Award Oral Presentation (Samaggi Abstract Competition 2022 by The Thai Students' Association in the UK)